

LEVEL II

12

ATC REPORT NO. -R-92000/1CR- 63

CONTRACT NO. N00019-80-C-0265

DTIC FILE COPY AD A109282

The Development of a Low Velocity Impact Methodology for Hybrid Material Systems

S. V. HAYES
E. F. RYBICKI

VOUGHT CORPORATION ADVANCED TECHNOLOGY CENTER
P. O. BOX 226144
DALLAS, TEXAS 75266

JULY 1981

FINAL REPORT FOR PERIOD APRIL 1980 - APRIL 1981

DTIC
COLLECTED
JAN 6 1982
H

12 102

APPROVED FOR PUBLIC RELEASE; DISTRIBUTION UNLIMITED

PREPARED FOR

NAVAL AIR SYSTEMS COMMAND
WASHINGTON, D.C. 20361

389797



VOUGHT CORPORATION
Advanced Technology Center

82 01 05 002

Handwritten mark

UNCLASSIFIED

SECURITY CLASSIFICATION OF THIS PAGE (When Data Entered)

REPORT DOCUMENTATION PAGE		READ INSTRUCTIONS BEFORE COMPLETING FORM
1. REPORT NUMBER	2. GOVT ACCESSION NO.	3. RECIPIENT'S CATALOG NUMBER
	AD A109287	
4. TITLE (and Subtitle) THE DEVELOPMENT OF A LOW VELOCITY IMPACT METHODOLOGY FOR HYBRID MATERIAL SYSTEMS		5. TYPE OF REPORT & PERIOD COVERED FINAL REPORT FOR PERIOD APRIL 1980 - APRIL 1981
		6. PERFORMING ORG. REPORT NUMBER R-92000/1CR-63
7. AUTHOR(s) S. V. Hayes E. F. Rybicki		8. CONTRACT OR GRANT NUMBER(s) N00019-80-C-0265
9. PERFORMING ORGANIZATION NAME AND ADDRESS Vought Corporation Advanced Technology Center P. O. Box 226144 Dallas, Texas 75266		10. PROGRAM ELEMENT, PROJECT, TASK AREA & WORK UNIT NUMBERS
11. CONTROLLING OFFICE NAME AND ADDRESS Naval Air Systems Command Washington, D.C. 20361 Code AIR-320B		12. REPORT DATE July 1981
		13. NUMBER OF PAGES 100
14. MONITORING AGENCY NAME & ADDRESS (if different from Controlling Office)		15. SECURITY CLASS. (of this report) Unclassified
		15a. DECLASSIFICATION/DOWNGRADING SCHEDULE
16. DISTRIBUTION STATEMENT (of this Report) APPROVED FOR PUBLIC RELEASE; DISTRIBUTION UNLIMITED		
17. DISTRIBUTION STATEMENT (of the abstract entered in Block 20, if different from Report)		
18. SUPPLEMENTARY NOTES		
19. KEY WORDS (Continue on reverse side if necessary and identify by block number) Impact, Hybrids, Composites, Damage Tolerance, Math Model, Delamination, Strain Rate Sensitivity		
20. ABSTRACT (Continue on reverse side if necessary and identify by block number) The development of a design methodology for hybrid structures which describes the extent of damage and associated failure modes due to low velocity impact has been undertaken. Hybrids can provide a synergistic improvement in damage resistance caused by foreign body low velocity impact over graphite/epoxy material and when properly designed, enhance the visual and NDI damage detection threshold of the baseline material. Improvements in the visible and NDI damage detectability threshold of graphite/epoxy material, (cont'd next pag		

DTIC
JAN 6 1982

DD FORM 1473 1 JAN 73

EDITION OF 1 NOV 65 IS OBSOLETE
S/N 0102-LF-014-6601

UNCLASSIFIED

SECURITY CLASSIFICATION OF THIS PAGE (When Data Entered)

UNCLASSIFIED

SECURITY CLASSIFICATION OF THIS PAGE (When Data Entered)

subject to low velocity impact, via proper placement and use of Kevlar plies and metallic coatings within this baseline material were exhibited. Correlation between the math model and the extent of both visible and invisible damage test panels experienced when subjected to low velocity impact were used to validate the model. Residual strength tests of damaged panels were run to quantify the static strength reduction experienced in the panel due to varying levels of visible and invisible damage.

Development of the math model was based upon physical parameters identified through experimental testing. These included transverse impact of hybrid and graphite/epoxy panels and tensile tests of the target materials at elevated strain rates. High speed photography of the impact event on the composite panels was used to provide the dynamic modes of failure for use in model. Reasonably good correlation between predicted and actual strains and resulting damage were achieved.

Accession For	
NTIS GRA&I	<input checked="" type="checkbox"/>
DTIC TAB	<input type="checkbox"/>
Unannounced	<input type="checkbox"/>
Justification	
By _____	
Distribution/	
Availability	
Dist	
A	

UNCLASSIFIED

SECURITY CLASSIFICATION OF THIS PAGE (When Data Entered)

FOREWORD

This final report is for the program entitled "The Development of a Low Velocity Impact Methodology for Hybrid Material Systems". The experimental work was conducted by Vought Corporation Advanced Technology Center with the analytical model development subcontracted to the University of Tulsa. This is the final report that covers the period extending from 28 April 1980 to 28 April 1981 and is sponsored by the Naval Air Systems Command under Contract No. N00019-80-C-0265.

Dr. D. Mulville is the Navy Project Manager and Dr. W. J. Renton is the Vought Program Manager. Other key personnel are Mr. S. V. Hayes, Principal Investigator and Dr. E. F. Rybicki, University of Tulsa, Technical Consultant.

TABLE OF CONTENTS

<u>SECTION</u>	<u>PAGE</u>
FOREWORD	i
1.0 INTRODUCTION	1
2.0 OBJECTIVES AND SUMMARY	3
2.1 OBJECTIVES	3
2.2 SUMMARY OF RESULTS	4
3.0 EXPERIMENTAL RESULTS	5
3.1 TRANSVERSE IMPACT OF THIN FLAT PANELS - TASK I	5
3.1.1 Dynamic Deflection Profile	5
3.1.2 Impact Strain Relationships	9
3.1.3 Task I Summary	9
3.2 EVALUATION OF STRAIN RATE EFFECTS ON MATERIAL PROPERTIES - TASK II	9
3.2.1 Longitudinal and Transverse Coupon Tests	15
3.2.2 Shear Coupon Tests	18
3.2.3 Conclusions and Discussion - Task II	18
3.3 LAMINATE IMPACT DAMAGE AND RESPONSE	18
3.3.1 Non-Hybrid Laminate Impact Tests - Series 1	19
3.3.1.1 Test Results - Series 1	23
3.3.1.2 Series 1 Conclusions	26
3.3.2 Hybrid Laminate Impact - Series 2	26
3.3.2.1 Test Results - Series 2	31
3.3.2.2 Series 2 - Conclusions	31
3.3.3 Test Results - Series 3	34
4.0 COMPUTATIONAL MODEL FOR LOW VELOCITY IMPACT DAMAGE OF HYBRID PANELS	37
4.1 MODEL BACKGROUND	37
4.1.1 Determination of the Deformation Mode	37
4.1.2 Math Model Approach and Objectives	38

TABLE OF CONTENTS
(Continued)

<u>SECTION</u>	<u>PAGE</u>
4.2 DEVELOP SIMPLIFIED COMPUTATIONAL MODEL - TASK IV	38
4.2.1 Method of Analysis	40
4.2.2 Deformation Profile	41
4.2.3 Damage Modes	44
4.2.4 Summary of Math Model Development	44
4.3 VERIFICATION OF THE MODEL - TASK V	44
4.3.1 Thin Laminate Experimental Comparisons	45
4.3.2 Complex Laminate Comparisons	48
4.3.2.1 Critical Stress Evaluation	48
4.3.2.2 Hybrid Impact Prediction	50
4.3.3 Summary of Model Verification	57
4.4 APPLICATIONS OF MODEL - TASK VI	57
4.5 DISCUSSION OF ANALYTICAL VERSUS EXPERIMENTAL DATA	63
5.0 SUMMARY AND CONCLUSIONS	66
6.0 SUGGESTIONS FOR FUTURE WORK	70
7.0 REFERENCES	71

LIST OF FIGURES

FIGURE NO.		PAGE NO.
3.1	EXAMPLE OF DEFLECTED PANEL SHAPE DERIVED FROM PHOTO	7
3.2	ARRANGEMENT OF EXPERIMENTAL SET-UP (TASK 1)	8
3.3	STRAIN GAGE PLACEMENT (TASK 1)	10
3.4a	THE UPPER AND LOWER TRACES CORRESPOND TO THE RESPONSE OF STRAIN GAGES A AND B, RESPECTIVELY. (SPECIMEN GR 2)	11
3.4b	THE UPPER AND LOWER TRACES CORRESPOND TO THE RESPONSE OF STRAIN GAGES D AND C, RESPECTIVELY. (SPECIMEN GR 2)	11
3.5a	THE UPPER AND LOWER TRACES CORRESPOND TO THE RESPONSE OF STRAIN GAGES A AND B, RESPECTIVELY. (SPECIMEN KE2)	12
3.5b	THE UPPER AND LOWER TRACES CORRESPOND TO THE RESPONSE OF STRAIN GAGES D AND C, RESPECTIVELY. (SPECIMEN KE2)	12
3.6	SAMPLE STRESS-STRAIN CURVE AT ELEVATED STRAIN RATE	16
3.7	SAMPLE STRAIN-TIME CURVE	17
3.8	IMPACT POSITIONS ON TASK III PANEL (SERIES 1 AND 2)	21
3.9	CONFIGURATION OF CENTER PANEL IMPACT	22
3.10	CONFIGURATION OF OFF-CENTER PANEL IMPACT	24
3.11	CENTER IMPACT DELAMINATION SIZE FOR SERIES 1 AND 2 LAMINATES	25
3.12	DIAMOND SHAPED DELAMINATION IN 14 PLY LAMINATE	27
3.13	ROUNDED DELAMINATION IN 18 PLY LAMINATE	28
3.14	OFFSET DELAMINATION RESULTING FROM OFF-CENTER IMPACT	29
3.15	OFF-CENTER IMPACT DELAMINATION FOR SERIES 1 AND 2 LAMINATES	33
3.16	IMPACT POSITIONS AND ENERGY OF SERIES 3 METALLIC COATED PANELS	35

LIST OF FIGURES

(Cont'd)

FIGURE NO.		PAGE NO.
4.1	SKETCH OF LAMINATED PANEL BEFORE AND AFTER IMPACT	39
4.2	EXPERIMENTAL DISPLACEMENT VERSUS MODEL PREDICTION FOR TASK I GRAPHITE PANEL (T = .067 SEC)	42
4.3	EXPERIMENTAL VERSUS PREDICTED DISPLACEMENT AT IMPACT POINT TASK I KEVLAR PANEL	46
4.4	EXPERIMENTAL VERSUS ANALYTICAL STRAINS DURING IMPACT TASK I KEVLAR	47
4.5	EXPERIMENTAL VERSUS PREDICTED DELAMINATION ZONE	49
4.6	EXPERIMENTAL VERSUS PREDICTED DELAMINATION ZONE	51
4.7	EXPERIMENTAL VERSUS ANALYTICAL DELAMINATION LENGTH (15 FT/SEC)	52
4.8	EXPERIMENTAL VERSUS ANALYTICAL DELAMINATION LENGTH(20 FT/SEC)	55
4.9	EXPERIMENTAL VERSUS ANALYTICAL DELAMINATION LENGTH (15 FT/SEC)	59
4.10	EXPERIMENTAL VERSUS ANALYTICAL DELAMINATION LENGTH (20 FT/SEC)	60
1A	THIN IMPACT PANEL (3 PLY) CONFIGURATION (TASK I)	71
2A	LONGITUDINAL (0°), SHEAR (+45°) AND STATIC TRANS- VERSE (90°) COUPON CONFIGURATION (TASK II)	74
3A	DYNAMIC TRANSVERSE COUPON CONFIGURATION (TASK II)	75
4A	IMPACT PANEL CONFIGURATION, 14 AND 18 PLY (TASK III)	76
5A	RESIDUAL STRENGTH COUPON CONFIGURATION (TASK III)	77
1B	C-SCAN OF IMPACT DADAGED NON-HYBRID PANEL (PANEL 1)	79
2B	C-SCAN OF IMPACT DAMAGED NON-HYBRID PANEL (PANEL 2)	80
3B	C-SCAN OF IMPACT DAMAGED NON-HYBRID PANEL (PANEL 3)	81
4B	C-SCAN OF IMPACT DAMAGED NON-HYBRID PANEL (PANEL 4)	82
5B	C-SCAN OF IMPACT DAMAGED NON-HYBRID PANEL (PANEL 5)	83
6B	C-SCAN OF IMPACT DAMAGED HYBRID (PANEL 6)	84
7B	C-SCAN OF IMPACT DAMAGED HYBRID (PANEL 7)	85
8B	C-SCAN OF IMPACT DAMAGED HYBRID (PANEL 8)	86
9B	C-SCAN OF IMPACT DAMAGED HYBRID (PANEL 9)	87
10B	C-SCAN OF IMPACT DAMAGED HYBRID (PANEL 10)	88
11B	C-SCAN OF IMPACT DAMAGED METALLIC COATED HYBRID (PANEL 11)	89
12B	C-SCAN OF IMPACT DAMAGED METALLIC COATED HYBRID (PANEL 12)	90

LIST OF TABLES

TABLE NO.		PAGE NO.
3.1	TASK I - TEST MATRIX	6
3.2	THIN PANEL IMPACT TEST RESULTS TASK I	13
3.3	SUMMARY OF TASK II TESTS	14
3.4	TASK III TEST MATRIX	20
3.5	SERIES I TEST RESULTS	30
3.6	SERIES II TEST RESULTS	32
3.7	SERIES III LAMINATES	34
3.8	SERIES 3 METALLIC COATING IMPACT RESULTS	36
4.1	SUMMARY OF DELAMINATION ZONES FOR 14 PLY LAMINATES (15 FT/SEC)	54
4.2	SUMMARY OF DELAMINATION ZONES FOR 14 PLY LAMINATES (20 FT/SEC)	56
4.3	SUMMARY OF DELAMINATION ZONES FOR 18 PLY LAMINATES (15 FT/SEC)	61
4.4	SUMMARY OF DELAMINATION ZONES FOR 18 PLY LAMINATES (20 FT/SEC)	62
4.5	ANALYTICAL VERSUS EXPERIMENTAL RESULTS	64

1.0 INTRODUCTION

The wide use of advanced composite materials and the rapid increase in their fields of application have necessitated a better understanding of the performance of composites. Although significant progress has been made, the behavior of hybrid laminates subjected to low velocity impact is still not well understood. This study is, thereby, directed at obtaining a better insight into the behavior of composites under low velocity impact loadings.

Some pertinent work on this subject is described in the literature. For example, Jones¹ has dealt with the mechanics of composites, giving constitutive relationships which are basic to this study. Ashton, Halpin and Petit² give insight into the changes of the material properties of composites with loading. Gottesman, Hashin and Brull³ give composites mechanical properties as a function of damage. The information provided by the above mentioned references provided important guidelines. Vinson and Zukas⁴ focused on fabrics and high velocity impact and made use of photographs of displacement in determining strains. Information regarding the inplane strains in plates as described by Daniel, Liber and Labedz⁵ is also pertinent to this study. Other papers and reports were also reviewed for applicability to this problem and are listed in the references section.

This research program was divided into two parts, an experimental and an analytical study. The experimental study was performed at Vought Corporation Advanced Technology Center (ATC). The analytical investigation was conducted at the Mechanical Engineering Department at the University of Tulsa.

In the experimental study, hybrid and nonhybrid composite laminates with different stacking sequences and lay-ups angles were impacted by low velocity projectiles. The resulting damage was determined utilizing various NDT methods, followed by destructive testing to obtain the residual strengths. These results have been compared with the predicted analytical results from the model. Coupon tests at several strain rates were conducted to quantify the strain rate sensitivity of the materials. The objectives of each task are described in the following:

Build a computational model to predict damage in hybrid laminates subjected to low velocity impact.

Validate the computational model with test data for a variety of laminates.
Use the model to design laminates with improved impact resistance.
The experimental program and analytical effort were done simultaneously
with extensive interactions between the two investigations.

2.0 OBJECTIVES AND SUMMARY

2.1 OBJECTIVES

The overall objectives of the research effort described in this document are to determine if hybrids do provide a synergistic improvement in damage resistance in comparison to a baseline (i.e., graphite/epoxy) material, and to determine if hybrids, when properly designed, may enhance the visual and NDI damage detection threshold of the baseline material. The net result may enable one to design with hybrids for improved low velocity impact resistance and for an improved damage detection capability. The specific objectives of this research program were:

- o To develop a design methodology (math model) for hybrid structures which accurately describes the structural response, extent of damage and associated failure mode(s) due to low velocity impact. Such a model should enable one to design an optimum hybrid panel to maximize the damage initiation threshold and/or damage resistance of a baseline material and minimize the number of tests required to optimize a hybrid design.
- o To verify that the math model can predict the extent of damage, both visible and invisible, a panel experiences when subjected to low velocity impact. Panels were impacted to provide the necessary analytical-experimental correlation.
- o To residual strength test all impacted test panels to ascertain their reduced static strength due to visible and invisible damage.
- o To improve the visible and NDI damage detectability threshold of a baseline material system subjected to low velocity impact by proper placement of a second and possibly a third material at the proper location within the baseline material. Enhanced damage detectability could be provided by a thin aluminum or titanium foil outer surface lamina. This layer would provide a permanent record of small particle impact events on the surface of the panel. The size of the dent in turn could possibly be correlated to the probability that the panel had been damaged internally.

2.2 SUMMARY OF RESULTS

The following contains a summary of the significant results from the computational modeling study is as follows:

- o A simple quasi-static computational model was developed to represent the low velocity impact behavior for hybrid Kevlar/graphite laminates.
- o Good agreement was obtained for comparison of experimental data and computed values for strains and displacements as a function of time for an impacted laminate.
- o The model showed good agreement with the delamination trends observed in the experimental study for most cases. However, correlation of analytical with experimental delamination data varied for some hybrids.

While the results shown here are very encouraging, the simplicity of the model indicates restrictions on its general applicability. Further verification and development is required.

A summary of experimental work conducted within the scope of the impact program yielded the following results:

- o Impact tests of both hybrid and non-hybrid laminates were conducted to determine their damage and response. Of the laminates tested, the hybrids did not exhibit significant synergistic damage tolerance. High speed photos and strain gage data were obtained on thin graphite/epoxy and Kevlar/epoxy panels from which deformation mode shapes and strain response were derived.
- o Metallic coatings were applied to the impact surface of selected composite laminates in an effort to enhance the visual detection of impact damage. Thin aluminum foil was secondarily bonded or cocured on one surface of the panel. The panels were impact tested. The aluminum did not contribute significantly to detecting impact damage.
- o Longitudinal, transverse and shear graphite/epoxy and Kevlar/epoxy tensile coupons were tested at three strain rates to determine the material's strain rate sensitivity. Some material properties did exhibit limited variation with strain rate. Further investigation is required.

3.0 EXPERIMENTAL RESULTS

3.1 TRANSVERSE IMPACT OF THIN FLAT PANELS - TASK I

The materials used in all phases of this program were obtained from Narmco Materials, Inc. Narmco 5208 epoxy resin was used on both T300 graphite fiber and Kevlar 49 fiber.

Four thin 3-ply composite panels were transversely impacted to determine their response for use in developing a math model of the impact event. Deflected shapes of all panels were recorded using high speed photography. Two panels were instrumented with strain gages to determine the impact induced strain levels and strain rates. All Task I panels were fabricated using woven material with overall dimensions of five inches by ten inches. Two of the four panels were fabricated using graphite/epoxy fabric. The remaining two were fabricated with Kevlar/epoxy. Thin laminates were used to allow deflections large enough to be photographed.

Twelve inch unidirectional prepreg tape was used in all Task II and III panels. Standard layup and cure processes were used in fabrication as prescribed by the vendor.

3.1.1 Dynamic Deflection Profile

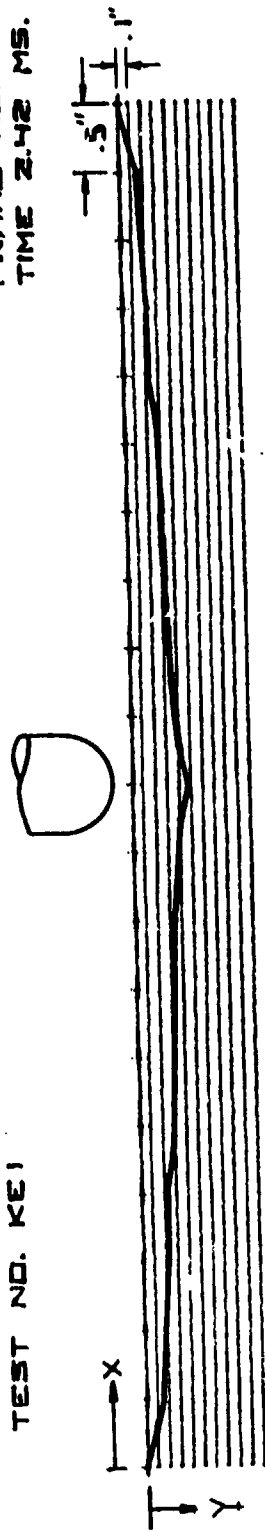
The deflected shape of the thin laminates was determined using high speed photographs of the impact event for use as a basis in the analytical model. The first impact test for each of the graphite/epoxy and Kevlar/epoxy panels, tests GR1 and KE1 as summarized in Table 3.1, utilized two cameras situated orthogonal to each other in a parallel plane to that of the test panel. Two 16mm cameras were used at speeds up to 4500 frames per second. Electronic controls were utilized to synchronize the camera triggers with the impact event. The two views were then used to verify symmetry in the deflected panel about the impact zone and determine the approximate shape of the deflected panel subjected to impacts by a one pound projectile from three and six foot drop heights (15 and 20 ft/sec, respectively). Figure 3.1 is an example of the deflected panel shape obtained from the photos. Subsequent to verifying axial symmetry in deformation, one camera was used to further substantiate the deflected panel shape. Figure 3.2 shows the test setup used.

TABLE 3.1
TASK I - TEST MATRIX

PANEL NO.	MATERIAL	IMPACT ENERGY (FOOT POUNDS)	IMPACT VELOCITY (FEET/SECOND)	INSTRUMENTATION
GR1	Graphite/Epoxy	3	15	2 Cameras
GR2	Graphite/Epoxy	6	20	1 Camera, 4 Strain Gages
KE1	Kevlar/Epoxy	3	15	2 Cameras
KE2	Kevlar/Epoxy	6	20	1 Camera, 4 Strain Gages

FRAME NO. 11
TIME 2.42 MS.

TEST NO. KE1



Y-DIST.	X-DIST.
0.140	0.50
0.166	1.00
0.204	1.50
0.215	2.00
0.271	2.50
0.302	3.00
0.317	3.50
0.332	4.00
0.353	4.25
0.376	4.50
0.412	4.75
0.412	5.00
0.375	5.25
0.353	5.50
0.332	5.75
0.317	6.00
0.302	7.00
0.271	7.50
0.215	8.00
0.204	8.50
0.166	9.00
0.140	9.50

FIGURE 3.1 EXAMPLE OF DEFLECTED PANEL SHAPE DERIVED FROM PHOTO

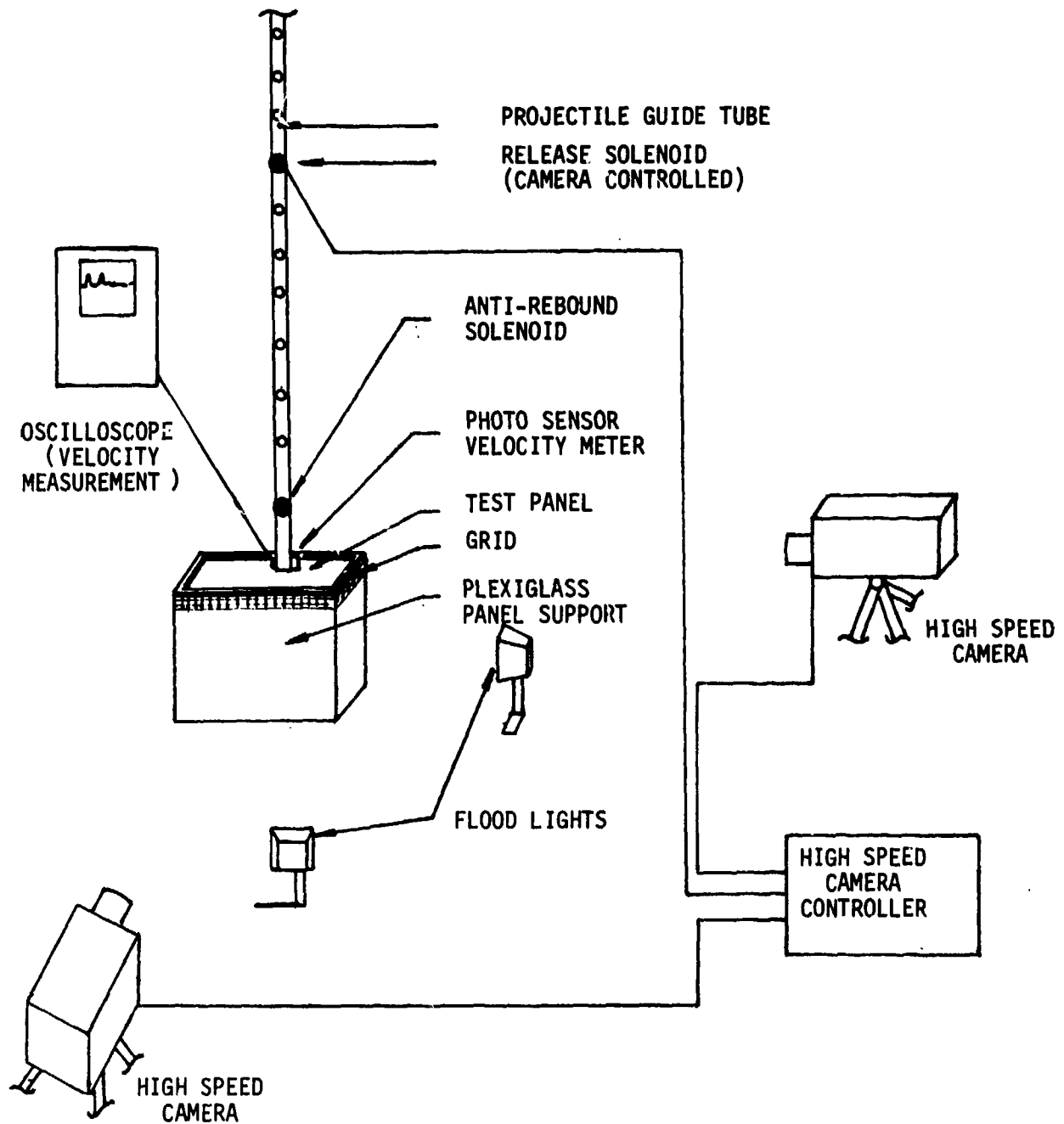


FIGURE 3.2 ARRANGEMENT OF EXPERIMENTAL SET-UP (TASK I)

3.1.2 Impact Strain Relationships

Panels GR2 and KE2 were instrumented using axial strain gages (see Figure 3.3) to determine the strain rates and levels encountered during the impact event. The strain gages were placed on radial axis, top and bottom at 0° and 90° at one inch from the point of impact. In addition, the strain values were used to provide additional documentation supporting the symmetry of the panel deflection. Figures 3.4 a-b and 3.5 a-b contain the strain vs. time plots of the graphite/epoxy panel GR2 and the Kevlar/epoxy panel KE2 when subjected to a 20 foot per second impact (6 foot pounds). Table 3.2 contains a summary of Task I strain and displacement results. Strain rate data was recorded for use in selecting the coupon strain rates in Task II.

Due to the high strain rates involved, several strain gages were ruined by individual fibers failing early in the test resulting in a loss of strain data.

3.1.3 Task I Summary

The principal purpose for performing the task outlined in this section was to provide the information necessary to develop a simple model of the low velocity impact event. Axisymmetric deformation was shown to be an accurate assumption from the tests conducted. Strain gage data indicates the principle strains in the deflected panels are due to in-plane stretching as both the top and bottom strain gages exhibited nearly equal tensile strains. Strain due to bending appears to assume a secondary role with the upper surface strains showing a slightly lower tensile component than the lower surface. This difference in strain corresponds to the pure bending mode which exhibits negative upper surface strains and positive lower surface strains of equal magnitude. Thicker laminates will obviously have greater strains due to bending which were accounted for in the model.

3.2 EVALUATION OF STRAIN RATE EFFECTS ON MATERIAL PROPERTIES - TASK II

A series of coupon tests as summarized in Table 3.3 were conducted on the baseline materials to determine the effects of varying the rate of strain to failure on the basic material properties. Appendix A contains a review of the specimen configuration. The properties investigated were ultimate stress and

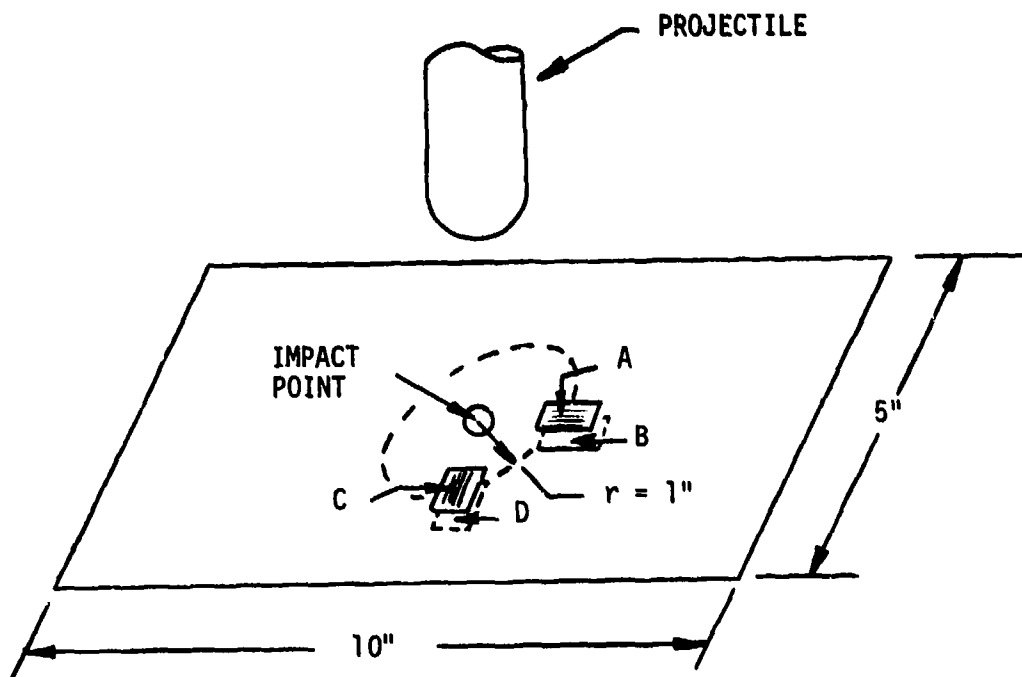


FIGURE 3.3 STRAIN GAGE PLACEMENT (TASK I)

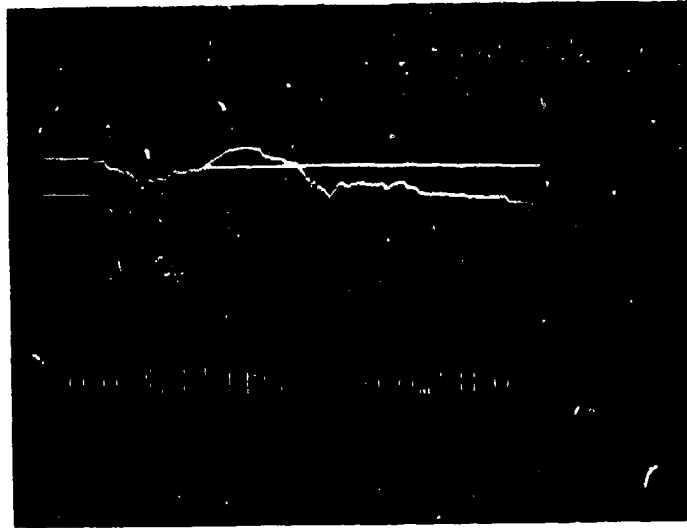


FIGURE 3.4a: THE UPPER AND LOWER TRACES CORRESPOND TO THE RESPONSE OF STRAIN GAGES A AND B, RESPECTIVELY. (SPECIMEN GR2)

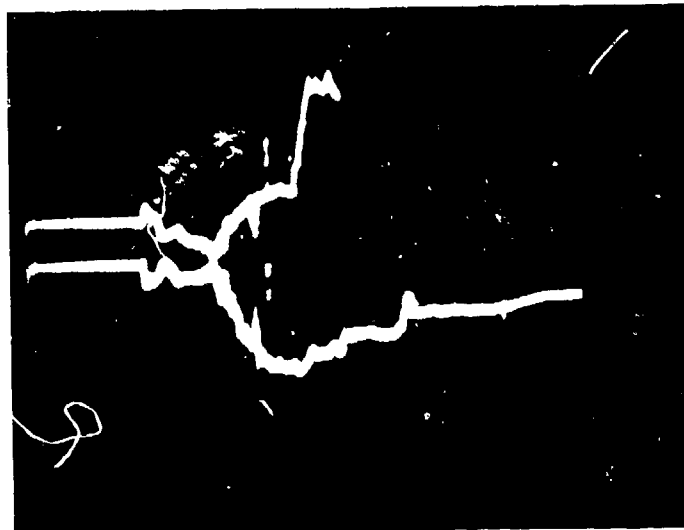


FIGURE 3.4b: THE UPPER AND LOWER TRACES CORRESPOND TO THE RESPONSE OF STRAIN GAGES D AND C, RESPECTIVELY. (SPECIMEN GR2)

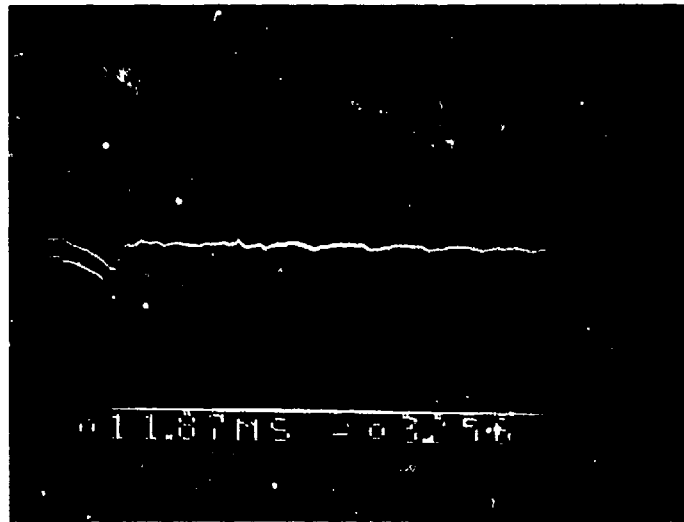


FIGURE 3.5a: THE UPPER AND LOWER TRACES CORRESPOND TO THE RESPONSE OF STRAIN GAGES A AND B, RESPECTIVELY. (SPECIMEN KE2)

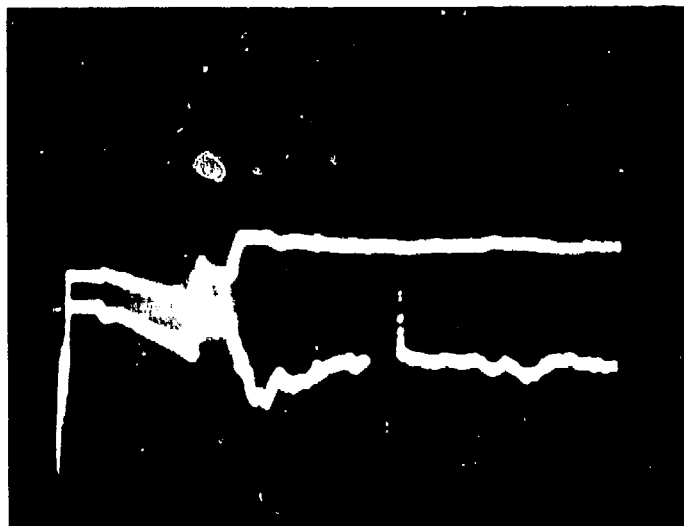


FIGURE 3.5b: THE UPPER AND LOWER TRACES CORRESPOND TO THE RESPONSE OF STRAIN GAGES D AND C, RESPECTIVELY. (SPECIMEN KE2)

TABLE 3.2 THIN PANEL IMPACT TEST RESULTS
TASK I

PANEL NO.	MATERIAL	IMPACT VELOCITY (FT/SEC)	ULTIMATE DISPLACEMENT (IN)	STRAIN GAGE NO.	ULT. STRAIN (ϵ IN/IN)	STRAIN RATE $\dot{\epsilon}$ IN/IN/SEC
G1	Graphite/ Epoxy	15	.37	NO GAGE		
G2		20	.52	A	1,700 $\mu\epsilon$	6.1
				B	1,700 $\mu\epsilon$	-
				C	1,700 $\mu\epsilon$.67
				D	- $\mu\epsilon$	1.4
K1	Kevlar/ Epoxy	15	.45	NO GAGE		
K2		20	.5	A	4,800 $\mu\epsilon$	2.2
				B	4,800 $\mu\epsilon$	2.2
				C	5,300 $\mu\epsilon$	2.7
				D	3,200 $\mu\epsilon$	1.9

TABLE 3.3 - SUMMARY OF TASK II TESTS

MATERIAL	FIBER ORIENTATION	TEST RATE (IN/SEC)	ULTIMATE STRESS (KSI)	YOUNG'S MODULUS (MSI)	STRAIN RATE (IN/IN/SEC)	SHEAR MODULUS (MSI)
GRAPHITE/ EPOXY	0°	STATIC	206	23.1	-	-
		2.5	207	27.8	0.15	-
		5.0	213	25.6	0.30	-
	90°	STATIC	7.1	1.4	-	-
		2.5	6.0	1.3	-	-
		5.0	8.5	1.4	-	-
	+45°	STATIC	22.9	3.3	-	-
		2.5	28.1	-	1.6	2.1
		5.0	30.0	4.0	1.15	-
KEVLAR/ EPOXY	0°	STATIC	210.3	10.9	-	-
		2.5	191	16.0	.16	-
		5.0	177	11.1	.38	-
	90°	STATIC	2.1	.8	-	-
		2.5	3.7	.8	-	-
		5.0	4.0	.8	-	-
	+45°	STATIC	13.1	.9	-	-
		2.5	13.6	1.1	-	.32
		5.0	13.7	1.3	2.9	.42
						.56

Young's modulus. Eight ply and twenty ply unidirectional coupons with fibers oriented longitudinal and transverse, respectively to the loading axis were investigated for their strain rate sensitivity (see Appendix A). In addition, eight ply shear coupons with fibers oriented at alternating plus and minus forty-five degrees were studied. Three test machine stroke rates were utilized in this test series, the highest being approximately five inches per second. This rate corresponds to the highest stroke rate attainable using the test equipment available. Static tests were conducted to provide a baseline for the data. As seen in Table 3.2, the thin Task I panels experience strain rates of 2 to 6 in/in/sec at one inch from the impact point.

A third set of tests were conducted at an approximate stroke rate of two and one half inches per second. The actual strain rates realized in the materials varied according to the coupon ply orientation and stroke rate as outlined in Table 3.3. Sample dynamic stress-strain and strain-time curves obtained in testing are shown in Figures 3.6 and 3.7.

3.2.1 Longitudinal and Transverse Coupon Tests

Analysis of static Young's modulus and ultimate strain for the longitudinal (0° fiber) and transverse (90° fibers) coupon test results at static and higher strain rates exhibited some variation. All variation in the coupon material properties with respect to the strain rate was within the data scatter band.

The longitudinal graphite specimens did show a slight increase in ultimate stress with little variation in Young's modulus at increased strain rate. The longitudinal Kevlar specimens exhibited a small decrease in the ultimate stress with increased strain rate. The transverse Kevlar specimens revealed the most dramatic increase in ultimate stress. This increase most likely resulted from a variation in coupon size. The transverse Kevlar coupons used for the static tests were found to be too fragile in the elevated strain rate tests. Specimens with a cross sectional area of 0.1 in^2 versus 0.02 in^2 for the static tests were fabricated for the dynamic tests (see Appendix A). Therefore, edge effects may account for the higher modulus and ultimate stress values encountered.

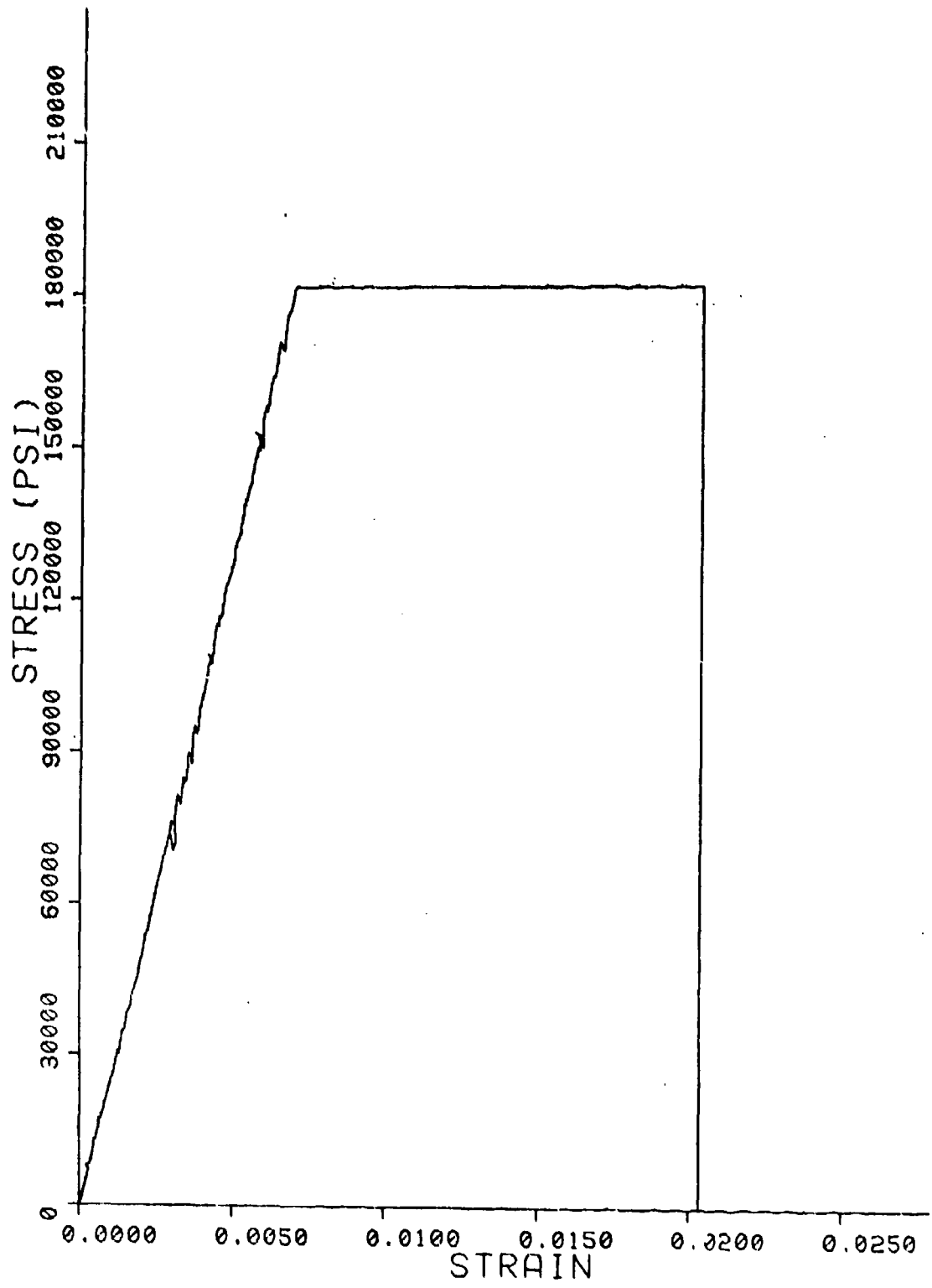


FIGURE 3.6 SAMPLE STRESS-STRAIN CURVE AT ELEVATED STRAIN RATE

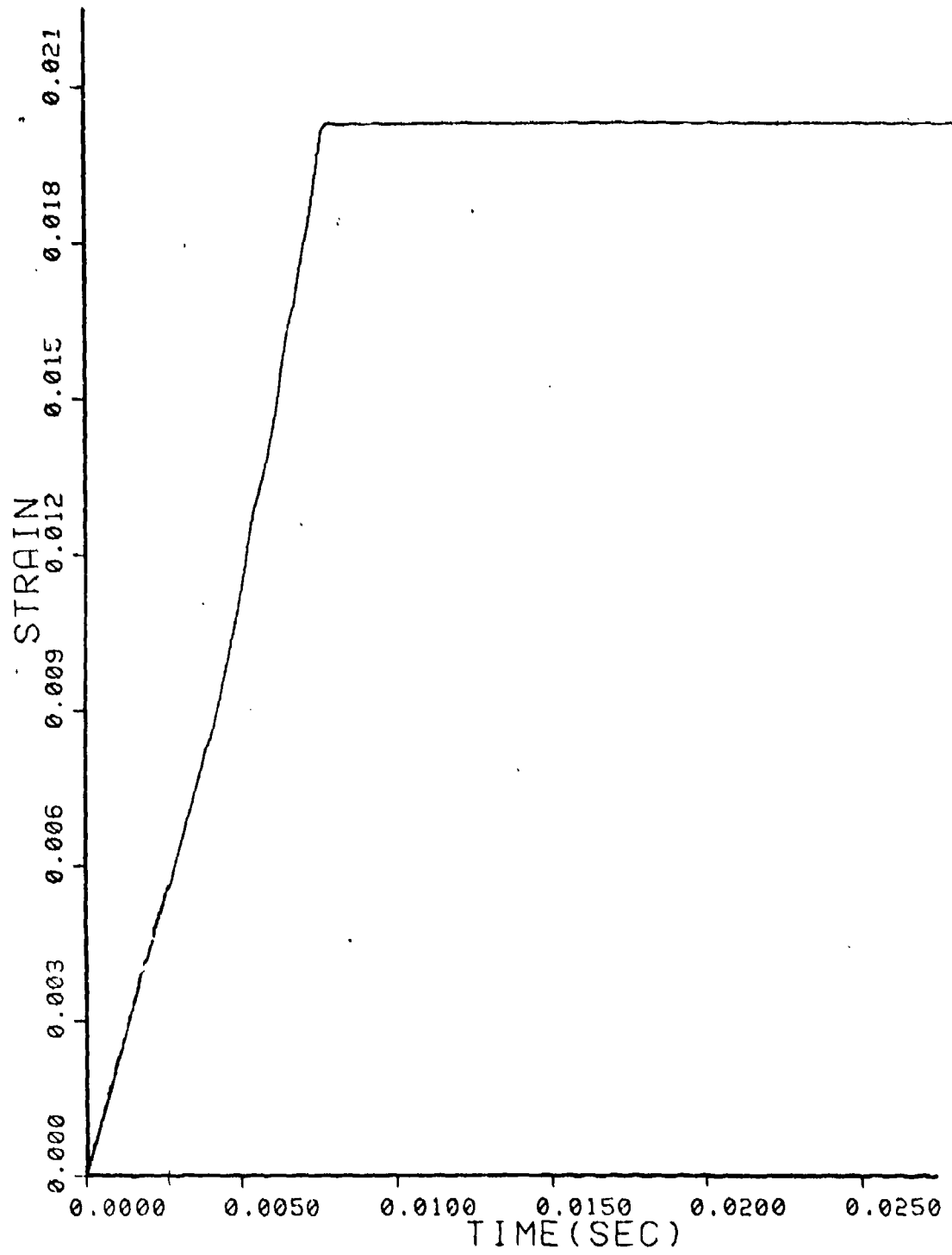


FIGURE 3.7 SAMPLE STRAIN-TIME CURVE

3.2.2 Shear Coupon Tests

The specimen configuration utilized in the shear tests was a one inch gage length, 8-ply, 0.5 inch wide, ± 45 degree fiber orientated coupon as shown in Appendix A. The graphite varied from a static shear modulus of 2.1 MSI to 3.8 MSI at 5.0 inches per second. A shear modulus on the Kevlar of .32 was obtained at the static load rate while .42 MSI and .56 MSI were obtained at stroke rates of 2.5 inches per second and 5.0 inches per second, respectively.

As shear modulus cannot be measured directly from the shear specimen, the longitudinal stresses and strains were measured directly from the ± 45 degree coupon. These longitudinal values were then used to calculate the shear modulus.

An increase in both the modulus and ultimate stress for the ± 45 graphite and Kevlar coupons with increased strain rate was noted. These increases were not considered significant at this point due to the considerable amount of scatter in the data. Further investigation is required.

3.2.3 Conclusions and Discussion - Task II

Test data indicate material properties were insensitive to strain rates at the levels used in these tests. The strain rates used in Task II tests varied from $0.3 (10^6)$ to $1.5 (10^6)$ microstrain per second on the 0° and 90° specimens, respectively. Strain rates approaching $3.0 (10^6)$ microstrain were measured at the point of impact in Task I panel impact tests.

The test apparatus available proved to be the limiting factor in the strain rates attainable. Further investigation into strain rate sensitivity of composite materials is necessary.

3.3 LAMINATE IMPACT DAMAGE AND RESPONSE - TASK III

Task III impact tests served to provide data to validate and develop the math model. In addition, an investigation of the visual damage threshold for the hybrid laminates was conducted. Section 4.0 contains an overview of the math model and the correlation between it and the experimental data presented here.

Task III laminates as summarized in Table 3.4 consist of two basic layups. A specially orthotropic 14-ply laminate and a quasi-isotropic 18-ply laminate were used. The 14 and 18-ply layups were $(0_2/90_2/0_2/90)_s$ and $(0_2/+45/90_2/+45/0)_s$, respectively.

Two material systems were employed in this program, T300 graphite/5208 epoxy and Kevlar 49/5208 epoxy unidirectional tape. Table 3.4 outlines the material's application in Task III laminates.

Task III tests were divided into three functional groups. The first group, Series 1 consisted of four non-hybrid laminates. These laminates included an all graphite/epoxy 14 and 18-ply laminates as well as corresponding 14 and 18-ply Kevlar/epoxy panels. Series 1 panels comprise the control or baseline tests with which the Series 2 hybrid laminate damage and response were compared. Test Series 2 laminates consisted of six hybrid laminates, three each of the 14 and 18-ply layups as outlined in Table 3.4. Selection of the particular hybrid laminates was based on the model predictions. Those selected were the three laminates which exhibited the least amount of damage, most damage and highest deflection during impact based on preliminary analyses of the laminates. Series 3 laminates consisted of two hybrid laminates, one with an aluminum foil cocured to the impact surface and a second panel with aluminum foil bonded to one surface.

3.3.1 Non-Hybrid Laminate Impact Tests - Series 1

Impact tests of the four Series 1 panels were conducted to provide impact data on the baseline materials. The baseline material data was used for comparison purposes to evaluate the Series 2 hybrid panels.

As noted in Table 3.4, impact and residual strength tests were conducted on graphite/epoxy and Kevlar/epoxy 14-ply and 18-ply panels. Each panel was divided into five equal sections (Figure 3.8) and impacted at the geometric center of four sections. The fifth section was left undamaged to provide a residual strength baseline for purposes of comparison. The panel sections were supported by a frame simulating pinned boundary conditions. The panel section could be positioned in a centered or off-centered impact position. The centered impact setup placed the impact point on the panel section in the geometric center of the impact support frame. This corresponds the tests run on positions 3 and 4 as seen in Figure 3.9. The impact point is positioned

TABLE 3.4 TASK III TEST MATRIX

PANEL NO.	LAYUP	LAMINATE TYPE	TEST SERIES	TESTS CONDUCTED
1	$(0_2/90_2/0_2/90)_s$	Nonhybrid (Series 1)	1	3 Ft-Lb Center Impact, 3 Ft-Lb Offcenter Impact, 6 Ft-Lb Center Impact, 6 Ft-Lb Offcenter Impact NDT Evaluation of Damage, Residual Strength Test All Damaged Sections and One Undamaged Section
2	$(0_2^k/90_2^k/0_2^k/90^k)_s$			
3	$(0_2/+45/90_2/+45/0)_s$			
4	$(0_2^k/+45^k/90_2^k/+45^k/0^k)_s$			
5	$(0_2^k/90^k/90/0_2/90)_s$	Hybrid (Series 2)	2	
6	$(0_2/90_2/0_2^k/90^k)_s$			
7	$(0_2/90_2/0/0^k/90^k)_s$			
8	$(0_2^k/+45^k/90_2/+45/0)_s$			
9	$(0/+45/90_2/+45^k/0_2^k)_s$			
10	$(0/+45/90_2/+45/0_2^k)_s$			
11	$(0_2/90_2/0_2^k/90^k)_s$	Hybrid/Metallic Coating	3	Incremental Impact (1-9 Ft-Lbs), One Impact Per Each 4"x5" Section, NDT Evaluation
12	$(0/+45/90_2/+45^k/0_2^k)_s$			

Note: Superscript "k" denotes Kevlar Ply

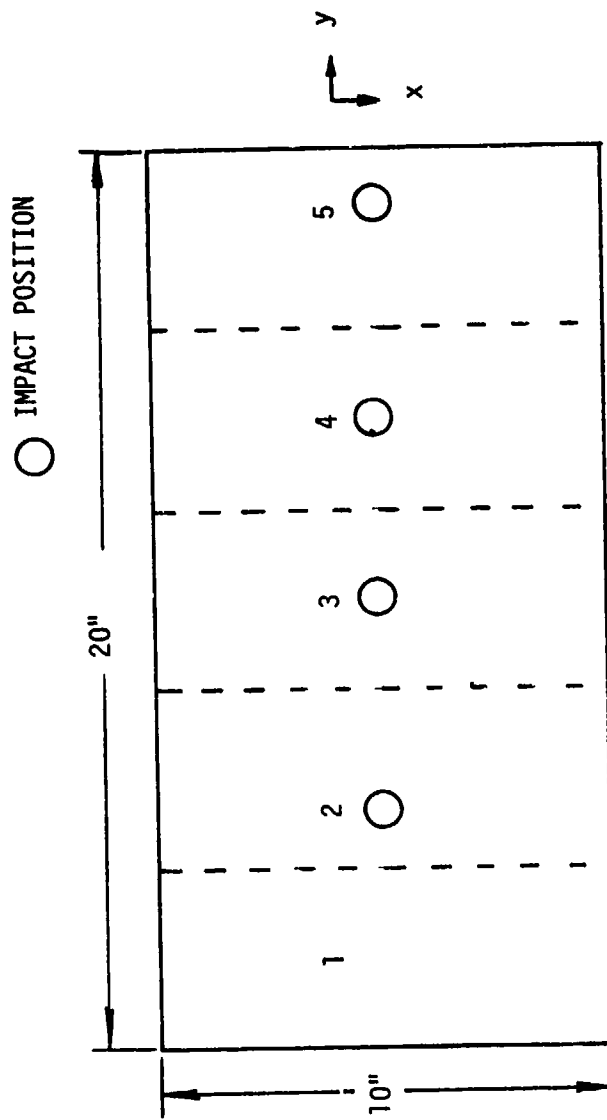


FIGURE 3.8 IMPACT POSITIONS ON TASK III PANEL (SERIES 1 AND 2)

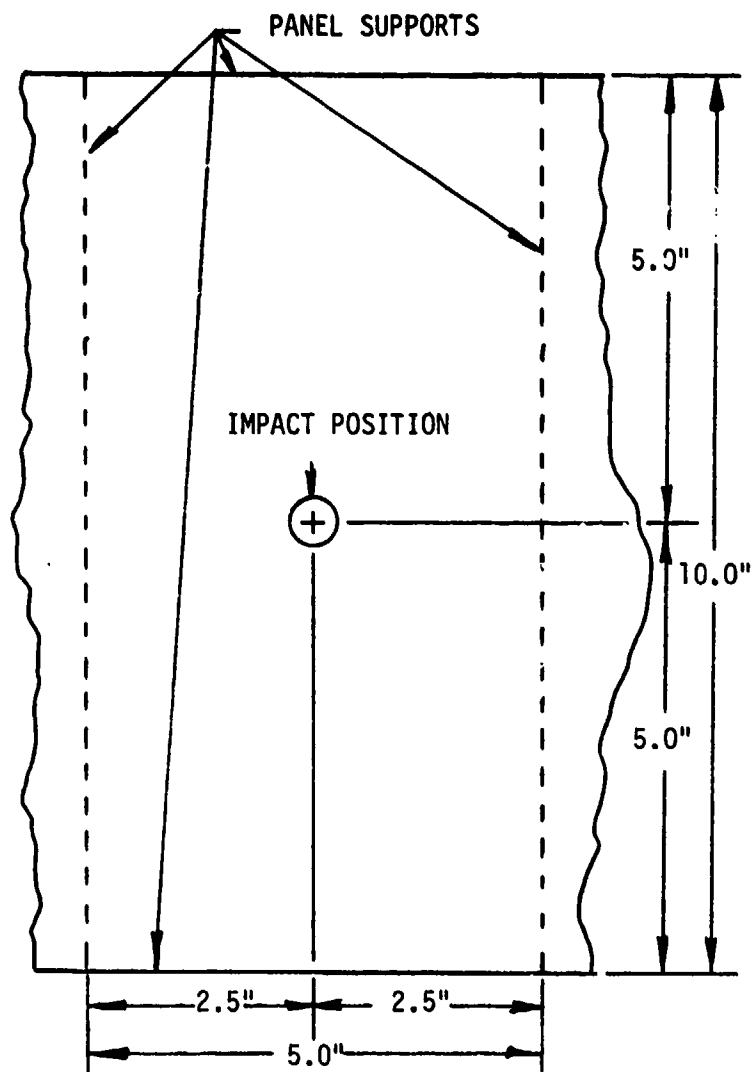


FIGURE 3.9 CONFIGURATION OF CENTER PANEL IMPACT

closer to one edge of the impact support frame for off-center impact (positions 2 and 5) as seen in Figure 3.10. A centered and off-center impact at 15 ft/sec and 20 ft/sec were conducted on each panel.

Strain gages were applied to the Series 1 panels to determine strain levels and strain rates at specific points on the panels during impact. These values were used in validating and fine tuning the math model. These data will be discussed in conjunction with Section 4.0, Analytical Math Model.

All panels were impacted using a one pound projectile with an 0.5 inch radius spherical head. To attain the 15 and 20 ft/sec drop rates, drop heights of 3.5 and 6.5 feet, respectively, were used. These drop heights of 3.5 and 6.5 feet correspond to 3.5 and 6.5 foot pounds of impact energy, respectively. Following impact, the panels were non-destructively tested using ultrasonic C-scan to determine the extent of damage.

Residual tensile strength tests of the damaged sections were conducted to determine the effects of impact on the composite sections. Three inch wide, ten inch long sections were cut from the impacted panels and tabbed. The impact point was centered on the coupon. The undamaged section, Section 1 in Figure 3.8 was also cut and tabbed for residual strength testing.

3.3.1.1 Test Results - Series 1

Table 3.5 contains a summary of Series 1 test results. The impact damage in all cases was a matrix failure. Visual inspection revealed cracks running parallel to the fibers on the side opposite the impact point. NDI inspection showed a delamination region surrounding the impact point. The delamination region and the area of matrix cracking on the panel backside were generally the same size. None of the panels investigated showed signs of broken fibers at the impact levels investigated.

NDT inspection of the impact area disclosed a delaminated area at the point of impact. The delamination area varied in size and shape according to the panel layup, thickness and material. The impact position also had an effect on the delamination zone. Figure 3.11 is a graphical representation of delamination size versus the test variables. As expected, the damage zone size increased with increasing impact energy. The ply orientation appeared to influence the damage zone shape. The 14-ply panels with zero and ninety degree fibers had an elongated diamond shaped delamination approximately .6 by

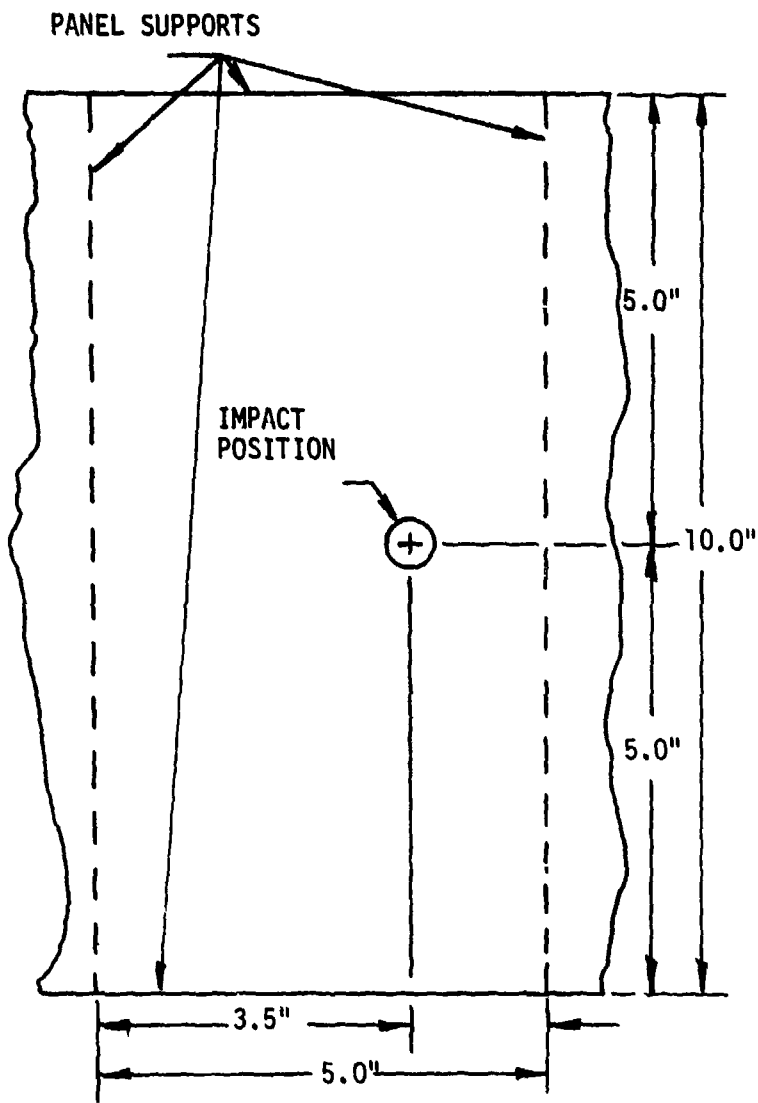


FIGURE 3.10 CONFIGURATION OF OFF-CENTER PANEL IMPACT

CENTER IMPACT

- ▲ 3 FT-LBS
- 6 FT-LBS

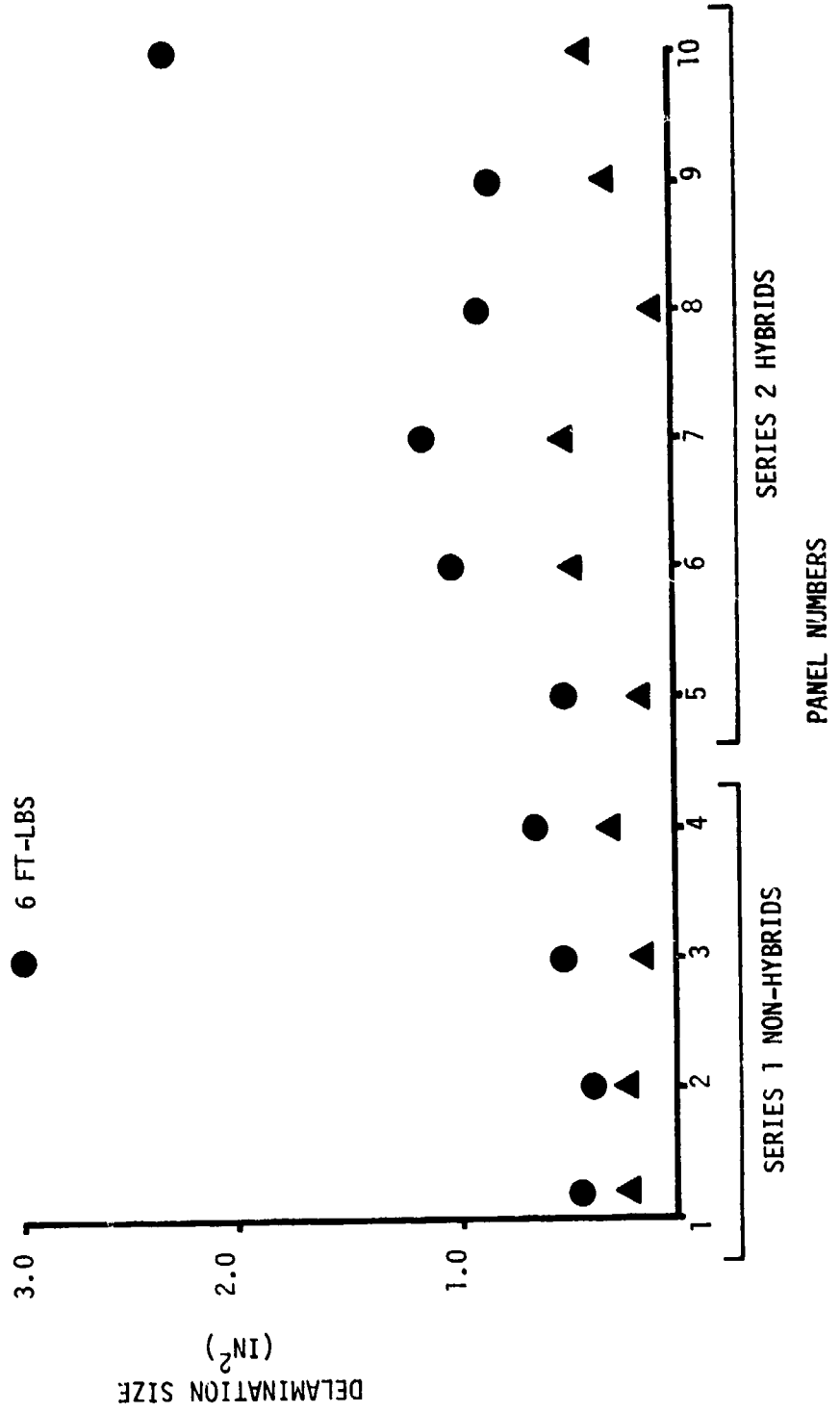


FIGURE 3.11 CENTER IMPACT DELAMINATION SIZE FOR SERIES 1 AND 2 LAMINATES

1.0 inches as shown in Figure 3.12. The 18-ply layup containing zero, ninety and forty-five degree lamina exhibited a round or elliptical damage area approximately .7 inches in diameter as seen in Figure 3.13. The off-center impact damage zones were not centered about the impact point. The damage zones were off-set as exhibited in Figure 3.14 and grew in the direction of the side closest to the impact point.

Residual strength tests of the damaged laminate revealed no loss in tensile strength for the damage incurred. Table 3.5 contains a listing of the residual strength test results. Comparing the tensile strength of the undamaged coupon to those containing damage, a slight increase in tensile strength with increased delamination size can be seen. A possible cause of this phenomenon may be related to the relief of residual stresses via matrix micro-cracking in the panel. These cracks and delaminations are the results of impact damage.

3.3.1.2 Series 1 Conclusions

Based upon the data shown in Table 3.5, the non-hybrid panels exhibited reasonably good damage tolerance under tensile loads for low energy impact. No degradation in tensile strength could be detected in any of the panels. A comparison of the delaminated damage zone size between the two materials failed to show any major advantage in the Kevlar material. This result could be due to the impact levels being lower than that required to fail the fibers. The damage was restricted to the epoxy matrix material, a common factor in both fiber systems. Delaminations are not extremely sensitive to tensile loads. A more pronounced degradation in strength may have been observed had an alternate residual strength test configuration been used. The shear component in the coupons did not seem to affect the ultimate tensile strength. If significant influence on material properties had been noted in the elevated strain rate tests, the properties used in the math model (Section 4.0) would have been adjusted to account for them.

3.3.2 Hybrid Laminate Impact - Series 2

Impact tests on the six Series 2 hybrid panels were conducted to provide hybrid impact data and to verify the predictive methodology capabilities.



FIGURE 3.12 DIAMOND SHAPED DELAMINATION IN 14 PLY LAMINATE

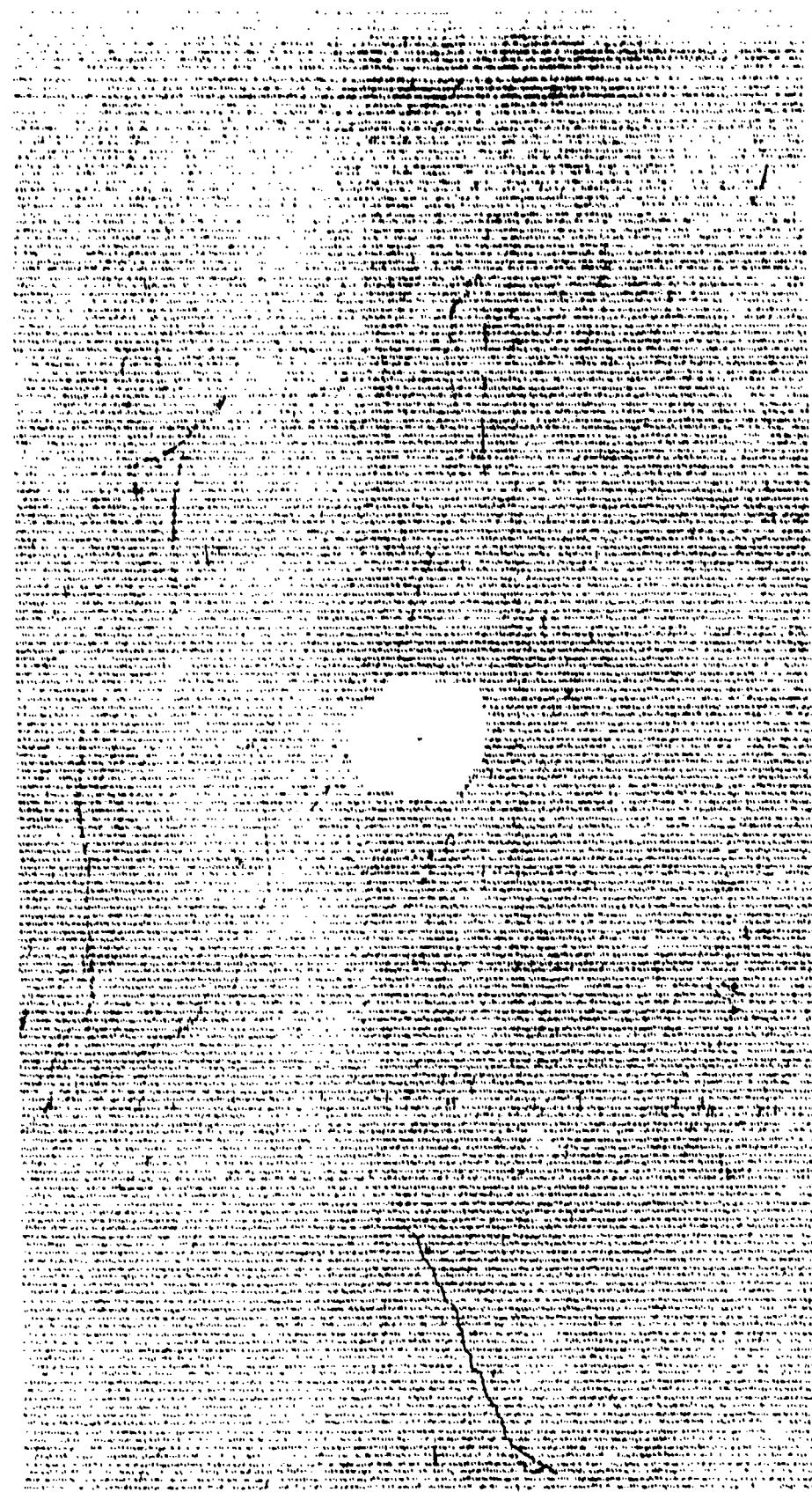


FIGURE 3.13 POUNDED DELAMINATION IN 18 PLY LAMINATE

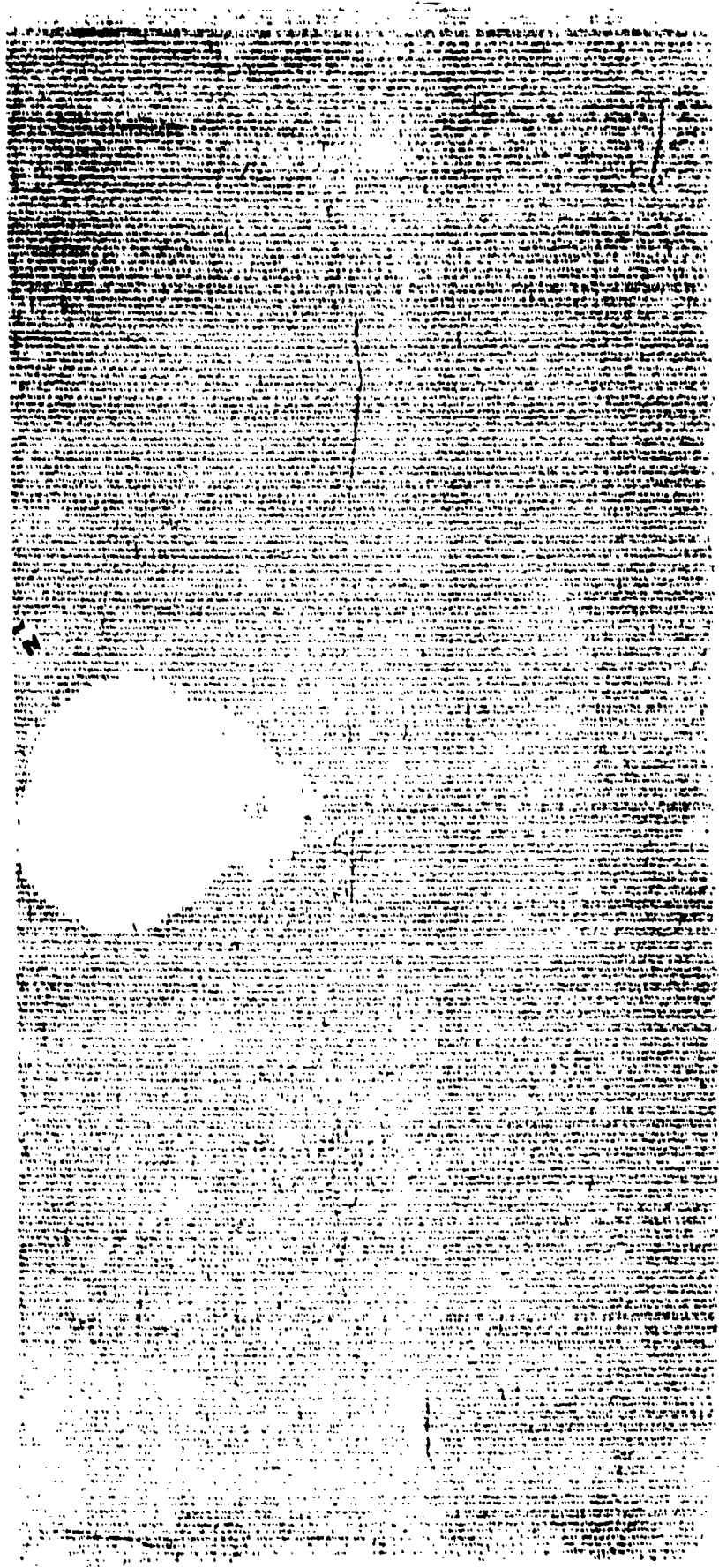


FIGURE 3.14 OFFSET DELAMINATION RESULTING FROM OFF-CENTER IMPACT

TABLE 3.5 SERIES I TEST RESULTS

LAMINATE NO.	LAMINATE DESCRIPTION	IMPACT POSITION	IMPACT ENERGY (FT-LBS)	DELAMINATION SIZE (IN ²)	RESIDUAL STRENGTH (PSI) [σ ULT/ σ_c]*
1	14 Ply Graphite	-	-	-	74100 [1.0]
		Center	3	.2	76300 [1.03]
		Center	6	.5	93500 [1.26]
		Off-Center	3	.15	85300 [1.15]
		Off-Center	6	.21	83200 [1.12]
2	18 Ply Graphite	-	-	-	66500 [1.0]
		Center	3	.16	58700 [0.88]
		Center	6	.50	75600 [1.14]
		Off-Center	3	.24	55800 [0.84]
		Off-Center	6	2.27	-
3	14 Ply Kevlar	-	-	-	75400 [1.0]
		Center	3	.24	75300 [1.01]
		Center	6	.32	78600 [1.04]
		Off-Center	3	.24	66600 [.88]
		Off-Center	6	.6	79900 [1.06]
4	18 Ply Kevlar	-	-	-	50300 [1.0]
		Center	3	.24	59300 [1.18]
		Center	6	.57	52700 [1.05]
		Off-Center	3	.20	54900 [1.09]
		Off-Center	6	.71	59500 [1.18]

* σ_c - Control Section Ultimate

Table 3.4 contains a summary of the laminates tested. Series 2 hybrid test data was compared with the Series 1 non-hybrid impact data.

Table 3.5 contains the results of Series 1 hybrid impact tests and residual strength data. Two laminate ply orientations were used, a 14-ply layup $(0_2/90_2/0_2/90)_s$ and an 18-ply $(0_2/+45/90_2/+45/0)_s$. These same layups were used in Series 2 testing. As outlined in Table 3.6, starting with a basic all graphite/epoxy panel, Kevlar plies were substituted into the laminate.

Impact and residual strength tests of the Series 2 hybrid panels were identical to those used on Series 1 non-hybrid panels as outlined in Section 3.3.1. That is, the damage was restricted to the epoxy matrix material in the form of matrix cracking and delamination.

3.3.2.1 Test Results - Series 2

Table 3.6 contains Series 2 hybrid specimen impact and residual strength test results. Impact energies of 3 ft-lbs and 6 ft-lbs caused matrix damage exclusively. No sign of broken fibers was found. The failure modes seen in the impacted hybrid specimens was identical to that of the non-hybrid Series 1 panels discussed in Section 3.3.1.1.

Residual strength tests resulted in a minor increase in tensile strength for most of the laminates tested when comparing the damaged to the undamaged coupons. This same phenomenon was observed in the non-hybrid coupons.

3.3.2.2 Series 2 - Conclusions

Results listed in Table 3.6 and shown graphically in Figures 3.11 and 3.15 indicate that for hybrid laminates the least damage, based on delamination size, occurred in the laminates fabricated using a shell or outer layer of Kevlar and a core or center of graphite. As in the case of the Series 1 non-hybrids, little degradation was seen in the ultimate tensile strength of the damaged coupons. A possible reason for this may be due to the relief of residual stresses from the cure process or an uncoupling of the interlaminar shear stresses.

A comparison of the hybrid and non-hybrid test data (Tables 3.5 and 3.6, Figures 3.11 and 3.15) failed to show any significant advantage to the hybrids tested over the baseline materials. A ranking of the laminates based on the

TABLE 3.6 SERIES II TEST RESULTS

Laminate No.	Impact Position	Impact Energy (Ft-lbs)	Delamination Size (in ²)	Residual Strength PSI
#5	Centered	3	.20	73400 (1.00)
	Off-Centered	6	.50	61400 (0.84)
#6	Centered	3	.48	64600 (1.00)
	Off-Centered	6	1.20	80400 (1.24)
#7	Centered	3	.64	75700 (1.17)
	Off-Centered	6	1.30	74400 (1.15)
#8	Centered	3	.48	80200 (1.00)
	Off-Centered	6	1.00	68400 (0.85)
#9	Centered	3	.07	66100 (0.82)
	Off-Centered	6	.60	79600 (0.99)
#10	Centered	3	.86	59300 (0.74)
	Off-Centered	6	1.20	47800 (1.00)
#11	Centered	3	.33	51600 (1.08)
	Off-Centered	6	.78	58300 (1.22)
#12	Centered	3	.44	52800 (1.10)
	Off-Centered	6	1.32	57300 (1.20)
#13	Centered	3	.38	39100 (1.00)
	Off-Centered	6	3.50	42800 (1.09)
#14	Centered	3	.50	48500 (1.24)
	Off-Centered	6	4.40	45700 (1.17)
#15	Centered	3	.38	49300 (1.26)
	Off-Centered	6	4.40	40800 (1.00)
#16	Centered	3	.38	51600 (1.27)
	Off-Centered	6	3.50	53100 (1.30)
#17	Centered	3	.50	49400 (1.21)
	Off-Centered	6	4.40	45600 (1.12)

OFF-CENTER IMPACT

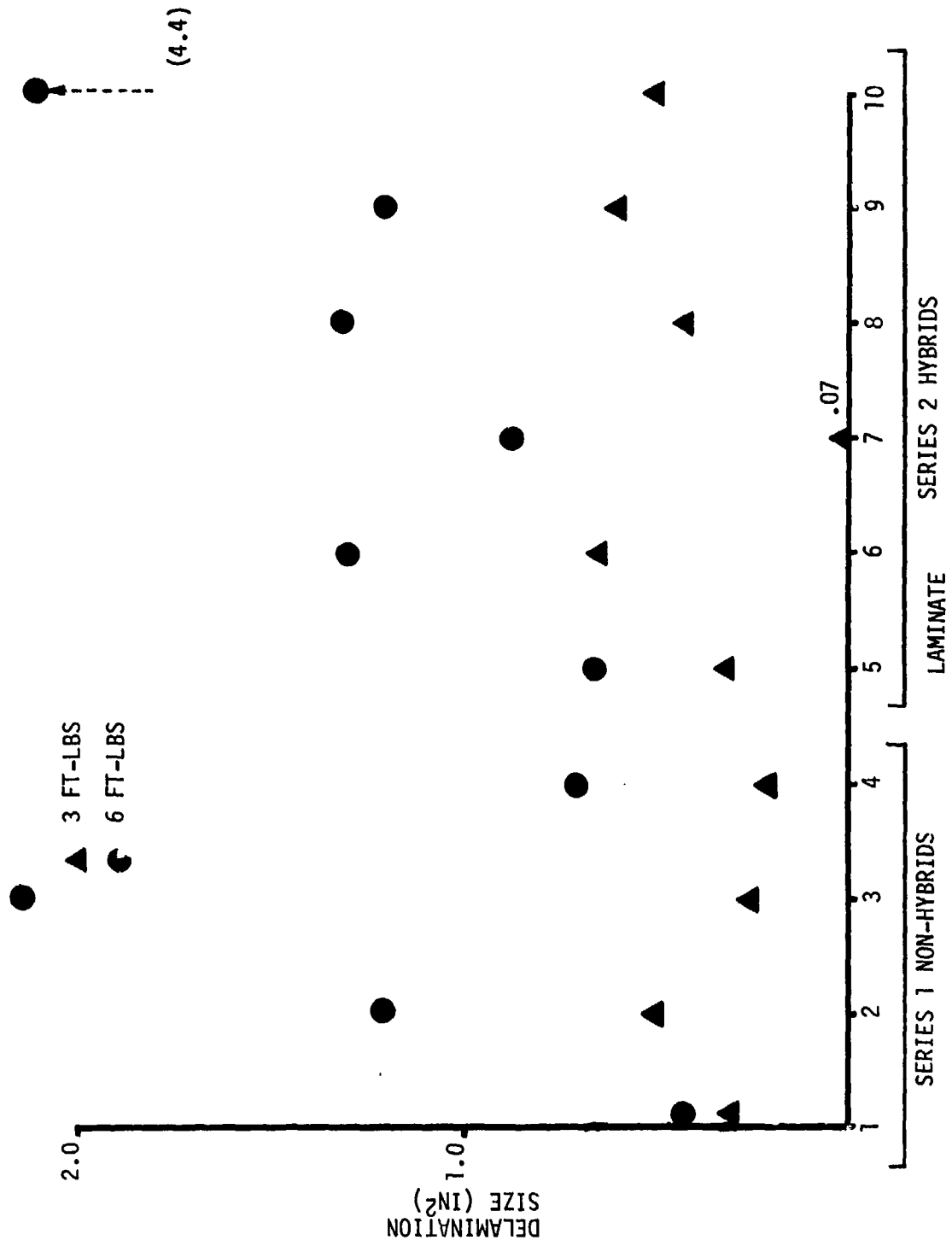


FIGURE 3.15 OFF-CENTER IMPACT DELAMINATION FOR SERIES 1 AND 2 LAMINATES

size of the delamination zone and ultimate tensile strength put the baseline graphite first, Kevlar second followed by the hybrids. Clearly, further work is required to define the useful regions for hybrid use and to optimize the hybrid laminate in those useful regions. Further discussion of the laminate rankings are found in Section 4.0.

3.3.3 Test Results - Series 3

Series 3 tests consisted of two hybrid laminates with an aluminum foil applied to the impact surface in an effort to enhance the visual detection of low level damage. Table 3.7 contains a description of the laminates.

TABLE 3.7 SERIES 3 LAMINATES

LAMINATE NO.	LAMINATE DESCRIPTION	METALLIC COATING DESCRIPTION
11	$(0_2/90_2/0_2^k/90^k)_s$	Cocured Aluminum Foil, Bonded During the Panel Cure
12	$(0/+45/90_2/+45^k/0^k)_s$	Aluminum Foil Bonded in a Secondary Process

Each panel was impacted at nine locations with impact energies ranging from 0 to 9.0 foot pounds at 1.0 foot pound increments (see Figure 3.16). Following impact, the panels were inspected both visually and with ultrasonic C-scan to determine the extent of damage. The appearance of the metallic coating at the impact point was of particular interest when conducting the visual inspection. It was hoped that the metallic coating might enhance the visual damage detectability of the laminates by leaving a dent in the material. A change in the projectile velocity upon rebound was recorded to provide a means of measuring the energy absorbed during impact.

Table 3.8 contains a summary of the Series 3 impact tests. Initial damage occurred at 2 and 1 foot pounds impact energy in the form of delamination for panels 11 and 12, respectively. Fiber breakage did not become visible until 9

foot pounds in panel 12 and no broken fibers were found in panel 11. As noted in the comment section of Table 3.8, the aluminum coatings did not significantly enhance the visual damage detection of the materials.

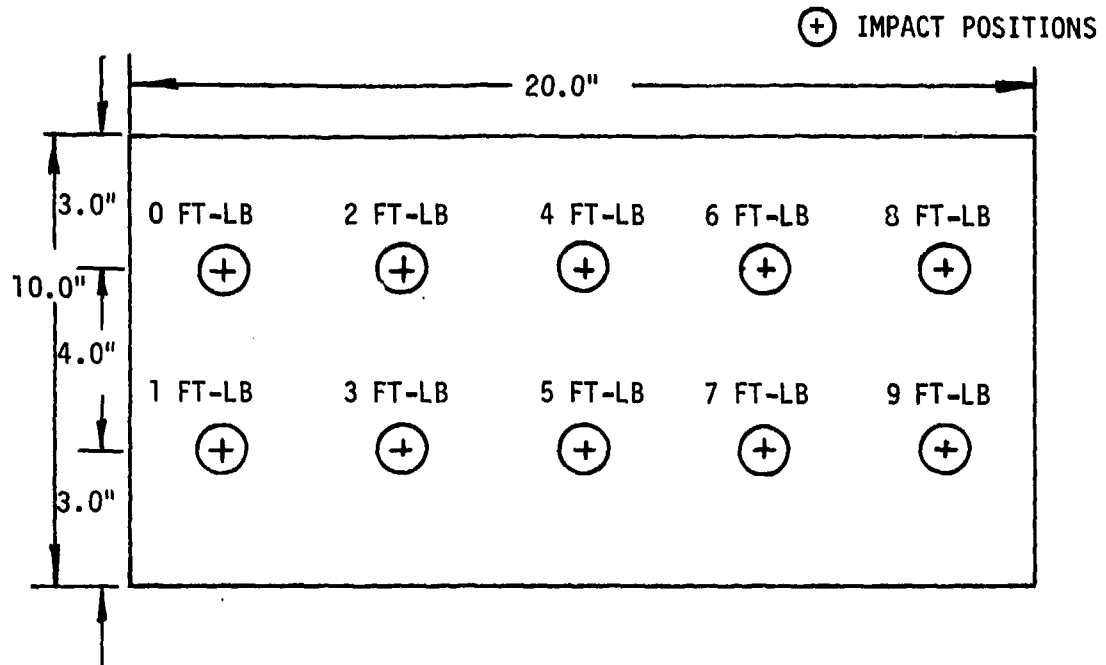


FIGURE 3.16 IMPACT POSITIONS AND ENERGY OF SERIES 3 METALLIC COATED PANELS

TABLE 3.8 SERIES 3 METALLIC COATING IMPACT RESULTS

PANEL NO.	PANEL DESCRIPTION	IMPACT ENERGY (FT-LBS)	ENERGY ABSORBED (FT-LBS)	DELAMINATION SIZE (IN ²)	COMMENTS
11	(0 ₂ /90 ₂ /0 ₂ ^k /90 ^k) _s Cocured Aluminum Foil	1	0.1	0	No visible damage
		2	1.2	0.6	No visible damage
		3	1.3	0.8	Single crack parallel to the fibers on backside
		4	1.9	1.5	Slight dent
		5	2.0	1.9	
		6	2.4	2.0	
		7	3.7	2.3	
		8	4.7	2.4	
		9	3.2	2.5	
12	(0/+45/90 ₂ /+45 ^k /0 ₂ ^k) _s Secondary Bonded Aluminum Foil	1	0.2	0.2	No visible Damage
		2	0.4	0.4	
		3	1.2	0.6	
		4	1.8	0.7	
		5	2.2	1.0	
		6	2.6	1.1	
		7	3.5	1.3	Very slight dent
		8	2.6	1.1	
		9	3.8	1.5	Broken fibers, large cracks

4.0 COMPUTATIONAL MODEL FOR LOW VELOCITY IMPACT DAMAGE OF HYBRID PANELS

4.1 MODEL BACKGROUND

A key part of this study was the development and verification of a mathematical model to represent the response and damage of hybrid laminated panels due to low velocity impact. In order for such a model to be useful, it must be simple yet representative of the deformation and damage mechanisms occurring. To place this study in proper perspective, it is pointed out that the full mathematical analysis of the transverse impact of a laminated plate is a complex and challenging analysis problem. Much progress has been made in understanding the low velocity impact problems as is evidenced by the work described in References 6 - 8.

An important ingredient to developing a simple yet representative mathematical model for low velocity impact is the combination of experimental results and the basic laws of mechanics. Specifically, such an approach has been successfully carried out by Vinson and Zukas⁹ in a high velocity impact study.

The authors of Reference 9 used photographs of the high velocity impact event to develop the response shape for this model. While there are several differences between the problem described in Reference 9 and the low velocity impact damage problem considered here, the approach of utilizing experimental observations to develop a computational model is equally applicable to both problems.

4.1.1 Determination of the Deformation Mode

The first step in developing the model for the low velocity impact study is to identify modes of deformation based on the experimental observations discussed in Section 3.1. Specifically, motion pictures were taken of an impacted laminated plate. Profiles for the deformations as a function of time were determined from these profiles. These profiles were examined and a representative shape was selected for use in the computational analysis. Only centered impact was investigated in the analytical study.

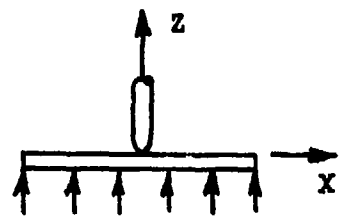
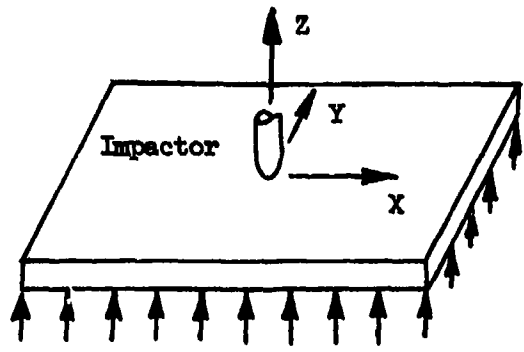
4.1.2 Math Model Approach and Objectives

The mathematical modeling study was divided into three tasks, Tasks IV-VI. Each task is closely integrated with the experimental study. The objective of Task IV was to develop a computational model to predict the response and damage of hybrid laminated panels subjected to transverse low velocity impact. In Task V, the primary objective was to obtain a degree of confidence in the computational model through comparisons with test data (Series 2 tests of Section 3.3.2) for a variety of laminates and impact conditions. The data that were compared with the results of the model include displacements, strains on the top and bottom surfaces of the panels, and the types and extent of damage for each panel. Following the development of the model and the evaluation of its capabilities in Tasks IV and V, the objective of Task VI is to utilize the computational model to rank laminates with respect to their resistance to low velocity impact damage. In this task, selected laminates were examined in terms of the extent of damage experienced for low velocity impact conditions. The procedure and results for these three tasks are described in the following sections.

4.2 DEVELOP SIMPLIFIED COMPUTATIONAL MODEL - TASK IV

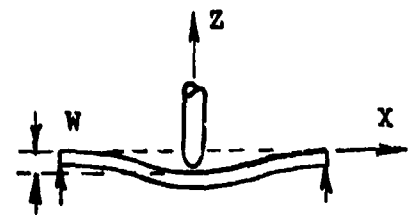
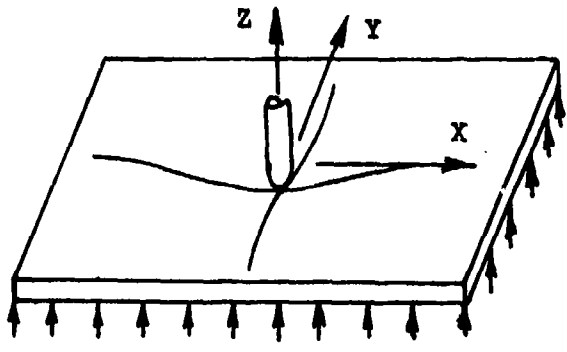
The computational model must represent certain characteristics of the low velocity impact problem. The model should include the effects of different lay-up angles, stacking sequences, the number of plies, the material properties of each ply and the dimensions of the panel. In addition, certain boundary conditions and initial conditions prior to impact must be contained in the model. This information includes the mass of the impactor, the initial velocity and the way in which the panel is secured at the edges. Figure 4.1 illustrates the geometry and coordinate system for the configuration considered here. The impactor is a one-pound cylinder with a rounded end and it is assumed that the impact area is at the center of the panel.

The computational model selected for this configuration represents the stacking sequences, individual ply lay-up angles and the material properties through use of a laminated plate theory formulation. This model also includes the mass of the impactor, impact velocity and specimen dimensions. A summary of the important features of the analysis method is given in the following.



Support Conditions

a. Incipient Impact



b. After Impact

FIGURE 4.1 SKETCH OF LAMINATED PANEL BEFORE AND AFTER IMPACT

4.2.1 Method of Analysis

The method of analysis is based on the conservation of energy principle and an assumed deformation mode selected to represent the experimentally observed response of impacted panels. The conservation of energy principle is a statement that the energy of the system before impact is equal to the total energy at any time thereafter. The mathematical model includes the initial kinetic energy of the impactor, the bending and stretching energy stored in the laminate and the potential and kinetic energy of the system. In equation form, the conservation of energy can be expressed as follows:

$$U_B(t) + U_S(t) + U_p(t) + U_K(t) = U_K(0) + U_p(0) \quad (1)$$

where the $U_B(t)$ represents the bending energy of the panel at any time, t . Similarly, $U_S(t)$ represents the tensile elongation energy and $U_p(t)$ and $U_K(t)$ are respectively the potential and kinetic energies of the system at any time, t . The terms $U_K(0)$ and $U_p(0)$ on the right hand side of Equation (1) are the kinetic and potential energy of the system just prior to impact at time $t=0$.

A brief description of each of the terms in Equation (1) is given here to facilitate describing of the model. The term $U_K(0)$ can be evaluated from $1/2 mV_0^2$, where m is the mass of the impactor and V_0 is the velocity just prior to impact, $U_p(0)$ is the sum of potential energies of the panel and impactor with respect to a datum plane which can be arbitrarily selected. If the datum is taken to be the midplane of the panel, this term has the form mgH , where H is the height of the center of gravity of the impactor about the midplane of the impactor at the time of impact. It was found that the potential and kinetic energy terms on the left hand side of the Equation (1) could be simplified. Examination of the panel contribution to these terms show them to be small and therefore negligible. Thus, the expression for $U_p(t) + U_K(t)$ is dependent on the impactor position and motion and equal to $Mg[H-W_1(t)] + 1/2 mV^2(t)$ where $W_1(t)$ denotes the deflection of the panel under the impactor at time t and $V(t)$ is the velocity of the impactor at time t .

The quantities $U_B(t)$ and $U_S(t)$ are the bending and stretching energies of the panel and are directly related to the deformation state of the panel at

time t . Selection of the deformation modes of the panel were based on high speed motion pictures taken of graphite and Kevlar panels impacted at various velocities. The photographs gave one profile of the deformed plates along one of the axes. A typical deformation mode obtained from the photographs is shown in Figure 4.2 along with the mathematical representation for this profile. The figure shows good agreement between the data points and the functional representation.

4.2.2 Deformation Profile

The analysis requires a deformation pattern throughout the entire plate. This was obtained from the profile shown in Figure 4.2 by assuming the deformation profile in the perpendicular direction to be similar to the measured shape and interpolating for locations between the major and minor axes of the panel. The procedure gave an expression for the deformation shape at all x and y points on the panel shown in Figure 4.1. It is important to emphasize that this procedure only provides the shape of the deformed panel and does not provide the amplitude of deformation or velocity at any time. However, knowing this mode of deformation, the response can be formulated so that there are only two unknowns. One is the displacement at the center of the panel. The other is the velocity of the impactor. If these two quantities are known, the deformation and the velocity at all points on the plate can be found. The amplitude $W_1(t)$, and velocity $V(t)$, are related according to Equation (1).

The procedure for using Equation (1) and the deformation shape requires that $U_B(t)$ and $U_S(t)$ be expressed in terms of $W_1(t)$. The transverse deflection of the panel at any point (x,y) at time t is given by the following equation.

$$W(x,y,t) = W_1(t) f(x,y) \quad (2)$$

where $f(x,y)$ is the displacement mode based on the photographs and the interpolation method and $W_1(t)$ is the displacement under the impactor at time t . The bending energy is obtained from an integral over the volume of the panel

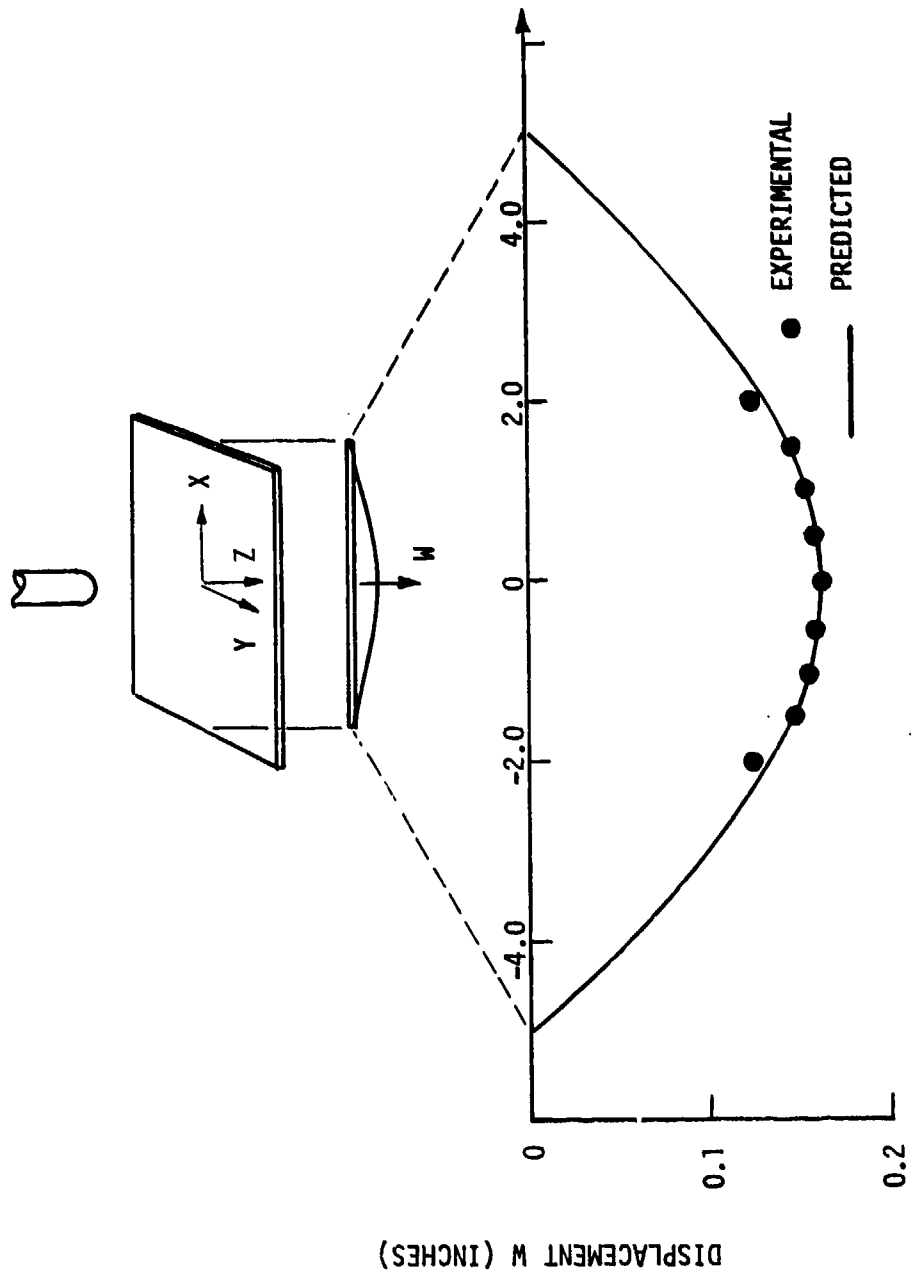


FIGURE 4.2 EXPERIMENTAL DISPLACEMENT VERSUS MODEL PREDICTION FOR TASK I GRAPHITE PANEL (T = .067 SEC)

involving second derivatives of the expression in Equation (2) with respect to x and y . Upon completing this integration, an expression of the form

$$U_B(t) = AW_1^2(t) \quad (3)$$

is obtained where A is a positive constant dependent on the material properties, stacking sequence, lay-up angle and panel dimensions.

The stretching energy is based on the change in length of the deformed panel. This term is assumed to be representable by the form

$$U_S(t) = BW_1^4(t) \quad (4)$$

where B is a positive constant dependent on the lay-up angles, material properties and panel dimensions. The expression in Equation (1) can now be rewritten using the preceding terms and Equations (2) through (4). The result is

$$AW_1^2(t) + BW_1^4(t) + mg[H - W_1(t)] + 1/2mV^2(t) = 1/2mV^2(0) + mgH \quad (5)$$

Equation (5) gives the relation between the displacement under the impactor, $W_1(t)$ and the velocity of the impactor, $V(t)$ at any time, t . The displacement and velocity are related from continuity by the integral

$$W_1(t) = \int_0^t V(t) dt \quad (6)$$

Equations (5) and (6) can be solved to obtain $W_1(t)$ and $V_1(t)$ for all times of interest. The procedure is to set a value of $W_1(t)$ in Equation (5) and then solve for $V(t)$. Starting with small values of $W_1(t)$, the computations are continued until $V(t)$ approaches zero. At this point, one has a table of $W_1(t)$ values and the corresponding values of $V(t)$. The value of time associated with each pair of displacement and velocity values is obtained through a numerical integration of Equation (6). Using these results and Equation (2) gives a deformation and velocity history for all points in the panel from the time of impact until the impactor comes to rest.

4.2.3 Damage Modes

The next step is to introduce damage modes into the model. The model represents three independent modes of damage. One is the fiber breaking. Another is matrix cracking between fibers for transverse loading. The third mode of failure which is very important in low velocity impact damage is delamination. Delamination zones are predicted based on estimates of the through-thickness stress σ_z . Estimates of the σ_z distribution are obtained from the distribution of the through thickness strain, ϵ_z , compatibility of the ply deformations between plies and the conditions of equilibrium. Other studies have shown that the σ_z stress can be associated with delamination. Example references include 10-12. While Reference 12 considers the actual separation due to delamination and uses a fracture mechanics approach to accurately represent the delamination process, a different approach was found to be effective in the simple mode here.

Because of the goals and simplicity of the model used in this study, separations and changes in material properties due to damage were not included. Rather, critical values of stresses or strains were used to designate damage regions by searching for points where these critical values were exceeded.

4.2.4 Summary of Math Model Development

In summary, the model affords a means to represent the deflection and strain history of the panel due to low velocity impact. Using the inplane stresses and strains and the estimate for the through thickness stresses provides a means of estimating three types of damage and the extent of damage. The next step is to determine the utility of this model in terms of its capability to predict the deformation and strain response of impacted laminates, the damage modes and extent of damage. This part of the study is described in Task V.

4.3 VERIFICATION OF THE MODEL - TASK V

The goal of the modeling effort is to develop a useful and economical tool to predict the response of hybrid laminates subjected to low velocity impact. To accomplish this requires that the model be capable of representing laminate

characteristics such as lay-up angles, stacking sequences, dimensions and material properties. Also the model must provide a qualitative description of modes of damage and the extent of damage due to low velocity impact. The model was formulated in Task IV to include the necessary descriptive features of the laminated panels. The goal of Task V is to evaluate the capability of the model to represent modes of damage and the extent of damage. In carrying out the verification task, it is important to keep in mind that for the purposes of this study, an exact prediction of the extent of damage is not necessary. Rather, the capability to rank a series of laminates according to the amount of impact damage each will incur is sufficient to provide guidance for the selection of laminates in the experimental program.

Several experimentally measured responses of impacted laminates were selected to be used as test cases to obtain confidence in the mathematical model. The measured responses include deformations or displacements at selected points on the laminate, strains at both the upper and lower surfaces of the panels and, finally and most relevant to this study, modes of damage due to low velocity impact. The philosophy for evaluating the model is to start with panels that are relatively simple and progress to increasingly complex configurations and material properties.

4.3.1 Thin Laminate Experimental Comparisons

The first set of comparisons with experimental data were for deflections and strains due to the impact of a 3-ply Kevlar laminate. The panel size is 5 inches by 10 inches. The panel is simply supported around the edges. A one-pound mass was dropped from various heights to produce an impact velocity of 15 and 20 feet per second. The laminate was modeled using the mathematical model developed in Task IV. Panel deflection directly under the impactor was measured along with the strains at a location one inch from the point of impact. Both deflection and strains were predicted as a function of time using Equations (5) and (6). Comparisons of displacement data from the experiment and the corresponding computed values are shown in Figure 4.3 for various times after impact. Figure 4.3 shows good agreement between results of the model and laboratory data. Next, strain behavior was examined. Comparisons of predicted and measured strain values on the laminate surface at a location of one inch from the point of impact are shown in Figure 4.4. Again, there is

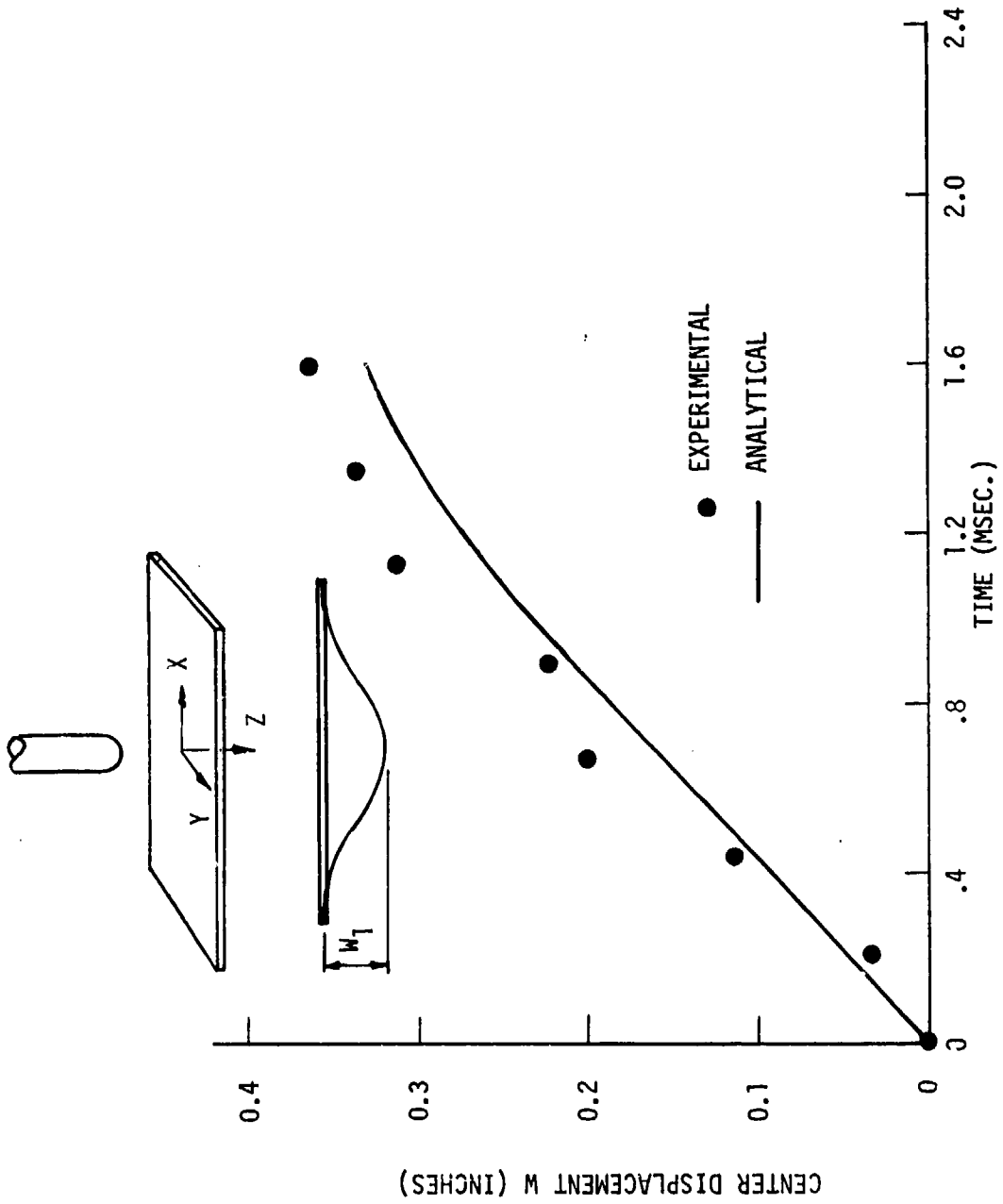


FIGURE 4.3 EXPERIMENTAL VERSUS PREDICTED DISPLACEMENT AT IMPACT POINT
TASK I KEVLAR PANEL

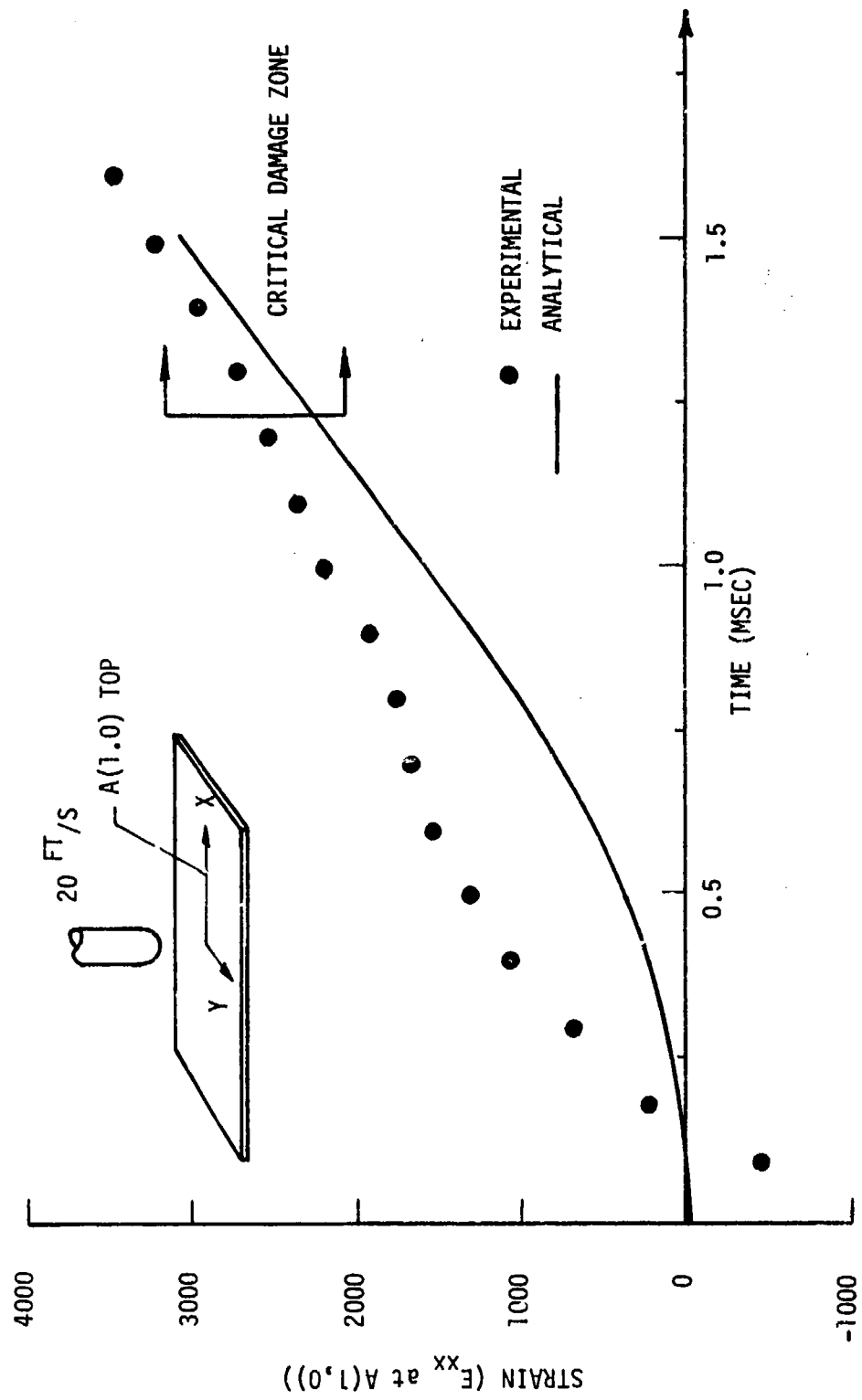


FIGURE 4.4 EXPERIMENTAL VERSUS ANALYTICAL STRAINS DURING IMPACT
TASK I KEVLAR

good agreement between the predicted strain history and strain data from the laboratory test. The agreement between these comparisons provides confidence that the computational model developed in Task IV will be a useful tool for evaluating laminate response due to low velocity impact.

4.3.2 Complex Laminate Comparisons

The next step in the verification process is to progress to more complex laminates. The comparisons in Figures 4.3 and 4.4 are for a laminate constructed of a unidirectional single woven material. It was noted that the primary mode of deformation was stretching rather than bending. This is because the laminate was too thin to develop high bending stresses. The next group of laminates are more complex than those previously examined in the sense that they are thicker and thus exhibit increased bending stiffness and have lay-up angles.

A series of 14-ply laminates with various stacking sequences were examined next. For these cases, the one mode of damage observed was delamination between plies near the surface of the panel opposite the impact region. In order to evaluate the extent of delamination, the procedure described in Task IV involving an evaluation of the through thickness stress, σ_z was used.

4.3.2.1 Critical Stress Evaluation

The first laminate in this series was a $(90_2/0_2/90_2/0)_S$ laminate made of graphite epoxy. The approach here is to examine two laminates and evaluate the level of predicted σ_z stress over the zone of measured delamination. This is done to calibrate the critical value of the σ_z stress and relate it to delamination. While this concept is very simple and does not represent all the salient features of fracture mechanics, it was found to be useful for the qualitative comparisons needed in this study. Figure 4.5 shows a comparison of the measured zone of delamination and the computed zone size for a $(90_2/0_2/90_2/0)_S$ laminate with an impact velocity of 15 ft/sec. The dashed boundary encribes the zone obtained from the C-scan and the blocked-shaped region represents the results from the computational model. Results from the computational model were obtained using a critical value of σ_z equal to 963 psi. The model has been discretized to a grid in order to

KEVLAR
(90₂, +45, 0₂, +45, 90)_S
6 FT-LB IMPACT

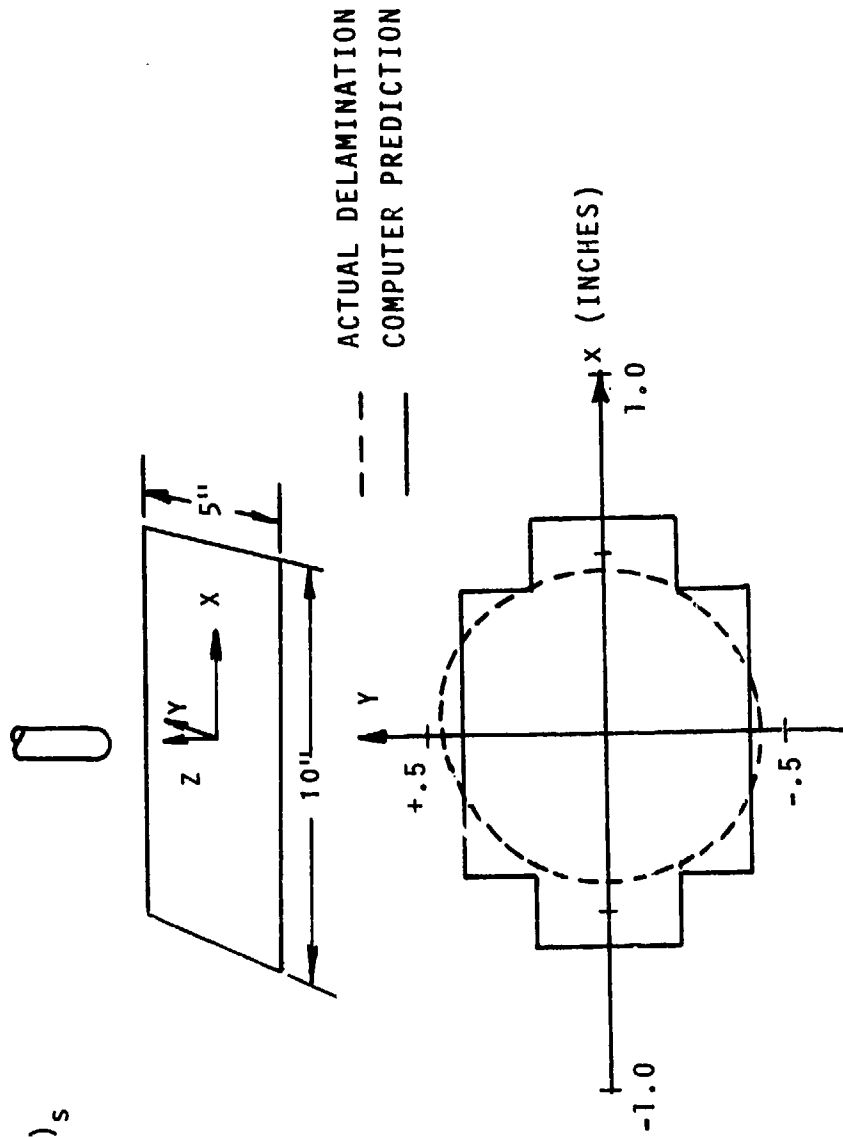


FIGURE 4.5 EXPERIMENTAL VERSUS PREDICTED DELAMINATION ZONE

determine stresses and strains at selected points. When a critical value of stress is exceeded at any grid point, the entire block region associated with this grid point is then assigned to be in the damage zone. Thus the model predicts a delamination zone containing square corners.

The second laminate examined was a $(90_2^k/0_2^k/90_2^k/0_2^k)_s$ lay-up made of Kevlar/epoxy plies. The superscript k is used to denote Kevlar plies. The objective is to identify a level of critical stress, σ_z , such that the computed zone of delamination and that obtained from the C-scan evaluation are comparable. Figure 4.6 shows a comparison of the experimentally determined zone of delamination and the region obtained using the computational model for an impact velocity of 15 ft/second. The computed zone size was based on a critical σ_z stress value of 899 psi. The area of the experimentally observed zone is .35 square inches. The area resulting from the computational model is .32 square inches.

4.3.2.2 Hybrid Impact Prediction

The capability of the model to predict the relative delamination response in terms of zone sizes was examined using three graphite/Kevlar hybrid laminates. These laminates were each subjected to an impact velocity of 15 ft/sec using a one-pound mass. Each laminate has 14 plies. The stacking sequences are $(0_2^k/90_2^k/90_2/0_2/90)_s$, $(0_2/90_2/0_2^k/90_2^k)_s$ and $(0_2/90_2/0/0^k/90_2^k)_s$. The first hybrid laminate has Kevlar plies on the outside. The second and third hybrid laminates have graphite plies on the outside. The impact event was modeled for each laminate.

In order to compare the results of the computational model with the data, two characteristics representing the delamination zone were selected. One was the maximum length of the delaminated zone. The other was the total area. Figure 4.7 gives a graphical illustration of the comparison of the data and computed values for the maximum length of delamination for the laminates. It can be seen from Figure 4.7 that the results of the model for ranking the laminates with respect to the maximum length of delamination are close to the experimental ranking. The other characteristic of the delamination damage is the total area of delamination. The delaminated area obtained by the computational model for each laminate shown in Figure 4.7 and the values obtained

KEVLAR PANEL
(90₂, 0₂, 90₂, 0)_s
6 FT-LB IMPACT

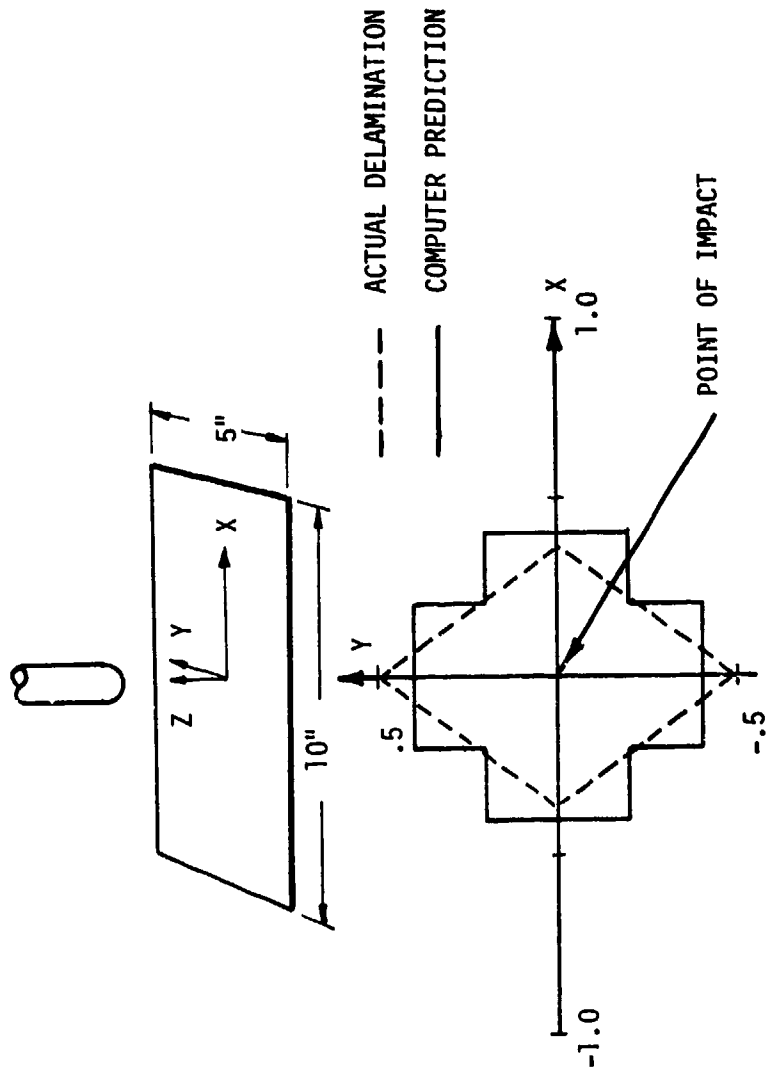
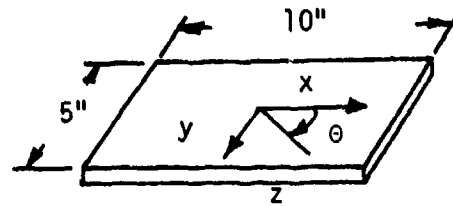


FIGURE 4.6 EXPERIMENTAL VERSUS PREDICTED DELAMINATION ZONE

DESIGNATION LAYUP

- 1 $(90_2, 0_2, 90_2, 0)_s$
- 2 $(90_2^k, 0_2^k, 90_2^k, 0^k)_s$
- 5 $(0_2^k, 90^k, 90, 0_2, 90)_s$
- 6 $(0_2, 90_2, 0_2^k, 90^k)_s$
- 7 $(0_2, 90_2, 0, 0^k, 90^k)_s$



- Computational Model
- ▲ Experimental Data

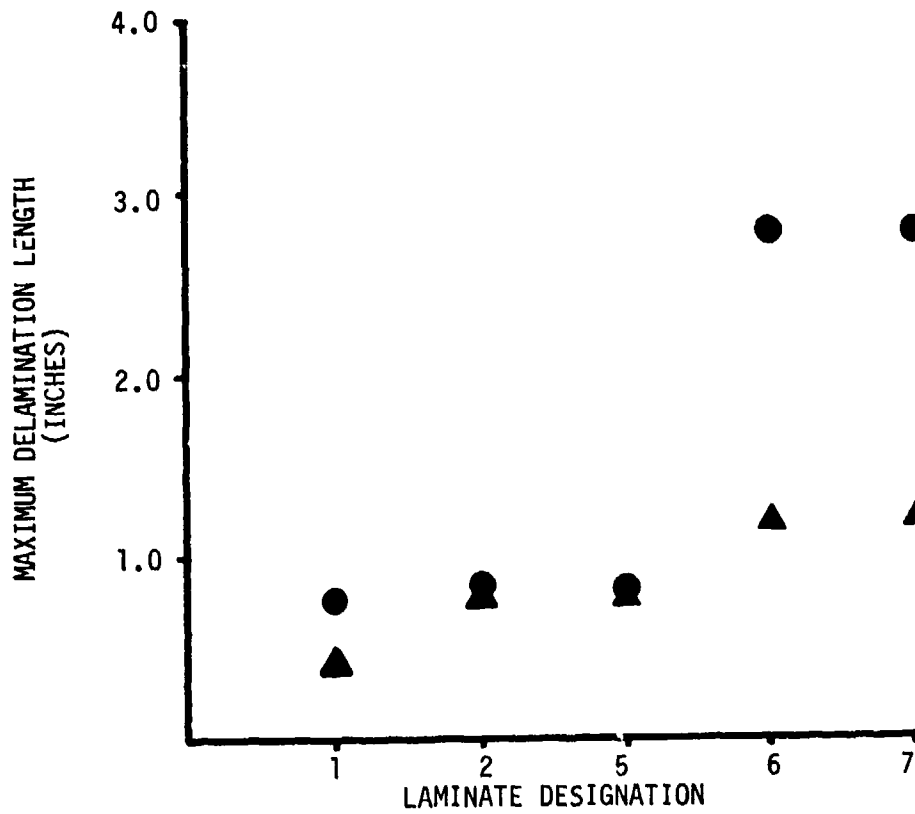


FIGURE 4.7 EXPERIMENTAL VERSUS ANALYTICAL DELAMINATION LENGTH (15 FT/SEC)

from the experiments are compared in Table 4.1. These comparisons also show that the ranking of the laminates by the model is in agreement with the experimental results.

The results shown in Figure 4.7 and Table 4.1 are encouraging in that they illustrate a degree of confidence in the model to rank the hybrid Kevlar/graphite laminates with respect to extent of damage due to delamination. Because of the simplicity of the model verification, studies were extended to include a higher impact velocity using the same laminate lay-up angles as described in Figure 4.7 and Table 4.1.

The procedure for verification of the computational model for the 14-ply hybrid laminates subjected to an impact velocity of 20 ft/sec was the same two-step process previously described for the impact velocity of 15 ft/sec. In the first step, a critical value of the delamination stress is established with respect to the experimental results using the non-hybrid laminates made of graphite or Kevlar. The critical level of delamination stress, σ_z , for the graphite laminate was 1213 psi, and for the Kevlar laminate was 1142 psi. As in the case of the 15 ft/sec impact velocity, the critical value of delamination stress for the Kevlar laminate was used to predict the delamination damage of laminate in No. 5 in Table 4.1. Similarly, the critical value of the delamination stress obtained for the graphite laminate was used to predict the delamination damage for laminates No. 6 and No. 7 in Table 4.1.

Two characteristics of the delaminated area were compared with the experimental data to check the capabilities of the computer model. One characteristic was the maximum length of the delamination area. Figure 4.8 shows the comparison of the computed values of the maximum length of the delaminated zones and the actual measured lengths. It can be seen from Figure 4.8 that there is good agreement between the results of the model and the data. That is, the model's ranking of the laminates is in agreement with the data. The other feature of the delamination damage zone that was compared with the data was the total delaminated area. Comparisons of the computed values and the measured areas are given in Table 4.2. The delaminated areas in Table 4.2 indicate there is agreement in the rankings of the laminates as obtained by the model and that observed from the experiments.

TABLE 4.1 SUMMARY OF DELAMINATION ZONES FOR 14 PLY
LAMINATES (15 FT/SEC)

NO.	LAMINATE LAY-UP ANGLES	DELAMINATION AREA (SQ. INCHES)		MAXIMUM LENGTH (INCHES)	
		EXPERIMENT	COMPUTER MODEL	EXPERIMENT	COMPUTER MODEL
1	$(90_2, 0_2, 90_2, 0)_s$.21	.16	.75	.40
2	$(90_2^k, 0_2^k, 90_2^k, 0^k)_s$.23	.32	.75	.80
5	$(0_2^k, 90_2^k, 90, 0_2, 90)_s$.17	.32	.75	.80
6	$(0_2, 90_2, 0_2^k, 90^k)_s$.45	3.52	1.19	2.8
7	$(0_2, 90_2, 0, 0^k, 90^k)_s$.48	3.36	1.19	2.8

DESIGNATION LAYUP

- 1 $(90_2, 0_2, 90_2, 0)_s$
- 2 $(90_2^k, 0_2^k, 90_2^k, 0^k)_s$
- 5 $(0_2^k, 90_2^k, 90_2, 0_2, 90)_s$
- 6 $(0_2, 90_2, 0_2^k, 90^k)_s$
- 7 $(0_2, 90_2, 0, 0^k, 90^k)_s$

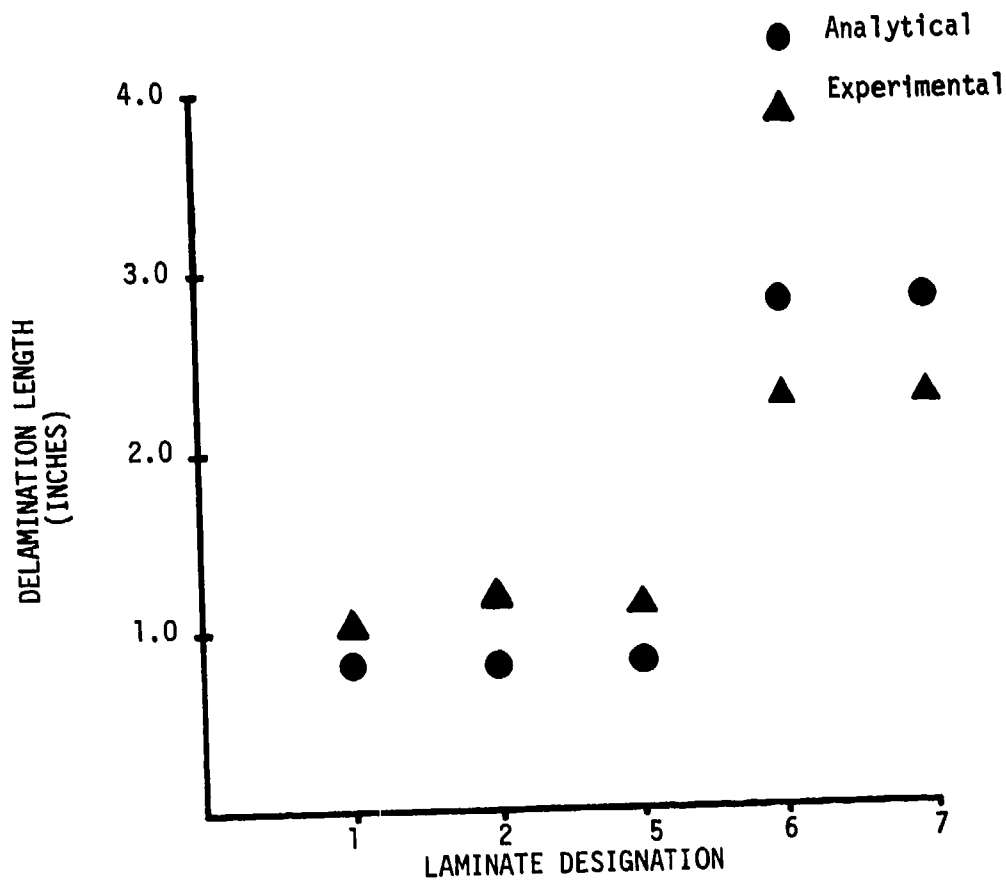
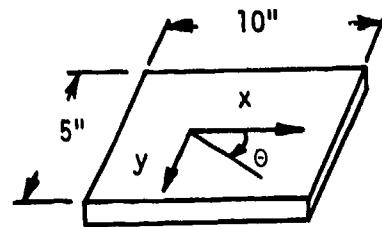


FIGURE 4.8 EXPERIMENTAL VERSUS ANALYTICAL DELAMINATION LENGTH (20 FT/SEC)

TABLE 4.2 SUMMARY OF DELAMINATION ZONES FOR 14 PLY
LAMINATES (20 FT/SEC)

NO.	LAMINATE LAY-UP ANGLES	DELAMINATION AREA (SQ. INCHES)		MAXIMUM LENGTH (INCHES)	
		EXPERIMENT	COMPUTER MODEL	EXPERIMENT	COMPUTER MODEL
1	$(90_2, 0_2, 90_2, 0)_s$.45	.48	1.20	.8
2	$(90^k_2, 0^k_2, 90^k_2, 0^k)_s$.35	.32	1.00	.8
5	$(0^k_2, 90^k, 90, 0_2, 90)_s$.50	.32	1.13	.8
6	$(0_2, 90_2, 0^k_2, 90^k)_s$	1.06	3.52	2.25	2.8
7	$(0_2, 90_2, 0, 0^k, 90^k)_s$	1.15	4.00	2.30	2.8

4.3.3 Summary of Model Verification

Recall that the primary objective of the modeling study is to develop a simple computational model capable of screening or ranking laminates with respect to low velocity impact damage. The combination of an assumed mode based on experimental observations and the basic laws of mechanics provided a simple model containing the important characteristics of the impact problem. Verification of the model capabilities consisted of comparisons of computed values with experimental data for displacements as a function of time (Figure 4.3), strains as a function of time (Figure 4.4), and the size of delamination damage zones (Figures 4.7 and 4.8, Tables 4.1 and 4.2). These comparisons provide a degree of confidence in the model's capability to represent the dynamic response of an impacted laminate as well as screen or rank laminates with respect to delamination damage. However, because of the model simplicity and the inherent complexity of the low velocity impact damage problem, these comparisons should not be interpreted as an all encompassing verification, but rather as a limited verification within the realm of the laminates considered. With this in mind, the next step in the study is to apply the model to a more complex set of laminates containing 0, 90, and ± 45 degree plies.

4.4 APPLICATIONS OF MODEL - TASK VI

The final portion of the computational modeling study is the application of the model to examine delamination response of more complex laminates. Specifically, five laminates containing 0, 90 and ± 45 degree plies were considered. Each laminate contains a total of 18 plies. Three laminates are Kevlar/graphite hybrids, one is all Kevlar and the other is all graphite. The impact velocities are 15 and 20 ft/sec.

The goal of the analysis is to rank the laminates with respect to extent of delamination damage sustained during impact. The procedure was the same as that followed for the 14-ply laminates. The delamination data for the two non-hybrid laminates was used to establish critical values of delamination stresses for this series of laminates. Critical stress values were then used to predict the behavior of the remaining three hybrid laminates. A summary of

laminates lay-up angles and results, in terms of the maximum dimension of the delaminated zone, are given in Figure 4.9 for the impact velocity of 15 ft/sec and in Figure 4.10 for an impact velocity of 20 ft/sec.

Figure 4.9 shows a similarity between the trend of the data and the trend of the computed values. That is, laminate 8 has less delamination than laminates 9 and 10 based on the analysis and the data. Laminate 8 also has less delamination than laminates 3 and 4 based on the model and the data. The primary difference between the computed values of the model and the data in Figure 4.9 is that the model indicates laminate 9 has a larger maximum length of delamination than laminate 10, while the data suggests the opposite. Because only one data point was obtained for each panel and impact velocity, it is difficult to determine how extensive the scatter in data will be and how the range of scatter will effect the trends of delamination response.

Figure 4.10 shows the results for the impact velocity of 20 ft/sec. The trends in the data are similar to those in Figure 4.9 with the exception that the maximum length of the delaminated zone for laminate 10 is about four times longer. This is very distinct from the experimental behavior shown in Figure 4.9 where the extent of delamination for laminates 9 and 10 are nearly identical. The data in Figure 4.10 also shows the extent of delamination of laminate 8 to be greater than laminates 3 or 4 while the data in Figure 4.9 shows laminate 8 to have less delamination than laminates 3 and 4. The trend of the results from the model in Figure 4.10 is very similar to that in Figure 4.9. Tables 4.3 and 4.4 give the numerical values for the curves in figures 4.9 and 4.10 and also the computed and measured areas of delamination. The data in Table 4.3 shows the delaminated areas to exhibit the same trend as the maximum length of the zone of delamination shown in Figure 4.9. Table 4.3 indicates generally good agreement between the trends of the delaminated areas obtained by the model and the experimental data for an impact velocity of 15 ft/sec. The exception, as was the case in Figure 4.9, is that model results point to a larger extent of delamination in laminate 9 than in laminate 10 while the data shows the opposite effect. However, the relative difference in the data for the areas of these two laminates is rather small at one tenth of a square inch.

Trends of the data for the area of delamination in Table 4.4 are similar to those for the maximum delaminated length shown in Table 4.4 and Figure 4.10. The explanation of this behavior in the data is not clear at this time. Two possibilities were mentioned. One is that there is scatter in the

DESIGNATION LAYUP

- 3 $(90_2, \underline{+45}, 0_2, \underline{+45}, 90)_s$
- 4 $(90_2^k, \underline{+45}^k, 0_2^k, \underline{+45}^k, 90^k)_s$
- 8 $(0_2^k, \underline{+45}^k, 90_2, \underline{+45}, 0)_s$
- 9 $(0, \underline{+45}, 90_2, \underline{+45}^k, 0_2^k)_s$
- 10 $(0, \underline{+45}, 90_2, \underline{+45}, 0_2^k)_s$

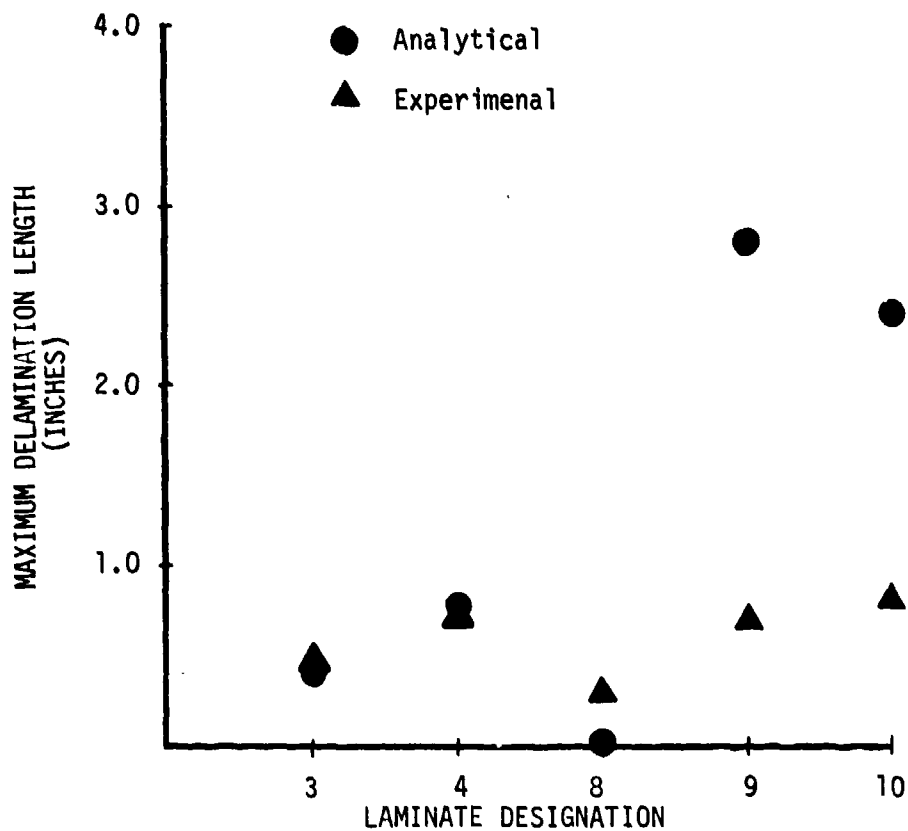
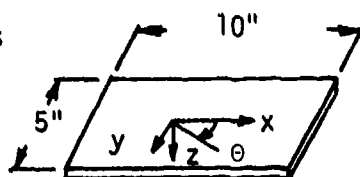
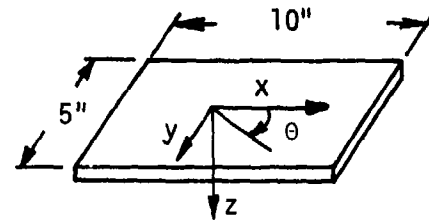


FIGURE 4.9 EXPERIMENTAL VERSUS ANALYTICAL DELAMINATION LENGTH (15 FT/SEC)

DESIGNATION LAYUP

- 3 $(90_2, \underline{+45}, 0_2, \underline{+45}, 90)_s$
- 4 $(90_2^k, \underline{+45}^k, 0_2^k, \underline{+45}^k, 90^k)_s$
- 8 $(0_2^k, \underline{+45}^k, 90_2, \underline{+45}, 0)_s$
- 9 $(0, \underline{+45}, 90_2, \underline{+45}^k, 0_2^k)_s$
- 10 $(0, \underline{+45}, 90_2, \underline{+45}, 0_2^k)$



● ANALYTICAL
▲ EXPERIMENTAL

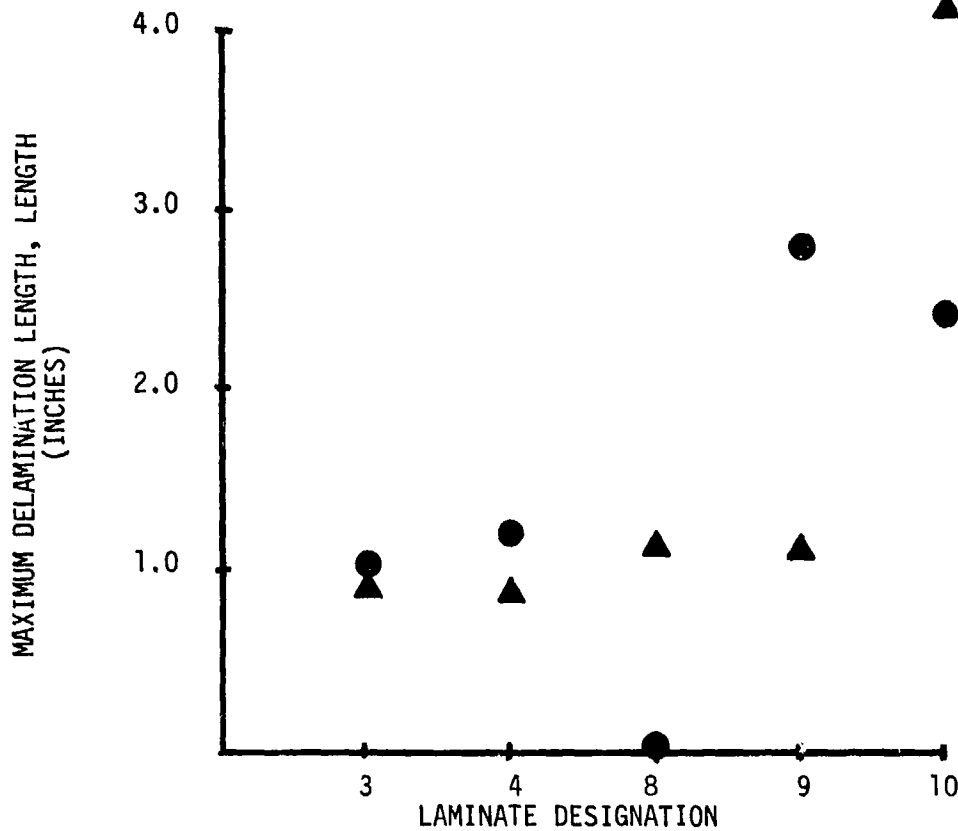


FIGURE 4.10 EXPERIMENTAL VERSUS ANALYTICAL DELAMINATION LENGTH (20 FT/SEC)

TABLE 4.3 SUMMARY OF DELAMINATION ZONES FOR 18 PLY
LAMINATES (15 FT/SEC)

NO.	LAMINATE LAY-UP ANGLES	DELAMINATION AREA (SQ. INCHES)		MAXIMUM LENGTH (INCHES)	
		EXPERIMENT	COMPUTER MODEL	EXPERIMENT	COMPUTER MODEL
3	$(90_2, +45, 0_2, +45, 90)_S$.17	.16	.50	.40
4	$(90_2^k, +45^k, 0_2^k, +45^k, 90^k)_S$.29	.32	.75	.80
8	$(9_2^k, +45^k, 90_2, +45, 0)_S$.06	.00	.31	.00
9	$(0, +45, 90_2, +45^k, 0_2^k)_S$.30	2.88	.69	2.80
10	$(0, +45, 90_2, +45, 0_2^k)_S$.40	2.40	.81	2.40

TABLE 4.4 SUMMARY OF DELAMINATION ZONES FOR 18 PLY LAMINATES (20 FT/SEC)

NO.	LAMINATE LAY-UP ANGLES	DELAMINATION AREA (SQ. INCHES)		MAXIMUM LENGTH (INCHES)	
		EXPERIMENT	COMPUTER MODEL	EXPERIMENT	COMPUTER MODEL
3	$(90_2, +45, 0_2, -45, 90)_s$.55	.56	.88	1.00
4	$(90_2^k, +45^k, 0_2^k, -45^k, 90^k)_s$.57	.64	.90	1.20
8	$(0_2^k, +45^k, 90_2, -45, 0)_s$.89	.00	1.13	.00
9	$(0, +45, 90_2, -45^k, 0_2^k)_s$.83	3.20	1.13	2.80
10	$(0, -45, 90_2, -45, 0_2^k)_s$	2.32	2.80	4.13	2.40

experimental data that did not show up due to the low number of tests run. Another possibility is that there is a dynamic effect in the delamination response of the laminates with ± 45 degree plies. If this is true, it may be possible that this dynamic response did not occur at the lower impact velocity of 15 ft/sec. In any event, it is recommended that both of these possibilities be examined in a later study.

4.5 DISCUSSION OF ANALYTICAL VERSUS EXPERIMENTAL DATA

Table 4.5 contains a summary of the analytical and experimental delamination data for panels one through ten. This includes both 14 and 18-ply laminates at impact energies of 3 and 6 ft-lbs (15 and 20 ft/sec). A ranking based on the delamination zone size is also shown for both the analytical predictions and experimental results. The assigned rank is based on the smallest delamination being first (1) and the largest last (10). An additional column is included which contains the difference between the experimental and analytical rank at 15 and 20 ft/sec. As discussed briefly earlier, the rankings are quite close between the analytical predicted and experimental damage zones. At an impact velocity of 15 ft/sec, the average variation in rank for the ten laminates is .6 and 1.7 at 20 ft/sec. This would indicate that the delamination damage tolerance of a laminate within a group of laminates could be accurately determined.

Referring again to Table 4.5 and comparing the analytically predicted damage zones with those obtained experimentally, a significant variation can be seen. The variation can be attributed to several factors. First, the experimental data shown was based on a single test or data point so that a larger cross section could be examined. Similar studies indicate extensive scatter can be expected in the delamination zone size for identical impact tests. A study conducted by Gause¹² revealed a variation in delamination zone size of 0.01 in.² to 3.48 in.² (average of 1.83) in six identical impact tests on composite laminates. Assuming a similar scatter band is present in the test data shown in Table 4.5 and the preceding figures discussed earlier in the report, further repetitions of the impact tests are essential.

A trend can be seen in Table 4.5 delamination data comparisons between the experimental and analytical predictions that the greatest variation occurs in

TABLE 4.5 - ANALYTICAL VERSUS EXPERIMENTAL RESULTS

LAMINATE NO.	LAYUP *	NO. OF PLYS	DELAMINATION AREA - IN ² (RANKING)		20 FT/SEC EXPERIMENTAL ANALYTICAL Δ**
			15 FT/SEC EXPERIMENTAL ANALYTICAL Δ**	20 FT/SEC EXPERIMENTAL ANALYTICAL Δ**	
1	(90 ₂ /0 ₂ /90 ₂ /0) _s	14	.22 (4)	.16 (2,3) 2	.45 (2) .48 (4) 2
2	(90 ^k ₂ /0 ^k ₂ /90 ^k ₂ /0 ^k ₂) _s	14	.23 (5)	.32 (4,5,6) 1	.35 (1) .32 (2,3) 1
3	(0 ₂ /+45/90 ₂ /+45/0) _s	18	.17 (2,3)	.16 (2,3) 0	.55 (4) .56 (5) 1
4	(0 ^k ₂ /+45 ^k /90 ^k ₂ /+45 ^k /0 ^k ₂) _s	18	.29 (6)	.32 (4,5,6) 2	.64 (5) .64 (6) 1
5	(0 ^k ₂ /90 ^k /90/0 ₂ /90) _s	14	.17 (2,3)	.32 (4,5,6) 2	.50 (3) .32 (2,3) 1
6	(0 ₂ /90 ₂ /0 ^k ₂ /90 ^k) _s	14	.45 (9)	3.52 (10) 1	1.06 (8) 3.52 (4) 1
7	(0 ₂ /90 ₂ /0/0 ^k /90 ^k) _s	14	.48 (10)	3.36 (9) 1	1.15 (9) 4.00 (10) 1
8	(0 ^k ₂ /+45/90 ₂ /+45/0) _s	18	.06 (1)	0.0 (0) 0	.89 (7) 0.00 (1) 6
9	(0/+45/90 ₂ /+45 ^k /0 ^k ₂) _s	18	.30 (7)	2.38 (8) 1	.63 (6) 3.20 (8) 2
10	(0/+45/90 ₂ /+45/0 ^k ₂) _s	18	.40 (8)	2.40 (7) 1	2.32 (10) 2.60 (7) 3

* k Superscript denotes Kevlar Ply
 ** Difference between experimental and analytical ranking

the Kevlar core, graphite shell laminates (panels 6,7,9 and 10). The critical σ_2 stress used in predicting the delamination zones was derived from the graphite/epoxy non-hybrid panels. This was based on the observed fact that the delamination occurs between the graphite plies on the side opposite the impact. Energy absorbed in the Kevlar plies at the center of the laminate is not accounted for in the critical σ_2 stress calibration obtained from the all graphite panel. A more refined method of determining this critical stress and further documentation would alleviate the analytical/experimental deviation.

5.0 SUMMARY AND CONCLUSIONS

The research effort described in this document was designed to determine if hybrids do provide a synergistic improvement in damage resistance in comparison to a baseline (i.e., graphite/epoxy) material and that hybrids, when properly designed may enhance the visual and NDI damage detection threshold of the baseline material. The overall objectives of this research program were:

- o Develop a design methodology (math model) for hybrid structures which accurately describes the structural response, extent of damage and associated failure mode(s) due to low velocity impact.
- o Verify that the math model can predict the extent of damage a panel experiences when subjected to low velocity impact.
- o Ascertain the effects of visible and invisible damage by residual strength testing all impacted test panels.
- o To improve the visible and NDI damage detectability threshold of a baseline material system subjected to low velocity impact by proper placement of a second and possibly a third material system within the baseline material.

The main thrust of the program consisted of development, validation and use of an analytical methodology capable of predicting the impact response and damage of a composite panel. A simple quasi-static computational model was developed to represent the low velocity impact behavior of hybrid Kevlar/graphite laminates. The model was based on a combination of experimentally observed deflection modes and the laws of mechanics. Good agreement was obtained for comparison of experimental data and computed values for strains and displacements as a function of time for an impacted laminate.

The goal of the model was to develop a simple analysis capable of ranking hybrid Kevlar/graphite laminates with respect to the amount of delamination due to low velocity impact. The procedure for predicting the extent of delamination was to use the delamination data for the two non-hybrid laminates made of graphite and Kevlar as calibration analyses. Then the critical values of delamination stress were used to predict the extent of delamination in three Kevlar/graphite hybrid laminates.

A verification study of the model's capabilities to rank laminates according to the extent of delamination damage was conducted. The model showed good agreement with the delamination trends observed in the experimental study for

both 15 ft/sec and 20 ft/sec impact velocities. The model was shown to have the capability of ranking a series of laminates in order, with respect to the size of the delamination zone. The model did exhibit significant variation in the predicted delamination zone size when compared to the experimental data for some laminates. Several factors were discussed which contributed to this variation. First, extensive data scatter on similar impact programs has been noted in the experimental data. This program opted to utilize only one test per data point so that a wider cross-section of laminates could be examined. Second, the greatest deviation in the analytical versus experimental correlation was observed in those hybrids containing a Kevlar core with exterior plies of graphite. Energy absorbed in the high strain to failure Kevlar effected the results. A totally graphite panel was utilized in obtaining the critical stress, σ_z . A more refined method of determining the critical σ_z stress to be used is required. Correction of these two factors would be a simple process and will be implemented in all future work.

The simple quasi-static model showed good agreement for the displacement and strain history response of a laminate as well as a capability to rank a series of 0, 90 degree Kevlar/graphite laminates. More complex laminates containing 0, 90 and +45 degree plies were also examined. The model showed good qualitative agreement with the delamination trends for those more complex laminates with an impact velocity of 15 ft/sec. The data for the 20 ft/sec impact velocity part of the experimental study showed some distinct differences when compared to the 15 ft/sec data. This suggested further studies to determine if there is a scatter in data or if there is a dynamic effect not seen in the 15 ft/sec data.

While the results shown here are very encouraging, the simplicity of the model indicates restrictions on its general applicability. Further applications of the model should be preceded by verification and developmental studies for the particular series of laminates of interest.

Use of high speed photographs in Task I was supplemented with strain gage data of the thin laminate impact response when deriving the basis for the analytical model. As mentioned earlier, thin 3-ply panels were used so that the deflections during impact would be large enough to be easily photographed. The strain rate sensitivity of a material's properties is a factor generally neglected in low velocity impact studies. Task II investigated the effects of elevated strain rates on the ultimate stress and strain for both

graphite/epoxy and Kevlar/epoxy. The modulus was also calculated. Longitudinal, transverse and ± 45 degree shear coupons were tested at three strain rates, one static and two dynamic rates. The properties at each rate were calculated and compared. Variation in the material properties was small, but the trends will be briefly discussed. Longitudinal graphite coupons showed a slight increase in tensile strength with an increase in strain rate while the corresponding Kevlar coupons revealed a decrease. The ± 45 degree shear coupons for both materials exhibited an increasing trend for both the ultimate stress and shear modulus with increasing strain rate. Further testing utilizing a greater number of specimens is essential as data scatter obtained coupled with the relatively small sample size renders any solid conclusions suspect.

Impact tests of the non-hybrid and hybrid panels were conducted under Task III tests. Two basic laminate layups, a 14 and 18 ply, were used throughout this section. The materials used within the laminate were varied, however. Task III was divided into three functional groups. Series 1 consisted of four non-hybrid laminates, a 14-ply Kevlar, 18-ply Kevlar, 14-ply graphite and an 18-ply graphite panel.

Series 1 panels comprised the control or baseline tests with which the six Series 2 hybrid laminate damage and response panels were compared. Following impact of the panels, the delaminated areas were identified using C-scan methods. The panels were then tested to determine their residual strengths.

Results of Series 1 and 2 tests indicated that for the hybrid laminates tested, only one hybrid exhibited a synergistic improvement over the non-hybrids based on total damage size. The maximum impact energy was a six-foot pound impact. At this low level, no fiber failures could be detected in the panel. All damage appeared to be matrix oriented. The residual tensile strength tests yielded interesting and noteworthy results in that a majority of the impact damaged coupons realized a net increase in ultimate stress. Again, it should be noted that no broken fibers were present and that the damage was matrix oriented. This damage would yield a definite hazard in compressive and fatigue loads.

Series 3 tests included two laminates on which thin aluminum foils were bonded. Impact tests on the metallic coating were conducted to determine the effectiveness of aluminum in enhancing the detection of low level damage. The

aluminum did not appear to aid in the detection of damage. A thicker, more ductile material may perform better although the concensus is that the stiff composite backing is not compatible with the idea of a dent in any surface coating.

6.0 SUGGESTIONS FOR FUTURE WORK

Several areas requiring further development or investigation have been outlined in this report. Much progress has been made and the groundwork now exists for even more substantial progress for low velocity impact work in the future.

The math model developed in the course of this study serves as the basic building block for a full-blown impact model. Additional repetitions of center impact tests are necessary to minimize the effects of scatter and to further validate the math model. With the addition of off-center and oblique impact modeling capabilities, a much more realistic model would be developed. Work is also necessary in adapting the model to account for the change in the impacted panel's properties as the damage increases during the impact event. This progressive failure would allow for a much more accurate prediction without complicating the model substantially. The model was used on a very limited spectrum of hybrid laminates due to the program restrictions. Extensive use of the model on other hybrid laminates would allow for the optimization of a laminate for specialized tasks. Further testing is required to determine the significance of the trends seen in the investigation of strain rate sensitivity in properties of graphite and Kevlar materials. Investigation into the cause of strain rate sensitive material properties would aid all segments of materials research. A possible correlation between the viscoelastic material properties and strain rate sensitivity may exist.

Future tasks should include the following:

- o Conduct additional repetitions of impact tests to minimize scatter
- o Refine the damage propagation methods in the model
- o Apply the model to a larger selection of laminates
- o Incorporate off-center impact into the model
- o Incorporate oblique impact into the model
- o Further investigate the effects of strain rate on the material properties

7.0 REFERENCES

1. Jones, R. M., "Mechanics of Composite Materials", Scripta Book Company, Washington, D.C.
2. Ashton, J. E., Halpin, J. C. and Petit, P. H., "Primer on Composite Materials: Analysis", Technomic Publishing Company, Westport, Conn.
3. Gottesman, T., Hashin, Z and Brull, M. A., "Reduction of Elastic Moduli of Fiber composites by Fatigue Crack Accumulation", Department of Materials Science and Eng., School of Engineering and Applied Science, University of Pennsylvania, Philadelphia, PA., April 1980.
4. Vinson, J. R. and Zukas, J. A., "On the Ballistic Impact of Textile Body Armor", Journal of Applied Mechanics, ASME Publication Paper No. 75-APM-12.
5. Daniel, I. M., Liber, T., and Labeledz, R. H., "Wave Propagation in Transversely Impacted Composite Laminates".
6. McQuillen, E. J, Llorens, R. E., and Gause, L. W., "Low Velocity Transverse Normal Impact of Graphite/Epoxy Composite Laminates", Interim Report, Naval Air Development Center, Warminster, PA., December 1975.
7. Llorens, R. E. and McQuillen, E. J., "Off-Center, Low Velocity Transverse Normal Impact of a Simply Supported Plate", Final Report, Naval Air Development Center, Warminster, PA., September 1979.
8. Llorens, R. E. and McQuillen, E. J., "Off-Center, Low Velocity Transverse Normal Impact of a Viscoelastic Beam", Final Report, Naval Air Development Center, Warminster, PA., September 1978.
9. Rybicki, E. F., Schmusser, D. W., and Fox, J., "An Energy Release Rate Approach for Stable Crack Growth in the Free-Edge Delamination Problem", Battelle Columbus Laboratories, Columbus, Ohio, June 1977.
10. Foy, R. L. and Bake, D. J., "Design of Orthotropic Laminates", Presented at the 11th Annual AIAA Structures, Structural Dynamics and Materials Conference, Denver, Colorado.
11. Pipes, R. B., Kaminski, B. E., and Pagano, N. J., "Influence of the Free Edge Upon the Strength of Angle Ply Laminates", an Analysis of the Test Methods for High Modulus Fibers and Composites, ASTM STP 521, 1973, pp. 218-228.
12. Gause, L. W., "Low Speed, Hard Object Impact on Thick Graphite/Epoxy Plates", Final Report, Naval Air Development Center, Warminster, PA., May 1978.

APPENDIX A

ULTRASONIC C-SCAN RESULTS OF IMPACTED TASK III PANELS

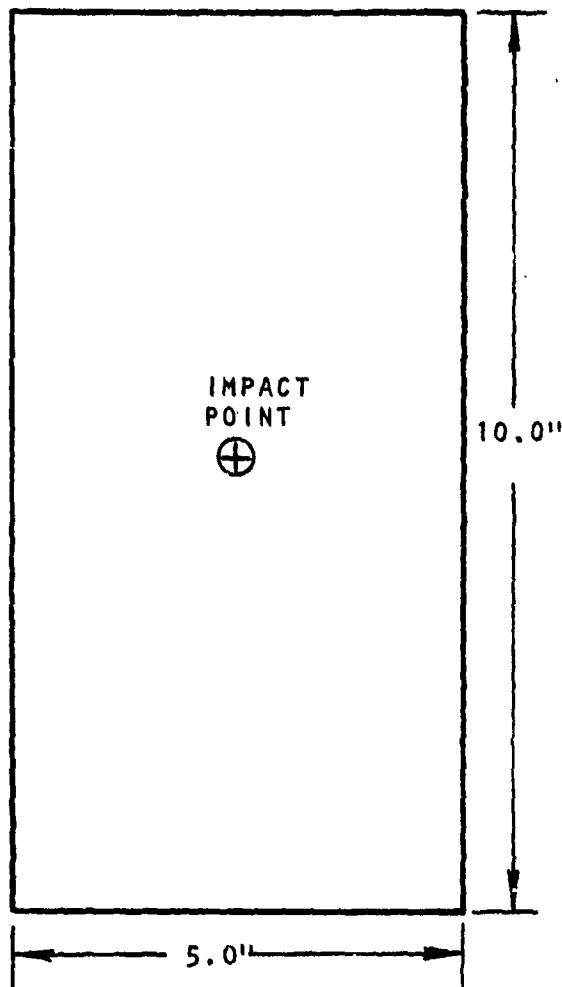


FIGURE 1A, THIN IMPACT PANEL (3 PLY) CONFIGURATION (TASK 1)

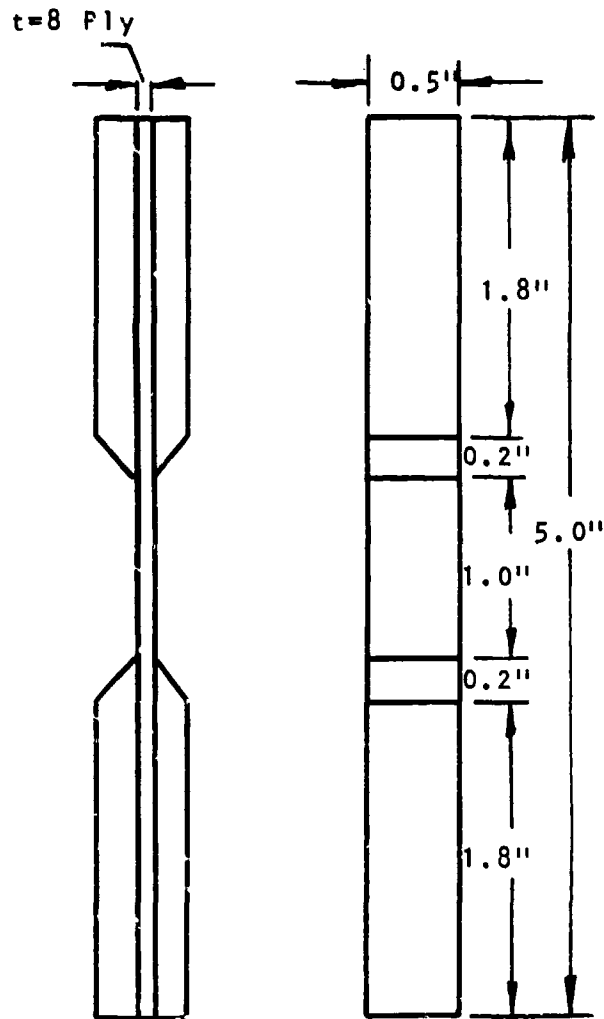


FIGURE 2A, LONGITUDINAL (0°), SHEAR ($+45^\circ$) AND STATIC TRANSVERSE (90°) COUPON CONFIGURATION (TASK I!)

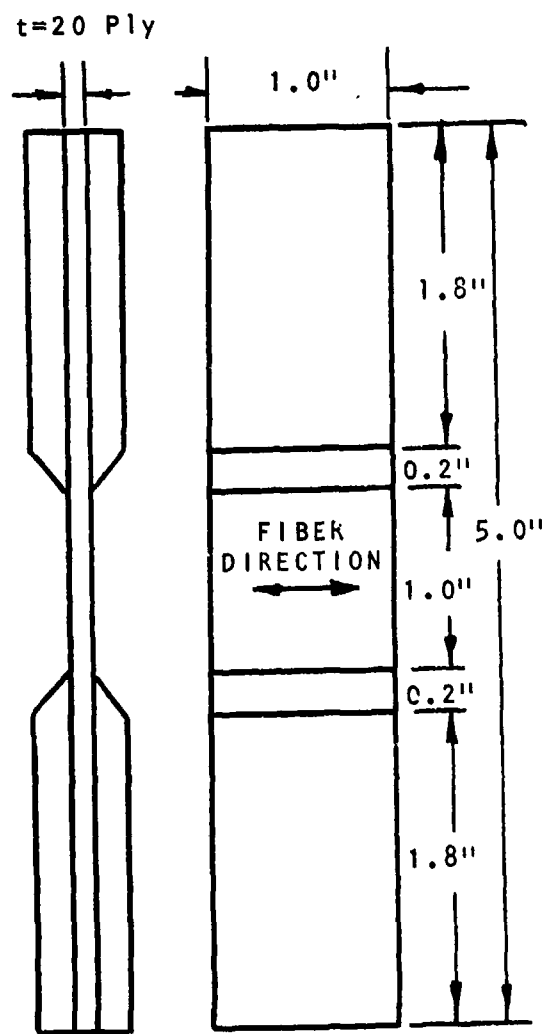


FIGURE 3A, DYNAMIC TRANSVERSE COUPON CONFIGURATION (TASK II)

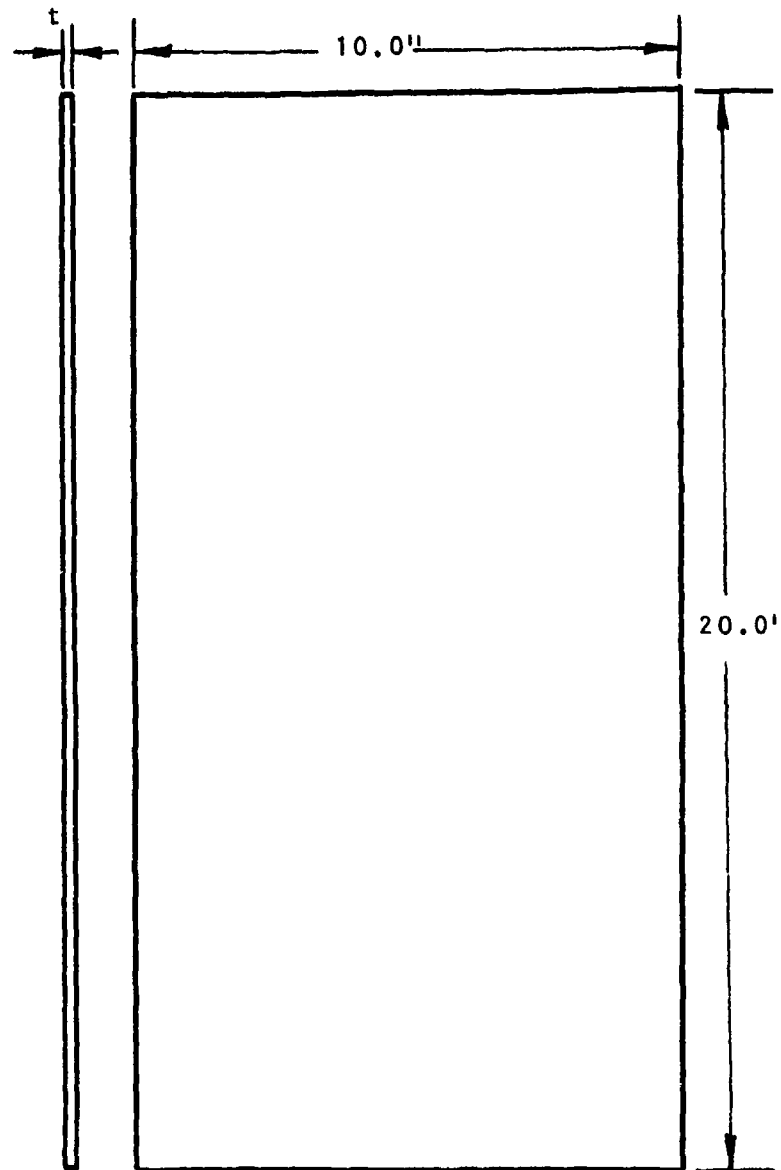


FIGURE 4A - IMPACT PANEL CONFIGURATION, 14 AND 18 PLY (TASK III)

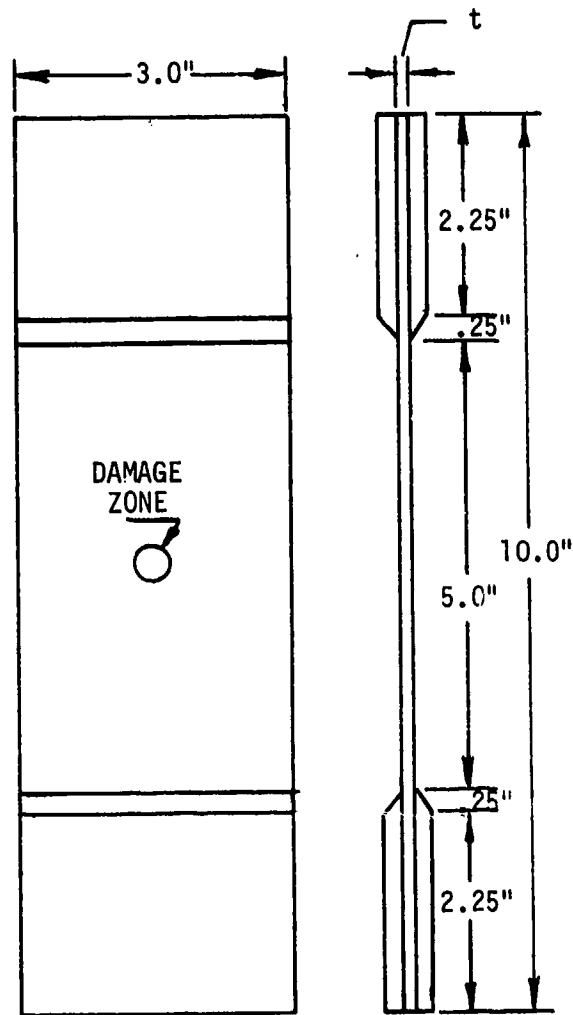


FIGURE 5A - RESIDUAL STRENGTH COUPON CONFIGURATION (TASK III)

APPENDIX B

ULTRASONIC C-SCAN RESULTS OF IMPACTED TASK III RESULTS

Several of the figures in this section exhibit a rectangular area of higher attenuation (lighter shade) which overlap the impact delamination area (white sections). The rectangular areas result from tape applied to the panel following impact to ensure no water penetrates the damage zone. The absorbed water would obscure the delamination during the ultrasonic tests. The tape induced region should be discounted when viewing the C-scans.

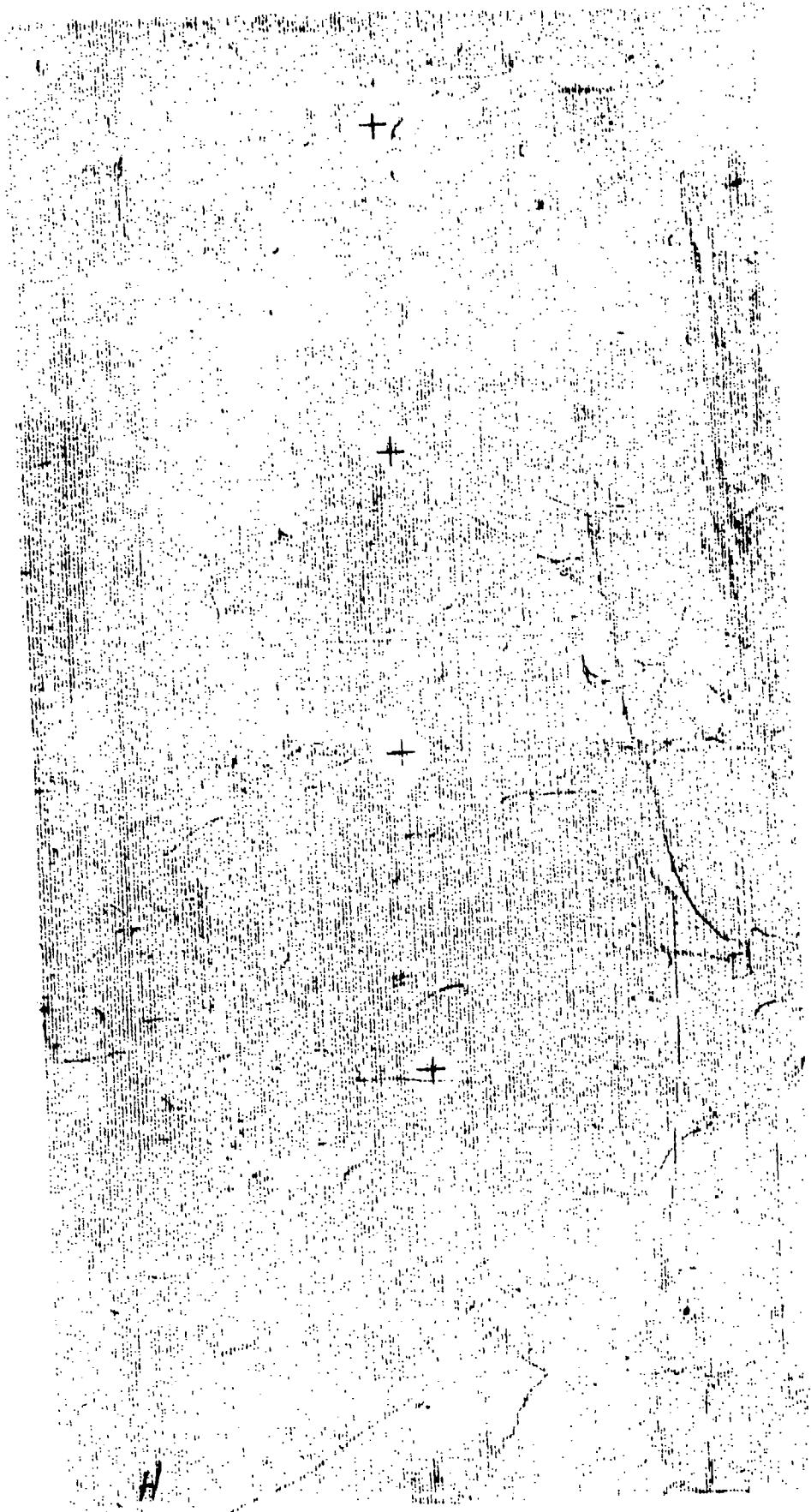


FIGURE 1B, C-SCAN OF IMPACT DAMAGED NON-HYBRID PANEL (PANEL 1)

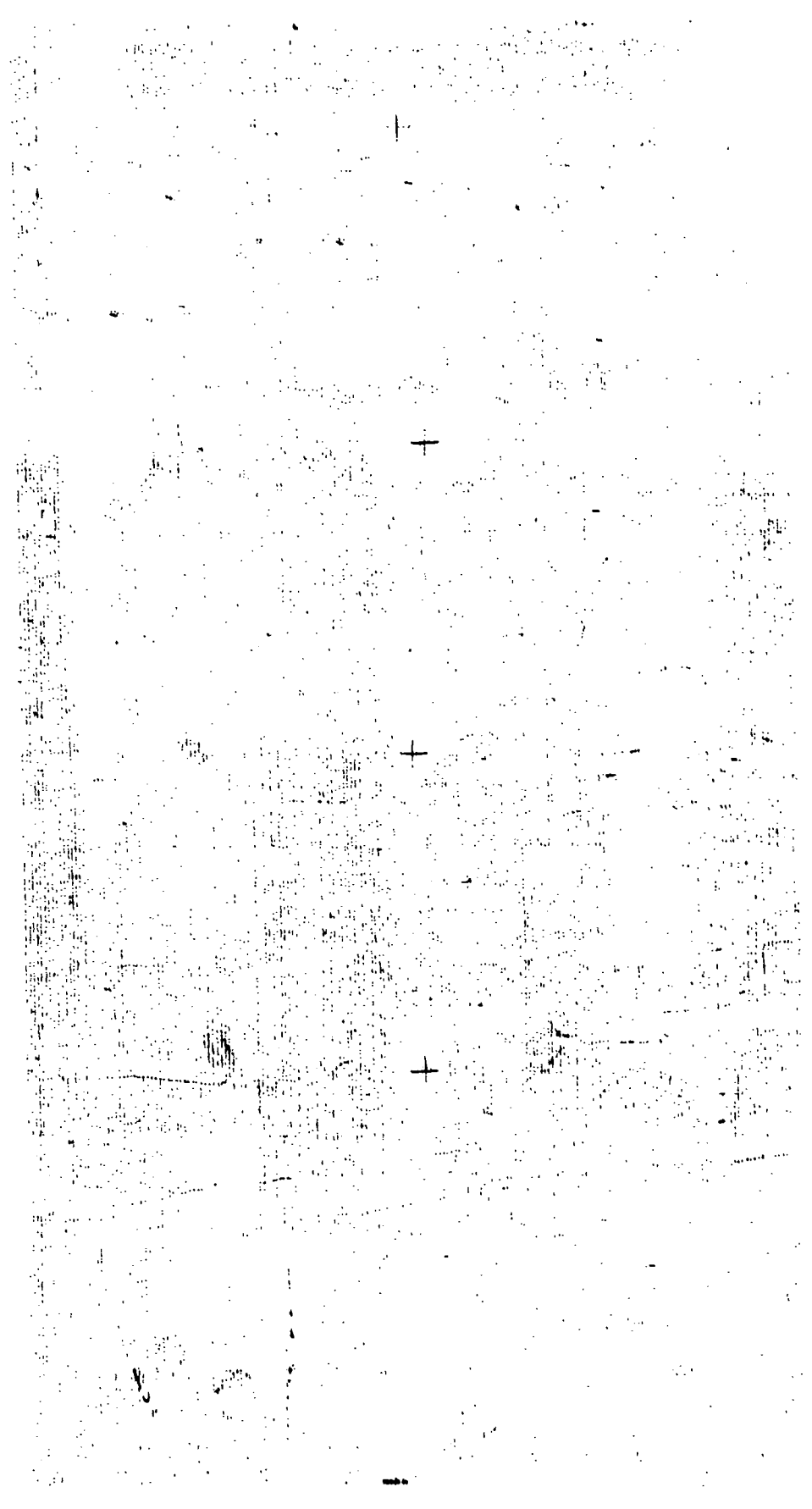


FIGURE 2B, C-SCAN OF IMPACT DAMAGED NON-HYBRID PANEL (PANEL 2)

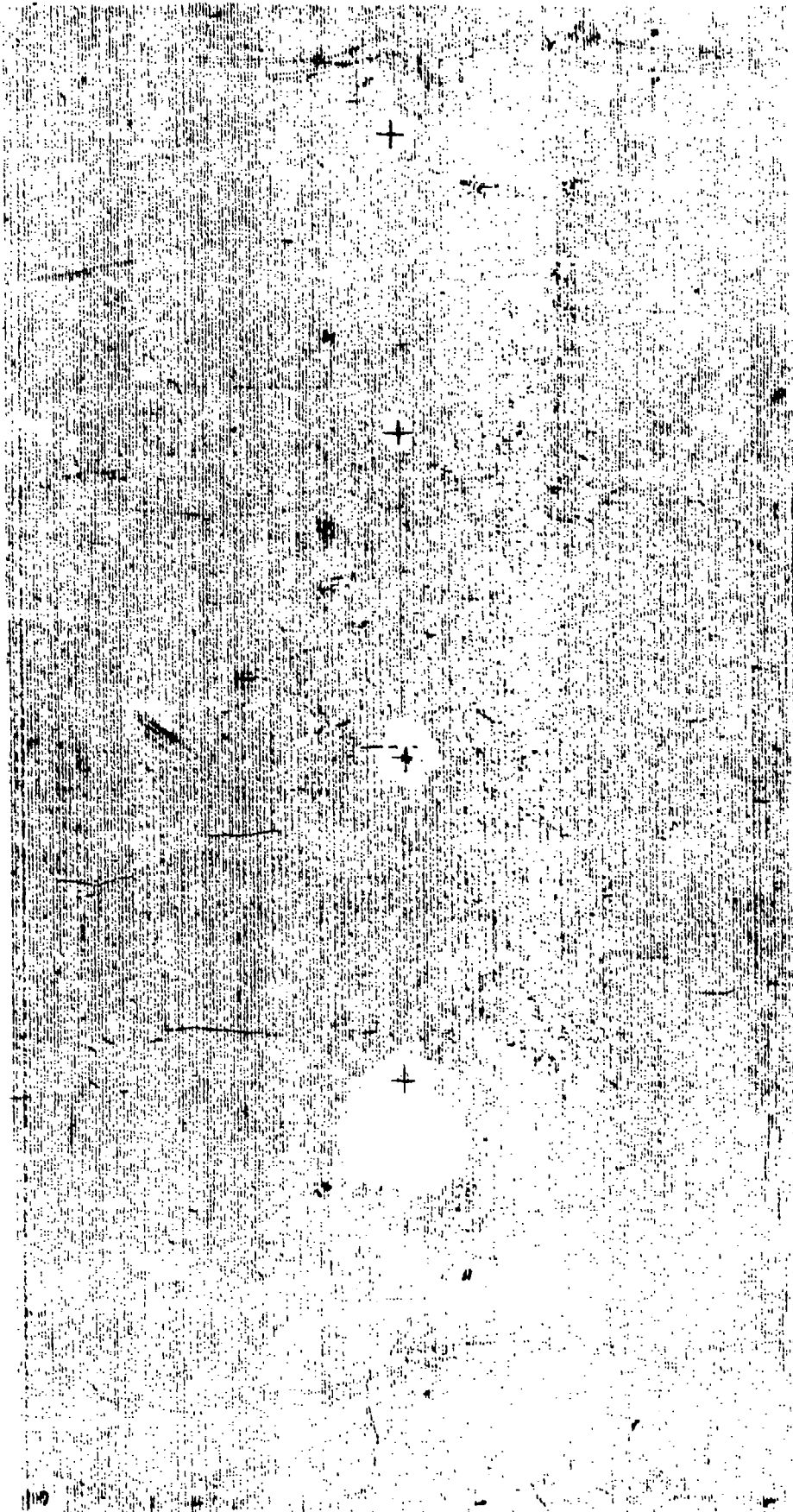


FIGURE 3B, C-SCAN OF IMPACT DAMAGED NON-HYBRID PANEL (PANEL 3)

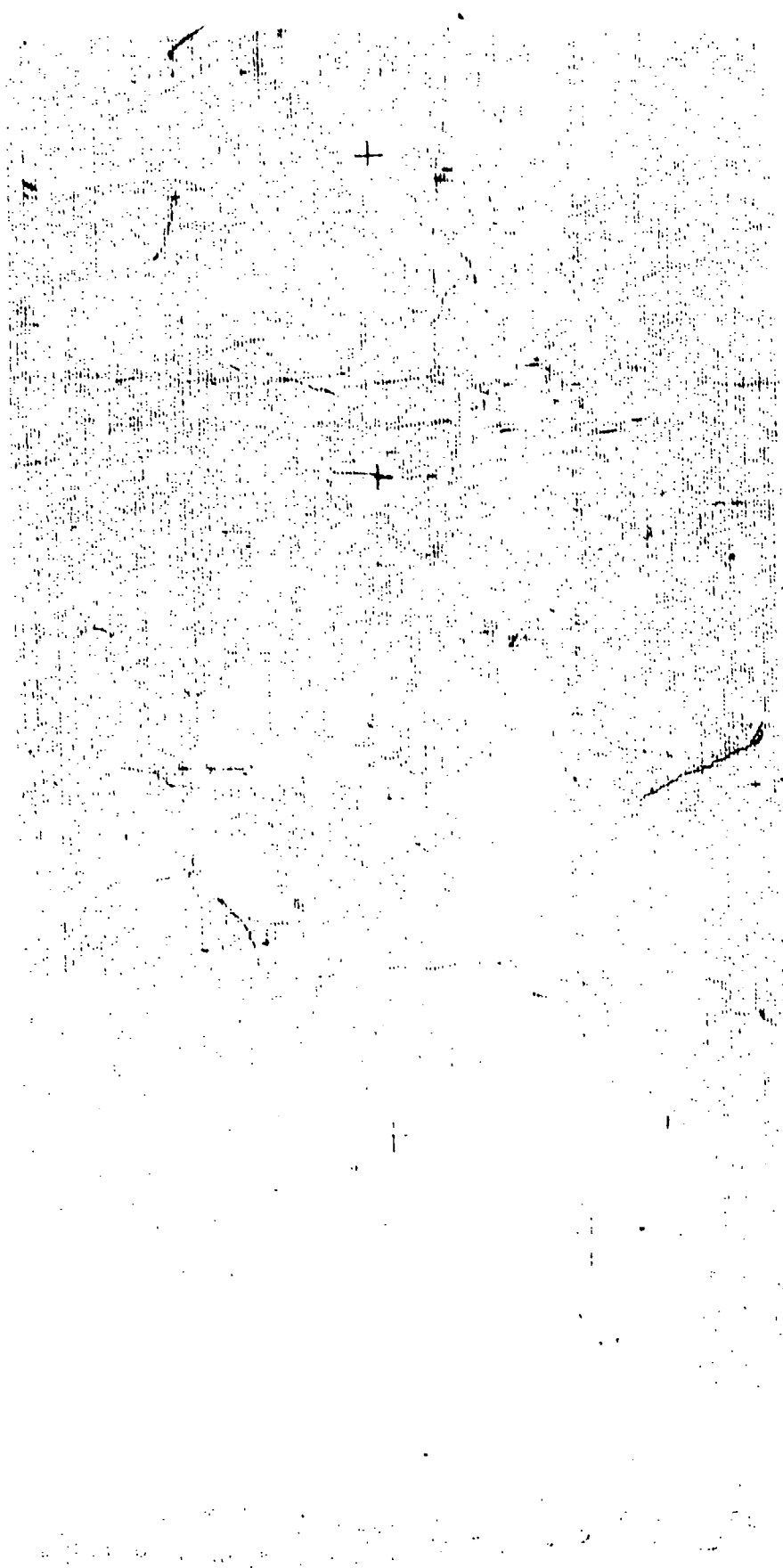


FIGURE 4B, C-SCAN OF IMPACT DAMAGED NON-HYBRID PANEL (PANEL 4)



FIGURE 5B, C-SCAN OF IMPACT DAMAGED NON-HYBRID PANEL (PANEL 5)

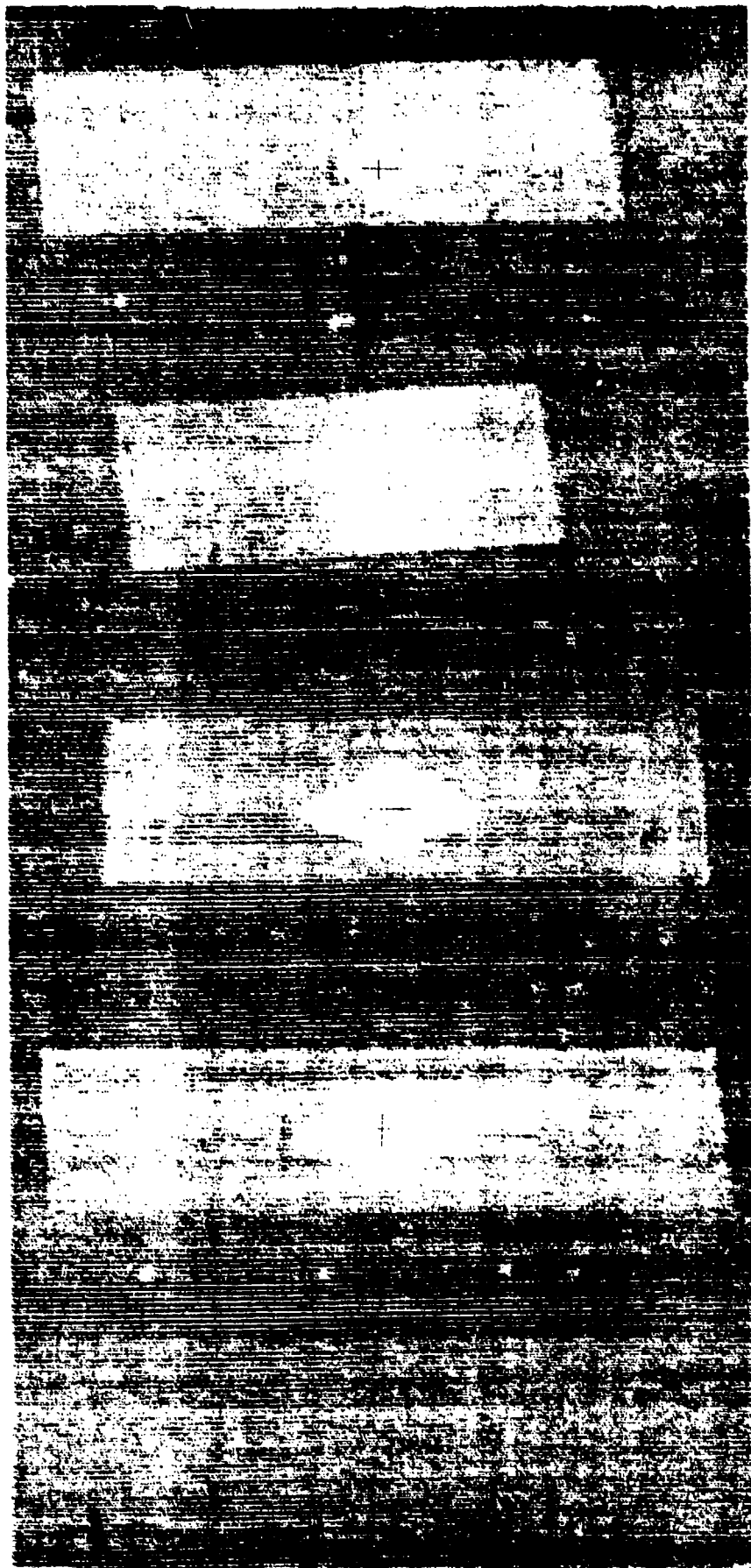


FIGURE 6B, C-SCAN OF IMPACT DAMAGED HYBRID (PANEL 6)

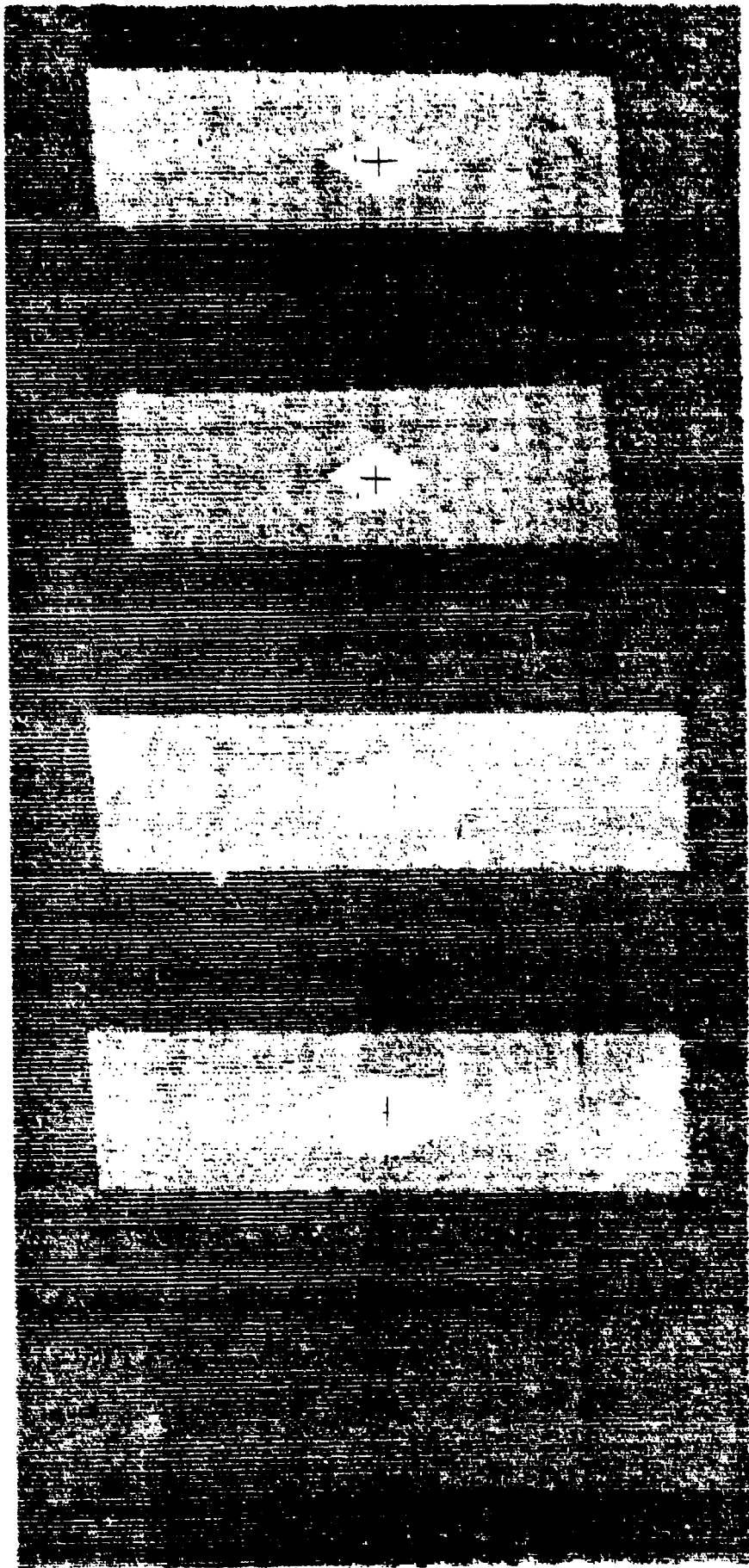


FIGURE 7B, C-SCAN OF IMPACT DAMAGED HYBRID (PANEL 7)

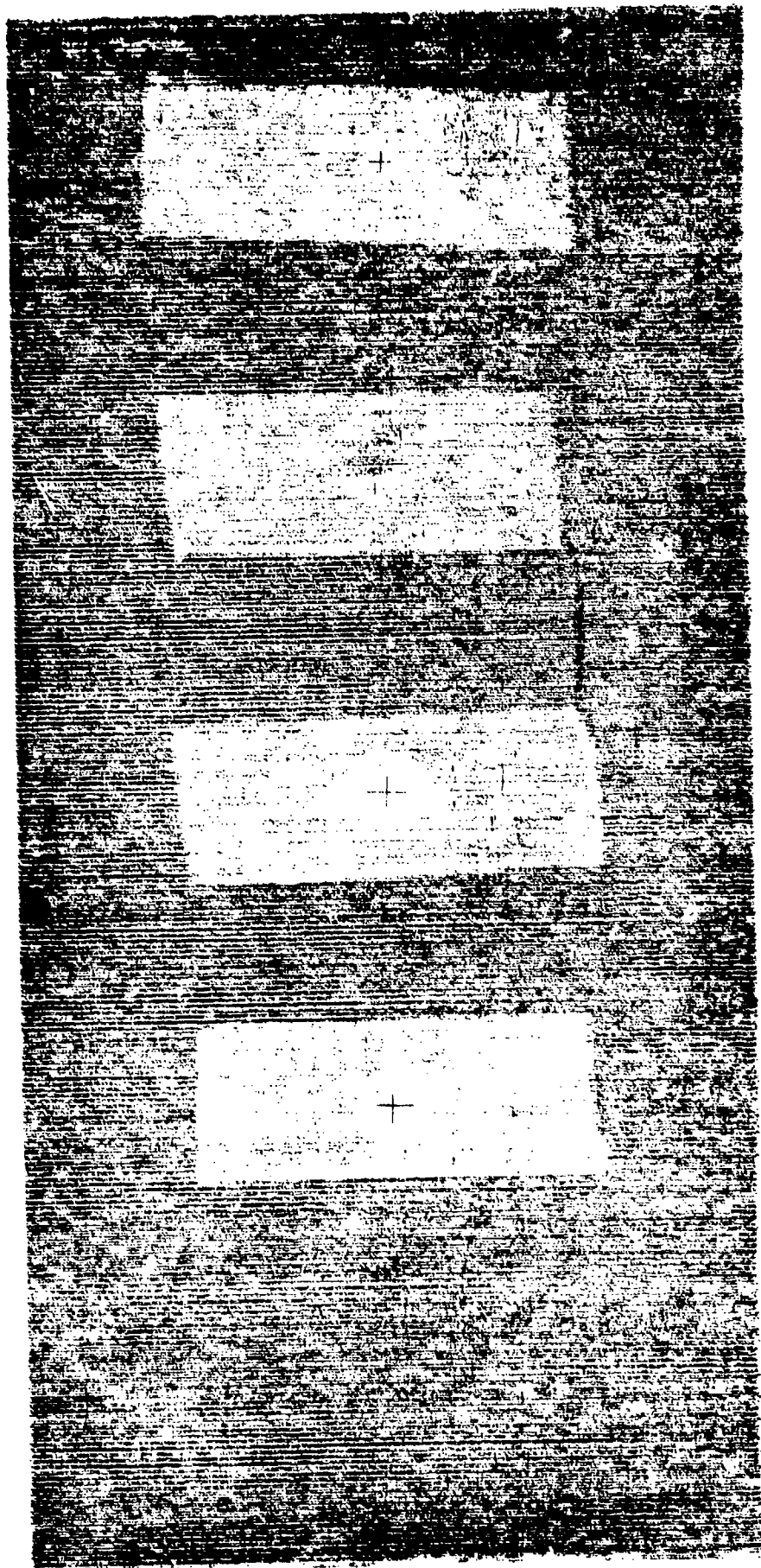


FIGURE 8B, C-SCAN OF IMPACT DAMAGED HYBRID (PANEL 8)

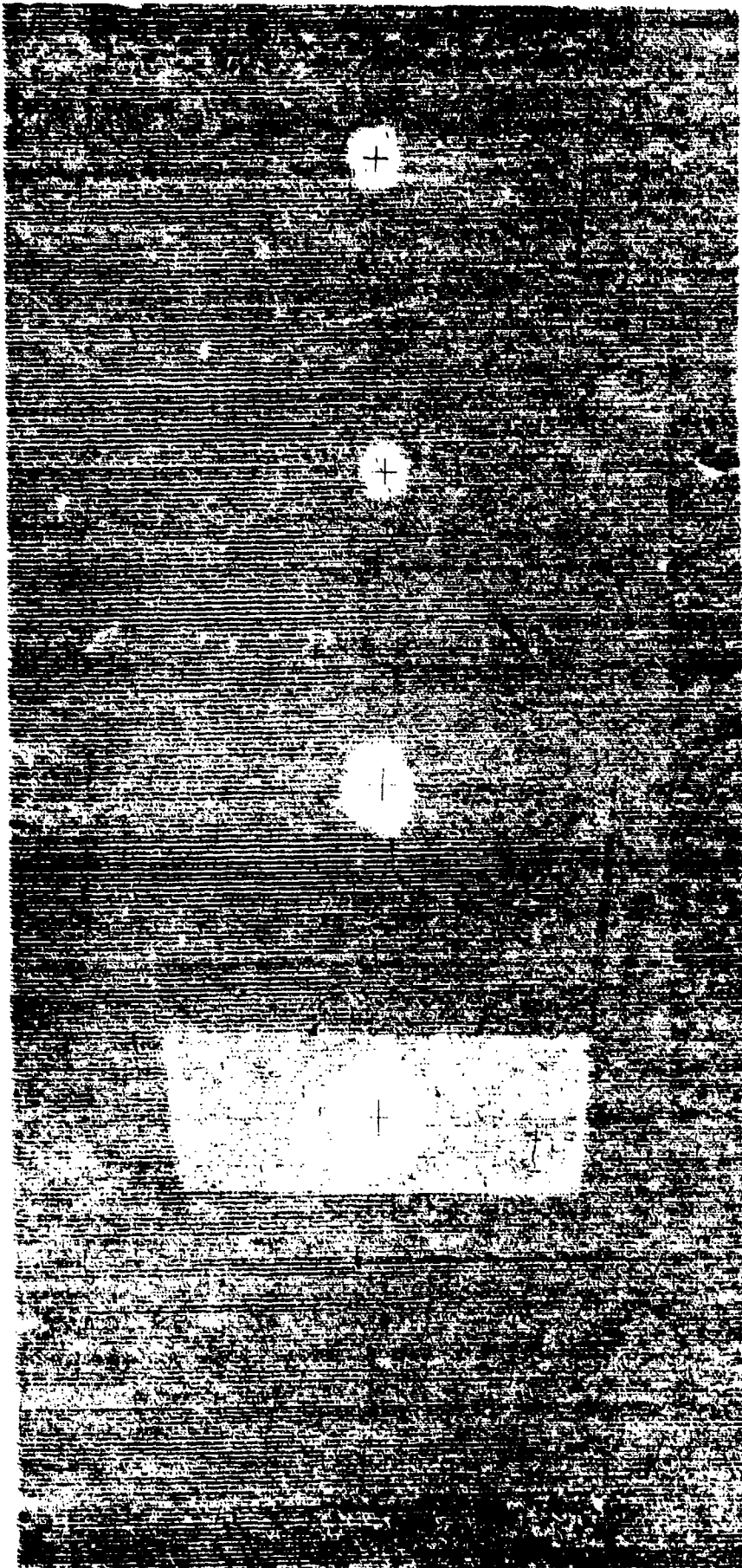


FIGURE 9B, C-SCAN OF IMPACT DAMAGED HYBRID (PANEL 9)

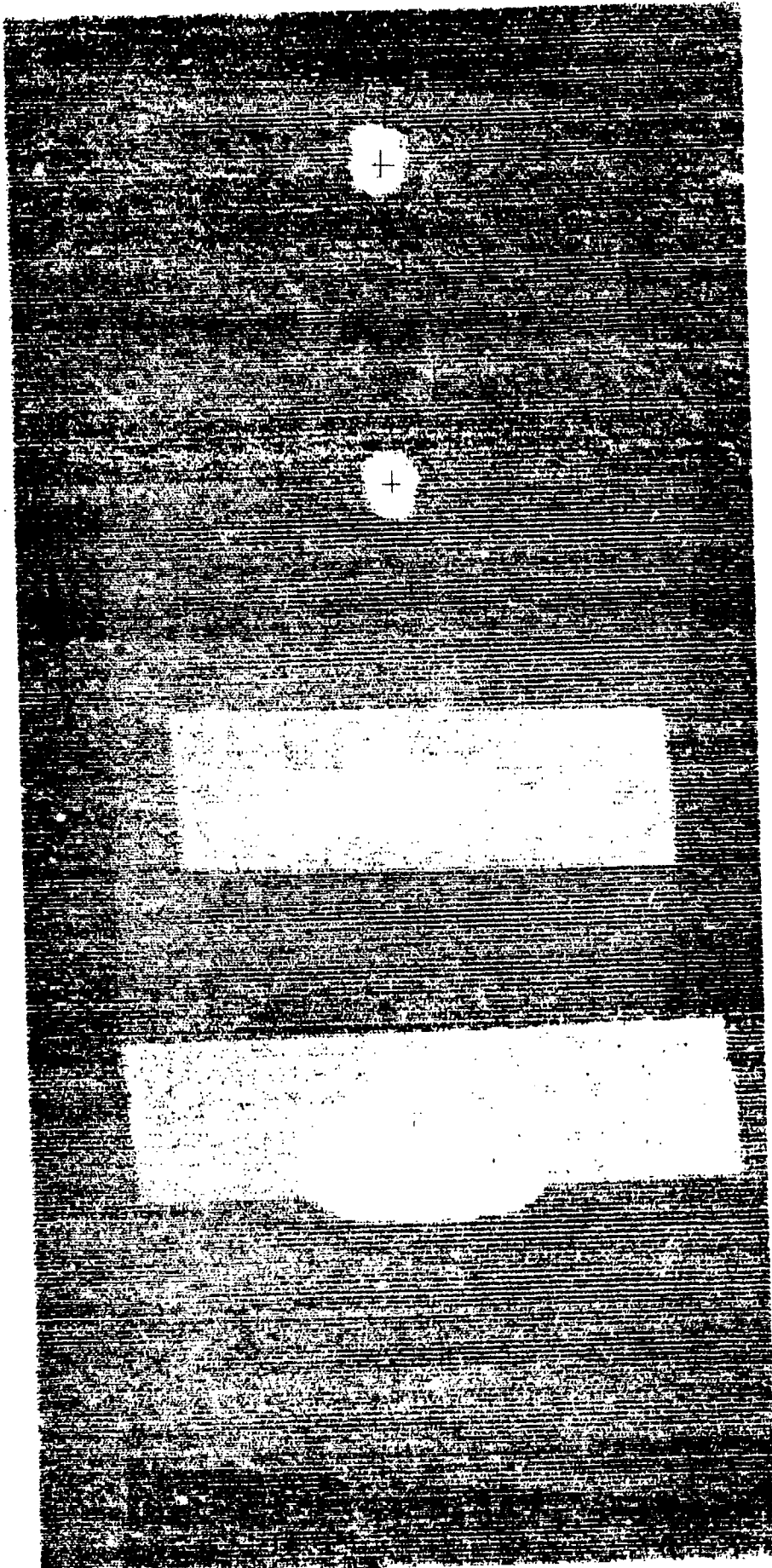


FIGURE 10B, C-SCAN OF IMPACT DAMAGED HYBRID (PANEL 10)

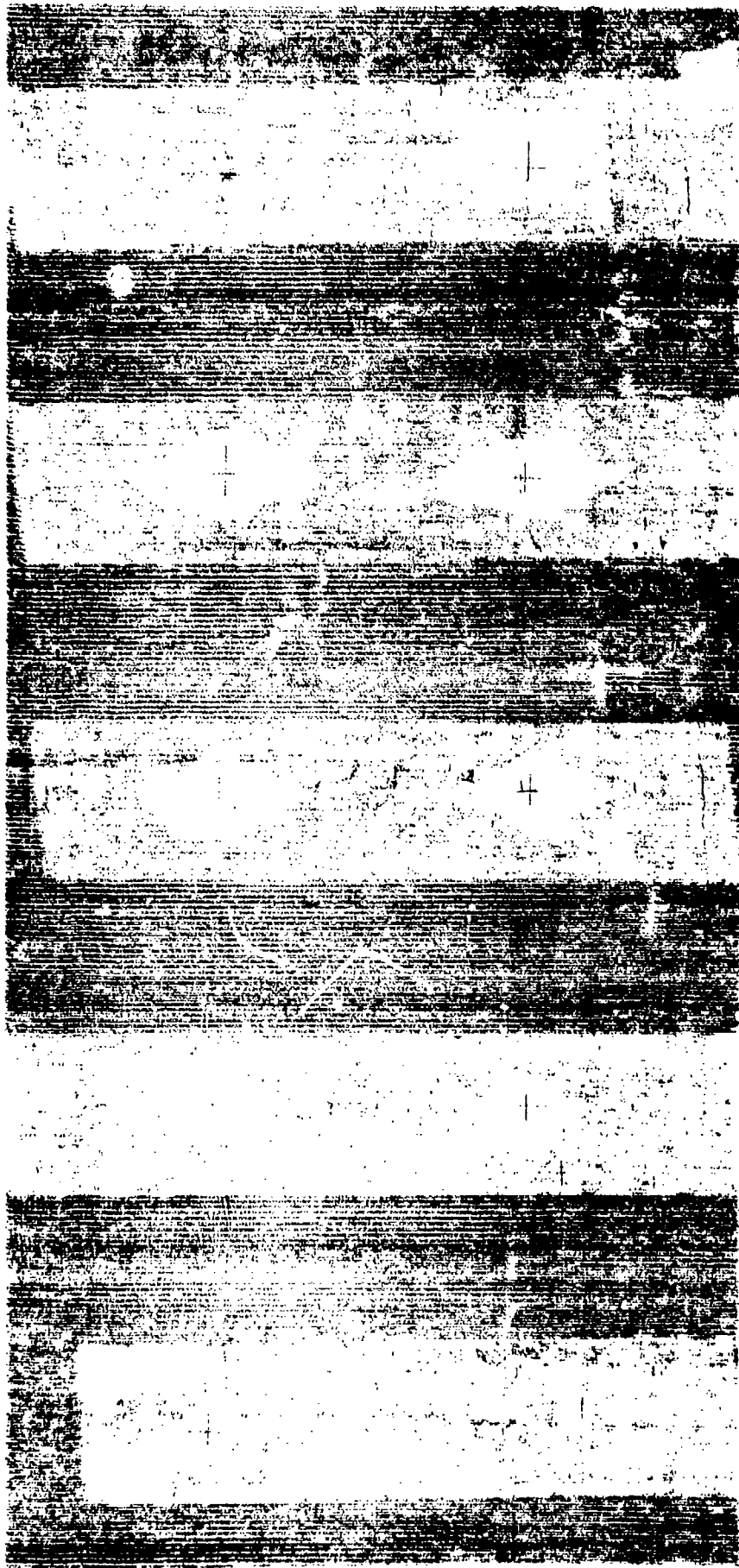


FIGURE 11B, C-SCAN OF IMPACT DAMAGED METALLIC COATED HYBRID (PANEL 11)

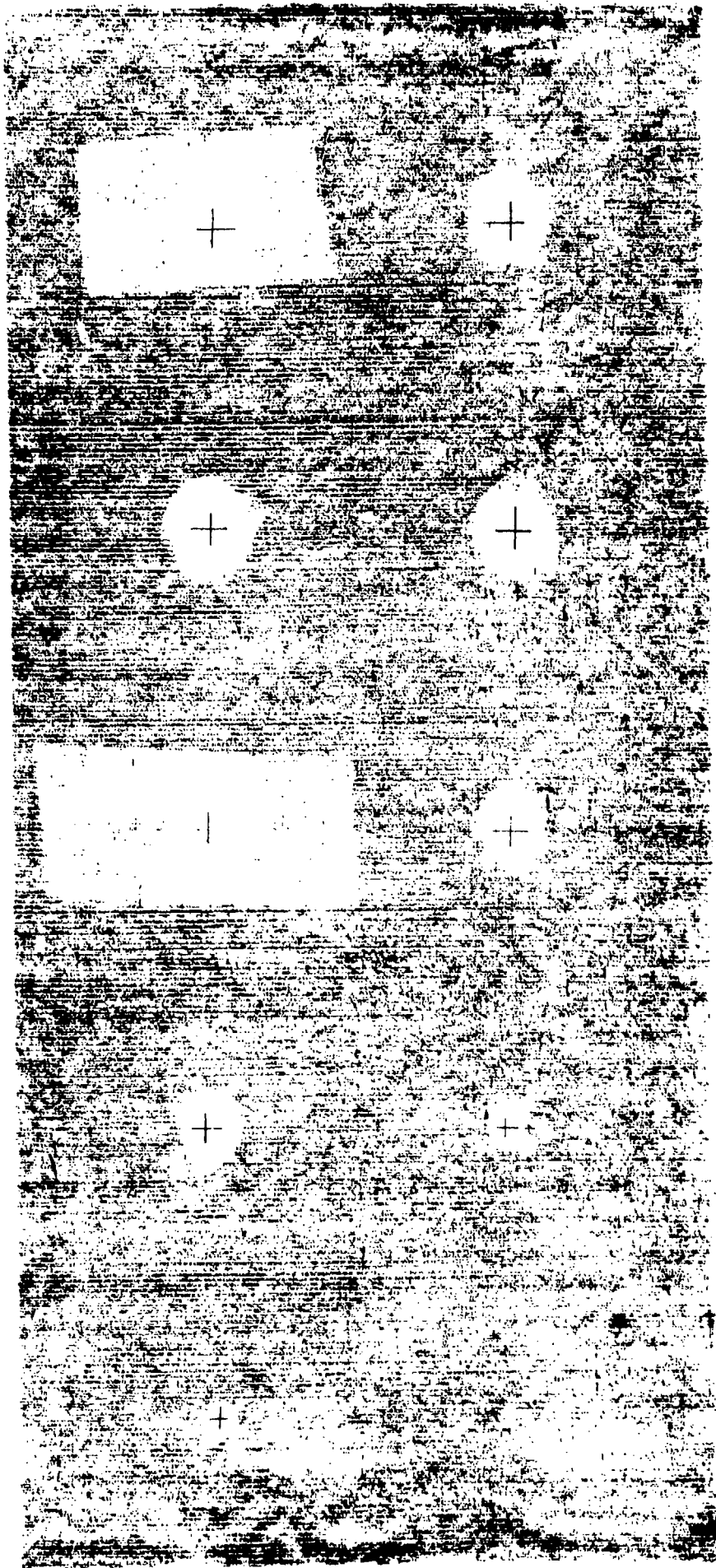


FIGURE 12 B, C-SCAN OF IMPACT DAMAGED METALLIC COATED HYBRID (PANEL 12)

Naval Air Systems Command
Code AIR-00D4
Washington, D.C. 20361

Naval Air Systems Command
Code AIR-320B
Washington, D.C. 20361

Naval Air Systems Command
Code AIR-5304
Washington, D.C. 20361

Naval Air Systems Command
Code AIR-5302
Washington, D.C. 20361

Naval Air Development Center
Attn: Mr. P. Kozel, Code 6043
Warminster, Pennsylvania 18974

Naval Air Development Center
Attn: Dr. S. L. Huang, Code 6043
Warminster, Pennsylvania 18974

Naval Air Development Center
Attn: Mr. T. Hess, Code 6043
Warminster, Pennsylvania 18974

Naval Air Development Center
Attn: Mr. L. Gauss
Warminster, Pennsylvania 18974

Naval Air Development Center
Attn: Dr. J. DeLuccia, Code 6052
Warminster, Pennsylvania 18974

Naval Sea Systems Command
Attn: Dr. H. Vanderveldt, Code 05R15
Washington, D.C. 20362

Naval Sea Systems Command
Attn: Mr. M. Kinna, Code 062R4
Washington, D.C. 20362

Naval Sea Systems Command
Attn: Mr. J. Gagorik, Code 03R24
Washington, D.C. 20362

Office of Naval Research
Attn: Dr. N. Perrone, Code 474
Arlington, Virginia 22217

Office of Naval Research
Attn: Dr. B. McDonald, Code 471
Arlington, Virginia 22217

Naval Ship R&D Center
Attn: Mr. Couch, Code 173.2
Bethesda, Maryland 20034

Naval Ship R&D Center
Attn: Mr. J. Gudas
Annapolis, Maryland 21401

Naval Surface Weapons Center
Attn: Mr. J. Agul
White Oak, Maryland 20910

Naval Research Laboratory
Attn: Dr. I. Wolock, Code 6383
Washington, D.C. 20375

Naval Research Laboratory
Attn: Dr. G. Yoder, Code 6384
Washington, D.C. 20375

Wright Aero Labs AFFDL
Attn: Mr. P. A. Parmley
Wright Patterson Air Force Base, Ohio 45433

Wright Aero Labs AFFDL
Attn: Mr. G. P. Senedekyj
Wright Patterson Air Force Base, Ohio 45433

Wright Aero Labs AFFDL
Attn: Mr. G. E. Maddux
Wright Patterson Air Force Base, Ohio 45433

Wright Aero Labs, AFML
Attn: Mr. T. G. Reinhard, Jr.
Wright Patterson Air Force Base, Ohio 45433

Wright Aero Labs, AFML
Attn: Mr. G. P. Peterson
Wright Patterson Air Force Base, Ohio 45433

Air Force Office of Scientific Research
Bldg. 410 Bolling AFB
Attn: Dr. A. Amos
Washington, D.C. 20332

Air Force Office of Scientific Research
Bldg. 410 Bolling AFB
Attn: Dr. M. Salkind
Washington, D.C. 20332

Defense Advanced Research Project Agency
1400 Wilson Boulevard
Attn: Dr. E. C. VanReuth
Arlington, Virginia 22209

NASA
Attn: Dr. J. Davidson
Langley Research Center
Hampton, Virginia 23365

NASA
Langley Research Center
Attn: Dr. R. Pride
Hampton, Virginia 23365

NASA
Langley Research Center
Attn: Dr. G. L. Roderick
Hampton, Virginia 23365

Army Air Mobility R&D Laboratory
Attn: Mr. H. Reddick
Fort Eustis, Virginia 23604

Army Materials & Mechanics Research Center
Attn: Dr. E. Lenoë
Watertown, Massachusetts 02172

Army Materials & Mechanics Research Center
Attn: Mr. D. Oplinger
Watertown, Massachusetts 02172

Army Mobility R&D Lab.
Ames Research Center
Attn: Dr. Raymond Foye
Moffett Field, California 94035

Army Research Office
Attn: Dr. F. Schmiedeshoff
Research Triangle Park, North Carolina 277

Materials Science Corporation
Merion Towle House
Attn: Dr. W. Rosen
Blue Bell, Pennsylvania 19422

McDonnell Douglas Corporation
McDonnell Aircraft Company
P. O. Box 516
Attn: Mr. K. Stenberg
St. Louis, Missouri 63166

McDonnell Douglas Corporation
McDonnell Aircraft Company
P. O. Box 516
Attn: Mr. R. Riley
St. Louis, Missouri 63166

McDonnell Douglas Corporation
McDonnell Aircraft Company
P. O. Box 516
Attn: Mr. R. Garrett
St. Louis, Missouri 63166

McDonnell Douglas Corporation
McDonnell Aircraft Company
P. O. Box 516
Attn: Dr. D. Ames
St. Louis, Missouri 63166

McDonnell Douglas Corporation
McDonnell Aircraft Company
P. O. Box 516
Attn: Dr. C. Whitsett
St. Louis, Missouri 63166

Northrop Corporation
3901 W. Broadway
Attn: Dr. N. Bhatia
Hawthorne, California 92050

Northrop Corporation
3901 W. Broadway
Attn: Dr. L. Jeans
Hawthorne, California 92050

Northrop Corporation
3901 W. Broadway
Attn: Dr. M. Ratwani
Hawthorne, California 92050

General Dynamics/CONVAIR Division
P. O. Box 80847
Attn: Mr. W. Scheck
San Diego, California 92138

General Dynamics
Aerospace Division
P. O. Box 748
Attn: Dr. R. Wilkins
Fort Worth, Texas 76101

General Dynamics
Aerospace Division
P. O. Box 748
Attn: Mr. S. Manning
Fort Worth, Texas 76101

Lockheed Missiles & Space Co.
Attn: Mr. H. Marshall
Sunnyvale, California 94088

Grumman Aerospace Corporation
Attn: Mr. R. Hadcock
Bethpage, New York 11714

Grumman Aerospace Corporation
Attn: Mr. S. Dastin
Bethpage, New York 11714

Grumman Aerospace Corporation
Attn: Mr. W. Grant
Bethpage, New York 11714

Sikorsky Aircraft
Attn: Mr. M. J. Rich
Stratford, Connecticut 06602

Bell Helicopter
P. O. Box 482
Attn: Mr. J. McGuigan
Fort Worth, Texas 76101

Hughes Helicopters
Centinela and Teale Street
Attn: Mr. G. Rock
Culver City, California 90230

Boeing Vertol Company
Attn: Mr. R. Peck
Philadelphia, Pennsylvania 19142

Kaman Aerospace Corporation
Old Windsor Road
Attn: Mr. J. Schauble
Bloomfield, Connecticut 06002

Rockwell International Corp./Science Center
P. O. Box 1085
1049 Camino Dos Rios
Attn: Dr. Neil Paton
Thousand Oaks, California 91360

Rockwell International Corp./Science Center
P. O. Box 1085
1049 Camino Dos Rios
Attn: Ms. R. Richards
Thousand Oaks, California 91360

Pratt & Whitney Aircraft
Division of United Aircraft Corp.
Florida Research & Development Ctr.
P. O. Box 2691
Attn: Mr. John Miller
West Palm Beach, Florida 33402

The Franklin Institute Research Laboratories
Twentieth & Parkway
Attn: Technical Director
Philadelphia, Pennsylvania 19103

Department of the Navy
Naval Air Systems Command
Attn: AIR-5302
Washington, D.C. 20361

Department of the Navy
Naval Air Systems Command
Attn: AIR-52032D
Washington, D.C. 20361

Naval Air Development Center
Attn: Code 6083
Warminster, Pennsylvania 18974